

SURFACE PLASMON ASSISTED SPECTROSCOPIES AND THEIR APPLICATION
IN TRACE ELEMENT ANALYSIS, THE STUDY OF BIOMOLECULAR
INTERACTIONS, AND CHEMICAL SENSING

Tsunghsueh Wu

Certificate of Approval

Holly R. Ellis
Associate Professor
Chemistry and Biochemistry

Curtis Shannon, Chair
Professor
Chemistry and Biochemistry

Vince Cammarata
Associate Professor
Chemistry and Biochemistry

Rik Blumenthal
Associate Professor
Chemistry and Biochemistry

George T. Flowers
Interim Dean
Graduate School

SURFACE PLASMON ASSISTED SPECTROSCOPIES AND THEIR APPLICATION
IN TRACE ELEMENT ANALYSIS, THE STUDY OF BIOMOLECULAR
INTERACTIONS, AND CHEMICAL SENSING

Tsunghsueh Wu

A Dissertation

Submitted to

the Graduate Faculty of

Auburn University

in Partial Fulfillment of the

Requirements for the

Degree of

Doctor of Philosophy

Auburn, Alabama

August 9, 2008

SURFACE PLASMON ASSISTED SPECTROSCOPIES AND THEIR APPLICATION
IN TRACE ELEMENT ANALYSIS, THE STUDY OF BIOMOLECULAR
INTERACTIONS, AND CHEMICAL SENSING

Tsunghsueh Wu

Permission is granted to Auburn University to make copies of this dissertation at its discretion, upon request of individuals or institutions and at their expense. The author reserves all publication rights.

Signature of Author

Date of Graduation

VITA

Tsunghsueh (Joseph) Wu, son of Yongyuan Wu and Chunhsian WuChen, was born on October 27, 1975 in Tsanghua, Taiwan. He is the youngest in the family with one elder brother, Tsungzhe Wu, and one elder sister, Tzuhui Wu. He obtained his high school diploma from Columbia College in 1996 in Vancouver, British Columbia, Canada. He then graduated with a Bachelor of Science degree in Chemical Engineering at Michigan Technological University in August 2000. He worked one year in General Electric Company before he entered the Department of Chemistry and Biochemistry at Auburn University in August 2003 to pursue a Doctoral degree in Analytical Chemistry. He married Shiara Farinah on August 8, 2001, and they have a son Brandon Michael Wu.

SURFACE PLASMON ASSISTED SPECTROSCOPIES AND THEIR APPLICATION
IN TRACE ELEMENT ANALYSIS, THE STUDY OF BIOMOLECULAR
INTERACTIONS, AND CHEMICAL SENSING

Tsunghsueh Wu

Doctor of Philosophy, August 9, 2008
(B.S. Michigan Tech. University, 2000)

123 Typed Pages

Directed by Curtis Shannon

The main objective of this dissertation is to apply the fundamental principles of surface plasmon assisted spectroscopies such as surface plasmon resonance spectroscopy and surface enhanced Raman spectroscopy in the trace analysis of selenite and tellurite concentration in an analyte solution, the study of the protein-protein interactions, and chemical sensing.

Chapter 1 presents the detailed literature review on two types of the surface plasmon assisted spectroscopies: surface plasmon resonance spectroscopy (SPR) and surface enhanced Raman spectroscopy (SERS). The principles of SPR and SERS based on the optical properties of the metallic thin film, their current applications in biochemical/chemical sensing, and the anticipated results are discussed in detail.

Chapter 2 provides a detailed discussion on the quantitative analysis of the selenite and tellurite concentration in an analyte solution. This study employs the combined electrochemistry and SPR technique (EC-SPR) to determine the concentration of an unknown solution containing selenite and tellurite ions. The motivation of determining selenium content in an aqueous solution, brief background of EC-SPR, the experiment setup, and the results of the research are presented.

Chapter 3 presents the application of surface Plasmon resonance spectroscopy in studying the protein-protein interaction as a surface based bioanalytical method. The two component protein system of alkanesulfonate monooxygenase was chosen as a model system for the study. The flavin reductase (SsuE) and flavin monooxygenase (SsuD) interact strongly to carry out enzymatic reactions. Their interaction has been studied using the solution based method. Herein, the surface based method such as SPR was used in this study and the current research results were compared to the results obtained from the solution based method. The discrepancy between two results was discussed.

Chapter 4 presents the application of surface enhanced Raman spectroscopy in studying the binary components of self-assembled monolayers and in developing a state-of-art filter based chemical sensor. The goal of this research project is to develop an optical based chemical sensor for monitoring the in-flight air quality. The development and the validation of the SERS based sensor are discussed.

Chapter 5 summarizes the finding of the research. The future work of the projects is stated.

ACKNOWLEDGEMENTS

I would like to express my deepest gratitude to my advisor Dr. Curtis Shannon for his dedicated teaching, constant guidance, and generous support during the entire course of this research. His stewardship of talents and his embracing cradle for the creativity will always be remembered as the role model for my teaching philosophy. I would like to recognize the tremendous contributions from my committee members, Dr. Cammarata, Dr. Ellis, and Dr. Blumenthal, over the past years of constant support in giving me numerous insightful suggestions for the research projects and for the preparation of this manuscript. I also want to extend my gratitude towards my mentor and my dedicated outside reader, Dr. Minseo Park, for sharing his unforgettable wisdom. I will always remember this department since I have received so much support from the faculty, administration assistants, and friends. Of course, I won't forget my colleagues, Dr. Kholis Abdurachim, Dr. Ugur Tamer, Dr. Lunsheng Zhang, Dr. Anand Sankarraj, Junxua Xin, Chaokang Gu, Sridevi Ramakrishnan, Rajakumari Ramaswamy, Weiping Li, Hongxia Zhang, Tanyu Wang, and Yajiao Yu. It is really fun working with all of them and I wish all the best to them.

I would like to thank my parents and family members for being extra supportive on my education since I was a kid. I want to say to my son, Brandon, that I will always love you and thank you for providing me the joy and the meaning of this world. Last but not least, I am forever indebted to my wife, Shiara, for her undivided love and her constant encouragement during the years of my graduate studies.

Style manual or journal used Journal of the American Chemical Society

Computer software used Microsoft Excel, Microsoft Word 2007, Origin Pro 7.5,

SIProScan 1.41b, KaleidaGraph3.5

TABLE OF CONTENTS

LIST OF TABLES	xii
LIST OF FIGURES	xiii
1. INTRODUCTION TO SURFACE PLASMON RESONANCE SPECTROSCOPY AND SURFACE ENHANCED RAMAN SPECTROSCOPY	1
1.1 Introduction	1
1.2 Dielectric constant of metals	2
1.3 Surface plasmon polariton	5
1.4 Excitation of surface plasmon	8
1.5 Localized surface plasmon resonance	12
1.6 Surface plasmon resonance spectroscopy	14
1.6.1 Attenuated total reflection and reflectance	15
1.6.2 Three modes of SPR measurements	20
1.6.3 SPR based affinity biosensors	21
1.6.4 Electrochemical SPR	22
1.7 Surface enhanced Raman Spectroscopy	24
1.7.1 Raman spectroscopy	24
1.7.2 Surface enhanced Raman spectroscopy	29
1.8 Conclusions	32
1.9 References	35

2. SIMULTANEOUS DETECTION OF TRACE SELENITE AND TELLURITE BY ELECTROCHEMICAL-SURFACE PLASMON RESONANCE TECHNIQUE	47
2.1 Introduction	47
2.2 Experimental	51
2.2.1 Materials	51
2.2.2 Electrochemistry	51
2.2.3 Instrumentation	52
2.3 Results and discussion	52
2.3.1 Study of stripping and formation of gold oxide	52
2.3.2 Study of selenium underpotential deposition	56
2.3.3 EC-SPR for selenite detection using constant potential deposition method	59
2.3.4 EC-SPR for selenite detection using electrochemical stripping method	62
2.4 Conclusions	73
2.5 References	74
3. STUDY OF PROTEIN-PROTEIN INTERACTION USING SURFACE PLASMON RESONANCE	78
3.1 Introduction	78
3.2 Experimental	82
3.2.1 Chemicals and proteins	82
3.2.2 Instrumentation	82
3.2.3 Covalent immobilization of SsuD on SPReeta sensing surface	84

3.3 Results and discussion	84
3.4 Conclusions	94
3.5 References	95
4. SENSITIVITY STUDIES OF SURFACE ENHANCED RAMAN SCATTERING ON Au/Ag FILM OVER NANOSPHERES AND SILVER COATED HIGH EFFICIENCY PARTICULATE AIR FILTER	98
4.1 Introduction	98
4.2 Experimental	100
4.2.1 Materials	100
4.2.2 SERS substrate fabrication	101
4.2.3 Self-assembled monolayer preparation	102
4.2.4 Electrochemical measurement	102
4.2.5 Atomic force microscopy imaging	103
4.2.6 SERS apparatus	103
4.3 Results and discussion	103
4.3.1 Characterization of the mixed monolayers of 4-ATP and DT using electrochemistry and SERS	104
4.3.2 Characterization of the Au/Ag coated HEPA filter	114
4.4 Conclusions	118
4.5 References	119
5. SUMMARY OF DISSERTATION	121

LIST OF TABLES

Table 1.1	The plasma frequency, the damping constants, and the Fermi velocity for copper, silver, and gold.	6
Table 1.2	Examples of applications of SPR in biomedical sciences.	23
Table 2.1	The calculated value for the concentration of TeO_3^{2-} and SeO_3^{2-} ions in the unknown analyte.	72
Table 3.1	The data fitting results.	93
Table 4.1	The assignment of selected SERS bands for 4-ATP.	109

LIST OF FIGURES

Figure 1.1	(a) Schematic representation of the mechanism of photon absorption for metallic materials in which an electron is excited into a higher-energy unoccupied state. (b) Reemission of a photon of light by the direct transition of an electron from a high to a low energy state.	3
Figure 1.2	Surface plasmon waves at a metal/dielectric interface.	7
Figure 1.3	The dispersion of surface plasmons at the metal-air interface.	10
Figure 1.4	(a) Kretschmann and (b) Otto configuration of an attenuated total reflection setup for coupling surface plasmons.	11
Figure 1.5	The localized surface plasmon.	13
Figure 1.6	Excitation of surface plasmon using the Kretschmann geometry	15
Figure 1.7	The reflectance curve of SPR measurements.	18
Figure 1.8	Quantum theory for (a) the Stokes and (b) anti-Stokes line. (c) Raman spectra of CCl ₄ showing Rayleigh, Stokes and anti-Stokes scattering.	27
Figure 1.9	Distance dependence of SERS.	33
Figure 2.1	The simultaneous measurement of cyclic voltammetry and SPR for a gold electrode in 0.1 M HClO ₄ .	53
Figure 2.2	The simultaneous measurement of cyclic voltammetry and SPR for a gold electrode in 1 mM SeO ₃ ²⁻ .	58
Figure 2.3	The changes in SPR response for three different potentials in the 200 μM selenite solution.	60

Figure 2.4	The changes in SPR angle for different SeO_3^{2-} concentrations at 200 mV.	61
Figure 2.5	The changes in SPR angle for different SeO_3^{2-} concentrations at 200 mV from Figure 2.4 at time 500 seconds.	63
Figure 2.6	Interference study of EC-SPR constant potential deposition.	64
Figure 2.7	The potential step programs for EC-SPR stripping analysis.	65
Figure 2.8	Effect of stripping potential on (a) selenium electroplated and (b) tellurium electroplated gold electrode.	67
Figure 2.9	The TeO_3^{2-} concentration effect on the EC-SPR stripping response.	68
Figure 2.10	The SeO_3^{2-} concentration effect on the EC-SPR stripping response.	69
Figure 2.13	The standard addition method to determine the concentration of an unknown analyte containing TeO_3^{2-} and SeO_3^{2-} ions.	71
Figure 3.1	The flow-cell setup for SPR measurement.	83
Figure 3.2	Schematic representation of the immobilization of the SsuD on gold surface.	85
Figure 3.3	The SPR sensorgram for the SsuD immobilization.	87
Figure 3.4	The SPR measurement of protein interactions between SsuE and immobilized SsuD.	88
Figure 3.5	The shifts in SPR angle upon the loading of SsuE at different concentrations.	92

Figure 4.1	The cyclic voltammogram of ATP self-assembled monolayer on gold electrode in 1 M HClO ₄ supporting electrolyte.	105
Figure 4.2	The relationship between surface coverage and the mole fraction of ATP in the solution.	107
Figure 4.3	The Raman spectrum of 4-ATP.	108
Figure 4.4	The AFM image of Au/Ag FONS on mica.	111
Figure 4.5	Raman intensity of the band 1077 cm ⁻¹ for 4-ATP as a function of mole fraction of the 4-ATP in the solution.	112
Figure 4.6	The relationship between the SERS intensity to the number of moles of ATP adsorbed on the Au/Ag FONS.	113
Figure 4.7	The scanning electron microscope image of the Au/Ag coated glass fiber.	
Figure 4.8	The uptake curve of the SERS intensity relative to the picomoles of ATP added to the Au/Ag modified HEPA filter from the addition of 10 μM ATP solution.	116
Figure 4.9	The standard addition method to determine the unknown concentration of ATP added to the Au/Ag modified HEPA filter.	117

CHAPTER 1

INTRODUCTION TO SURFACE PLASMON RESONANCE SPECTROSCOPY AND SURFACE ENHANCED RAMAN SPECTROSCOPY

1.1 Introduction

A surface plasmon is a quantum of a collective plasma oscillation confined at a dielectric-metal interface.^{1,2} It can be excited by electromagnetic radiation by matching the momentum of the incident photons to that of the surface plasmon or so-called surface plasmon resonance (SPR) condition. The excited surface plasmon or the surface plasmon polariton can propagate along a planar metal surface or can be localized on metallic nanoparticles or nanostructures. The induced electromagnetic field on metal surface decays exponentially into both media as a surface confined evanescent wave. Since the induced field is very sensitive to the variations of the dielectric medium in proximity to a metal surface, a small change in the optical properties of the dielectric medium can be quantitatively analyzed for the sensing purposes.

Sensors based on surface plasmon resonance have gained increasing popularity. One example is surface plasmon resonance spectroscopy, which is able to measure the binding of analytes to the functionalized surfaces without any labeling and is able to measure the binding events in real time.³⁻⁶ Its label-free advantage has been exploited for biosensing applications such as the development of immunosensors,⁷⁻⁹ proteomic technology,^{10,11} drug discovery,^{12,13} DNA sensors,^{14,15} and as a tool for studying

biomolecular interactions.^{16,17} Several reviews of surface plasmon resonance spectroscopy have been published.¹⁸⁻²⁰ On the other hand, the large field enhancement associated with SPR provides a basis for many surface analytical techniques such as surface enhanced Raman spectroscopy,²¹⁻²⁴ surface enhanced fluorescence spectroscopy,^{25,26} and surface enhanced infrared absorption.²⁷⁻²⁹ The field enhancement will be discussed in more detail in section 1.7.2

1.2 Dielectric constant of metals

Optical properties of a material often relate to the dielectric constant of the material and they can be determined by exposing the material to electromagnetic radiation such as visible light. The incident radiation of the visible light can excite the electrons of the materials into the unoccupied energy states above the Fermi energy level and the electron transition is demonstrated in Figure 1.1a. Metals have continuous empty electron states available for such electron transitions; therefore, metals can absorb all frequencies of visible light. However, most of the absorbed radiation by the metal is reemitted as the reflected light. Figure 1.1b depicts the electron transition accompanying the reemission of the light. The amount of reflected light energy can be measured and normalized with the incident light energy to yield the reflectivity of the materials. The reflectivity for most metals is between 0.90 and 0.95 since a small fraction of the incident energy is dissipated as heat during the non-radiative decay process.

Most metals are opaque, but certain metals such as copper and gold appear colored due to their unique optical property in selectively absorbing some certain wavelengths of the visible light without the light re-emission.

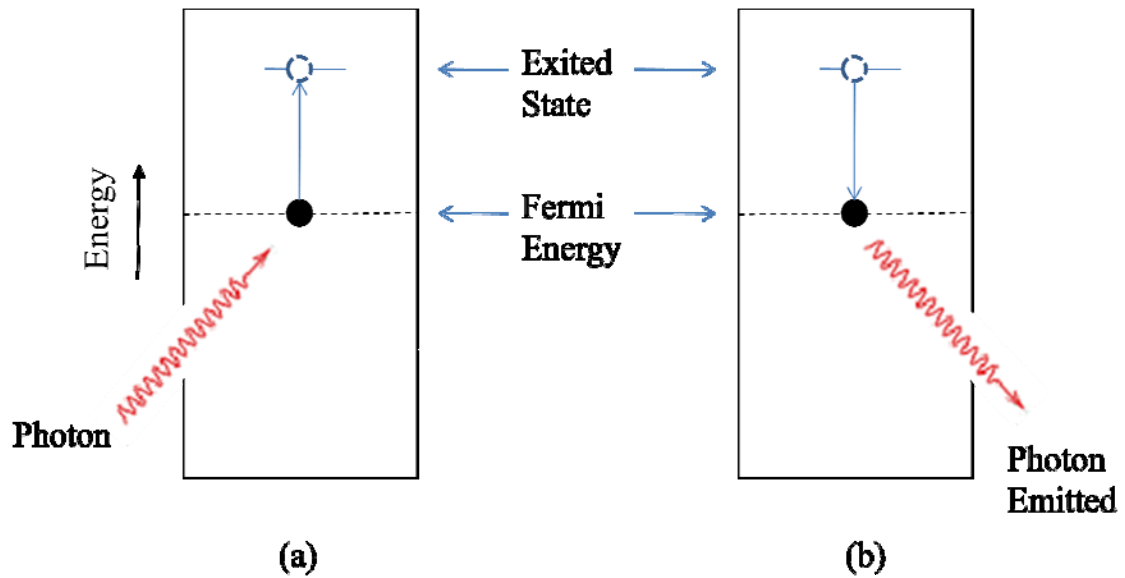


Figure 1.1 (a) Schematic representation of the mechanism of photon absorption for metallic materials in which an electron is excited into a higher-energy unoccupied state. The change in energy of the electron is equal to the energy of the photon. (b) Reemission of a photon of light by the direct transition of an electron from a high to a low energy state (reference 30).

The optical properties of metals can be explained by the Drude model,¹ The complex, frequency-dependent (ω) dielectric constant for metals can be expressed as the following equation.

$$\varepsilon_m(\omega) = \varepsilon_r^f(\omega) + \varepsilon_r^b(\omega) \quad \text{Eq. 1.1}$$

where the first term is associated with free electrons in the conduction band, and the latter is associated with bound electrons (those in filled band) and ions associated with the underlying lattice. To simplify the model, only the contribution from the free electrons is considered. The Drude model describes the dielectric constant of the free electrons, ε_r^f while the Lorentz harmonic-oscillator model describes the equation of motion of a free electron. The combination of these two models yields the dielectric constant of the metal.

$$\varepsilon_m(\omega) = 1 - \frac{\omega_p^2}{\omega^2 + i\Gamma\omega} \quad \text{Eq. 1.2}$$

$$\omega_p = \sqrt{\frac{Ne^2}{m\varepsilon_0}} \quad \text{Eq. 1.3}$$

where ω_p is plasma frequency, Γ is the damping constant, N is the free electron density, e is the electron charge, m is the effective mass of the electron, and ε_0 is the dielectric constant of free space. The damping constant Γ is related to the electron mean free path, l , and the Fermi velocity, v_F .

$$\Gamma = \frac{v_F}{l} \quad \text{Eq. 1.4}$$

When $\omega \ll \omega_p$, $\epsilon_r(\omega)$ is negative and the metals will reflect the incoming electromagnetic waves below the frequency of the applied radiation. When $\omega \gg \omega_p$, $\epsilon_r(\omega)$ is positive and the metals are transparent above the frequency of the applied radiation. Table 1.1 shows the plasma frequency, the damping constants, and the Fermi velocity for copper, silver, and gold.

1.3 Surface plasmon polariton

Excitation of a surface plasmon by a photon is called a surface plasmon polariton or a surface plasmon wave. It is a collective oscillation of electrons or a plasma wave near the surface of a metal, also known as the nonradiative evanescent wave.¹ Figure 1.2 depicts the surface plasmon waves at a metal-dielectric interface. Maxwell's equations consist of four partial differential equations which describe the properties of the electric and magnetic fields under an electromagnetic perturbation. We can use Maxwell's equations to describe the generation of a surface plasmon polariton.^{1,31} Figure 1.2 shows a system with two media, a dielectric and a metal. When light impinges at the interface between the two media, the linear momentum of the light is conserved across the two medium. The derivation of Maxwell's equation leads to a simple relationship between the relative permittivity and the normal components of the wavevectors of the applied field in both media shown in equation 1.5.¹

$$\frac{\epsilon_d}{k_{dz}} = -\frac{\epsilon_m}{k_{mz}} \quad \text{Eq. 1.5}$$

where k_{dz} and k_{mz} are the z-components of the wavevectors of the radiation in a dielectric medium and in a metal respectively.

Table 1.1 The plasma frequency, the damping constants, and the Fermi velocity for copper, silver, and gold.¹

	Copper	Silver	Gold
ω_p (10^{15} s^{-1})	13.4	14.0	13.8
Γ (10^{-15} s)	6.9	31	9.3
v_F (10^8 cm/s)	1.57	1.39	1.39

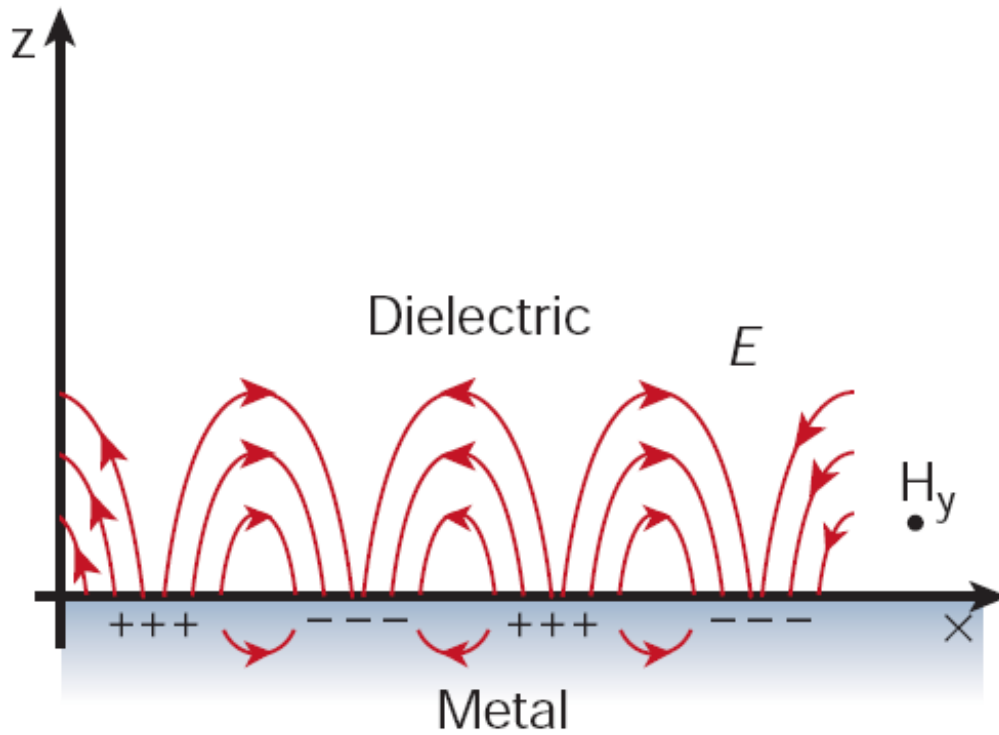


Figure 1.2 Surface plasmon waves at a metal/dielectric interface. The arrows show the electric field lines at the interface. The magnetic field is along y direction. Reproduced with permission from citation 21 Copyright 2006 Annual Reviews.

By satisfying Maxwell's equations with the boundary conditions, the wavevector of the surface plasmon polariton (k_{SPW}) can be related to the wavevector of the radiation (k) and the dielectric constants of dielectric material (ϵ_d) and metal film (ϵ_m) as the following:

$$k_{SPW} = k \sqrt{\frac{\epsilon_d \epsilon_m}{\epsilon_d + \epsilon_m}} \quad \text{Eq. 1.6}$$

From the equation above, the generation of surface plasmon polaritons requires a negative dielectric constant for the metal and $|\epsilon_m| > \epsilon_d$. Metals with a negative dielectric constant include silver, gold, copper and aluminium and of which silver and gold are more commonly used. Silver is used as it provides a sharp SPR resonance peak while gold is used due to its stability.

There are two types of surface plasmon polariton: propagating and localized surface plasmon polariton. The generation of a propagating surface plasmon polariton on the planar surface is discussed in section 1.4 while the generation of a localized surface plasmon polariton is discussed in section 1.5. The properties related to surface plasmon polariton are discussed further in section 1.6 and section 1.7.2.

1.4 Excitation of surface plasmons

The optical excitation of SPs requires matching of the energy and the momentum of the photons to that of plasmons. From equation 1.6, the wavevector of the radiation is always smaller than the wavevector of the SPs at the interface of the metal and the dielectric. This means that we cannot excite SPs by imposing the visible light on a smooth planar surface,³² but a momentum enhancing configuration is required. Figure 1.3

shows the dispersion of surface plasmon polaritons on a planar metal surface at the air interface. The photon line is to the left of the SP dispersion curve at all frequencies and this implies the inability of light to excite SPs at planar metal surface via direct illumination.

There are two other conditions that must be met simultaneously to excite SPs on the planar metal surface besides the metal must have negative value of dielectric constant. First, the incident light must have nonzero z-component wavevectors. Since P-polarized light has the electric field in the plane of incidence and a wavevector normal to the surface, it can excite surface plasmon on the planar surface. Secondly, the momentum of the incident photons has to be increased by a certain surface modification or a certain optical setup. For example, coupling the photons through a higher refractive index medium can increase the momentum of the photons. The wavevector of the light can be increased by a factor of n when the light passes through a medium that has a refractive index value of n . Figure 1.4 shows the early demonstration of prism coupling reported as Otto geometry³³ and Kretschmann-Raether geometry (or Kretschmann geometry).³⁴ In Kretschmann geometry, a glass slide coated with a thin gold film is brought into contact with a high refractive index prism. The surface plasmon polaritons are generated when the light is illuminated on the gold film through the prism at an angle higher than the critical angle for the total internal reflection. Due to the simplicity of Kretschmann configuration, SPR instrumentation using Kretschmann geometry was developed into commercial products such as BIAcore³⁵ and SPReeta.³⁶

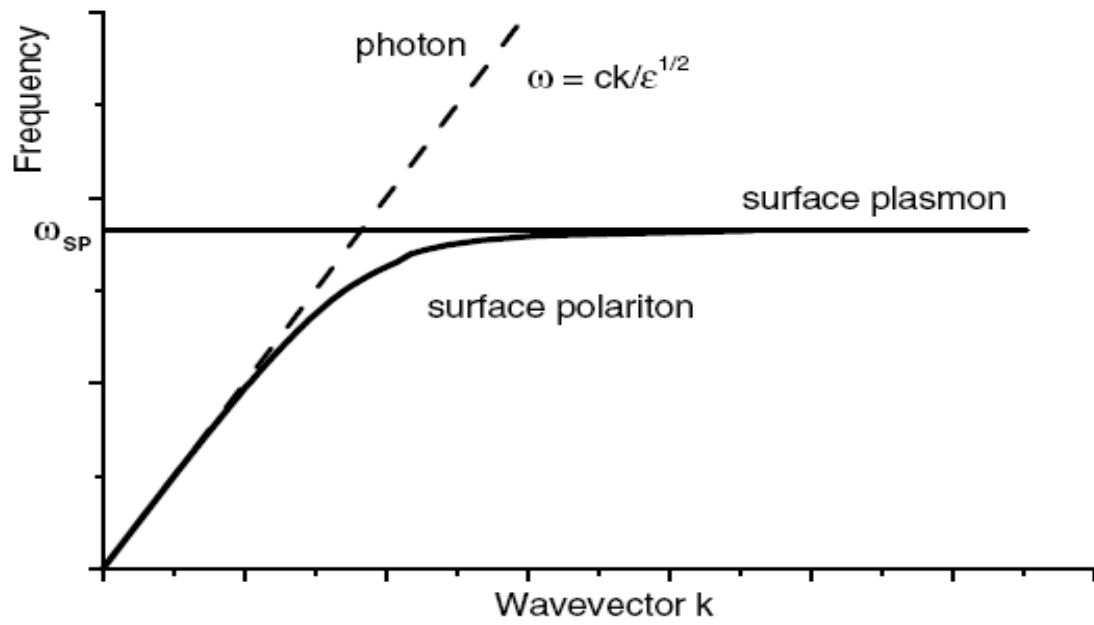


Figure 1.3 The dispersion of surface plasmons at the metal-air interface. Re-drawn from the diagram in reference 1.

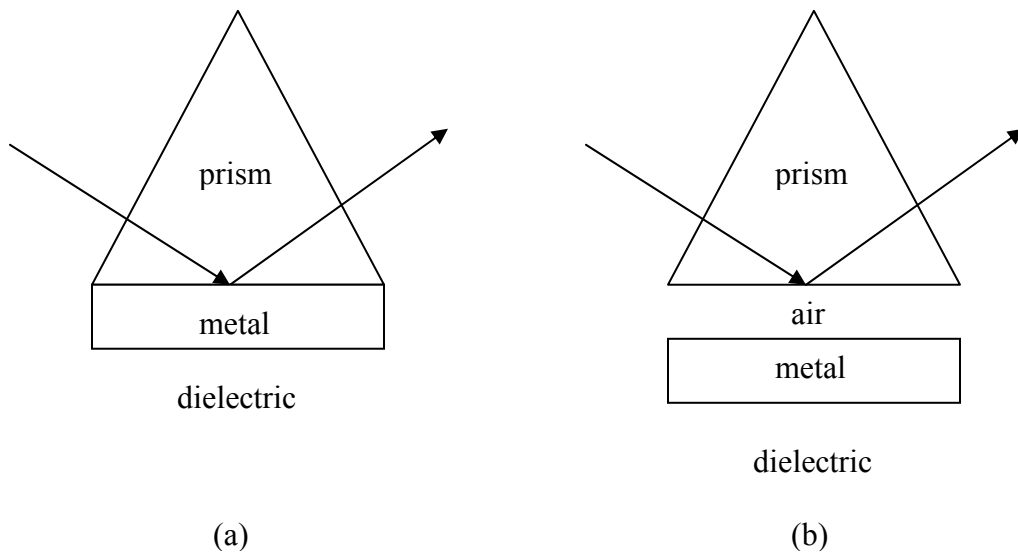


Figure 1.4 (a) Kretschmann and (b) Otto configuration of an attenuated total reflection setup for coupling surface plasmons. (Redrawn from reference 33 and 34).

1.5 Localized surface plasmon resonance

Another method to excite the surface plasmons optically is to use objects which have physical dimensions less than the wavelength of the light such as metallic nanoparticles, nanoscaled island array, and the metallic nanostructures. The evanescent field generated from this method is known as localized surface plasmon resonance (LSPR). The nanoscaled features alter the momentum conservation condition and removes the kinematic constraints imposed on the excitation of surface plasmons on the planar surface. A nanoscaled object such as a metallic nanoparticle can produce localized surface plasmons after being illuminated with light. Once the metallic nanoparticle is irradiated by light, the oscillating electric field causes the conduction electrons to oscillate coherently. This is schematically depicted in Figure 1.5. When the electron cloud is displaced relative to the nuclei, a restoring force arises from Coulomb attraction between electrons and nuclei that results in oscillation of the electron cloud relative to the nuclear framework.

Nanoparticles exhibit unique optical properties. Small colloidal particles of some metals, such as gold, show varied colors in absorption or scattering within visible wavelength range. When the nanoparticles coalesce to form a particle pair, cluster, one-dimensional array or two dimensional array, two remarkable optical phenomenon are observed: (1) an enhanced light scattering and absorption which is sensitive to the external refractive index and (2) a large local electromagnetic field enhancement. The enhanced light scattering or absorption can be exploited to develop chemical and biological sensor in fluorescence, Raman, or IR spectroscopy.

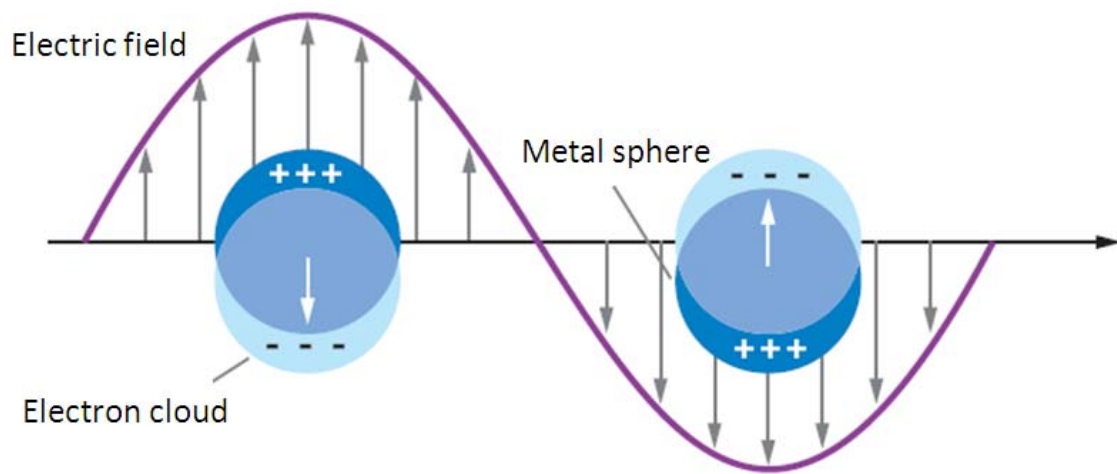


Figure 1.5 The localized surface plasmon. Reproduced with permission from citation 21

Copyright 2007 Annual Reviews.

1.6 Surface plasmon resonance spectroscopy

In principle, surface plasmon resonance spectroscopy (SPR) is like a thin-film refractometer which measures the changes in the refractive index occurring at a metal-dielectric interface. Since the introduction of the BIAcore® SPR instrument,³⁵ SPR has been generally accepted as an effective way to characterize the ultra-thin organic, biopolymer, or biomolecular films. Due to its capabilities in label-free, real time, and ultra-sensitive measurements, biochemists have relied on this technique to characterize biological surfaces and to monitoring the binding interactions between bio-molecules such as antibody-antigen binding,^{37,38} DNA hybridization,³⁹⁻⁴¹ and protein-DNA interactions⁴²⁻⁴⁵ to name a few. Many analytical chemists attempt to develop so-called hyphenated analytical methods where SPR is integrated with other techniques such as electrochemistry,⁴⁶⁻⁴⁸ electrochemical quartz crystal microgravimetry,^{49,50} and mass spectrometry⁵¹⁻⁵³ to increase the specificity of the SPR method.

The most common setup of SPR consists of the prism coupling in the Kretschmann configuration shown in Figure 1.6. Within this experimental setup, there are three distinctive layers. First is the glass prism layer which has the highest refractive index and is used to couple the photons with surface plasmons. Another layer is a thin metal layer (~50 nm thick) deposited in contact with a glass prism. Gold is the most used metal due to its stability although silver gives the best SPR resolution. The third layer is the dielectric layer or sensing layer where SPR is used to probe the changes of refractive

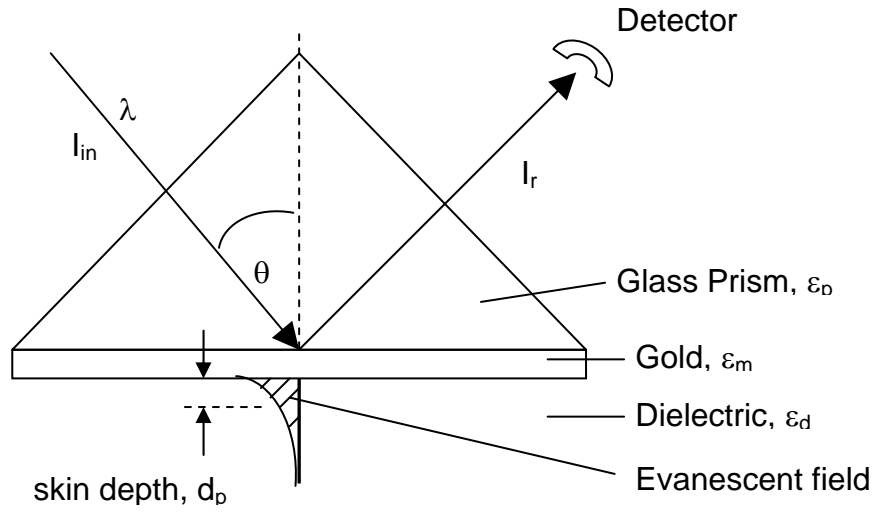


Figure 1.6 Excitation of surface plasmon using the Kretschmann geometry.

index during the experiment. As the light is reflected at the metal-prism interface, the surface plasmons on the gold surfaces were excited, producing the evanescent waves outward to the dielectric layer. During the experiment, the intensity of the reflected light is recorded and is normalized with the intensity of incident light to yield the reflectance or % reflectivity.

1.6.1 Attenuated total reflection and reflectance

As mentioned earlier, the attenuated total reflection (ATR) method with a prism coupler is widely used as an optical method for SP excitation because it is simple and it can enhance the momentum of the incident light by a factor equal to the refractive index of the prism.⁵⁴⁻⁶¹ SPR requirements are fulfilled by using Kretschmann geometry shown in Figure 1.6. To achieve total internal reflection, it is required that light is incident at an incident angle (θ) greater than the critical angle (θ_c). This critical angle can be calculated from the equation shown below.

$$\theta_c = \sin^{-1}\left(\frac{n_m}{n_p}\right) \quad \text{Eq. 1.7}$$

where n_p and n_m are the refractive index of the prism and metal respectively and $n_p > n_m$.

As the light is reflected from the metal surface, the surface plasmons are excited and collectively oscillate along the metal surface, producing evanescent wave or evanescent field. From the solution of Maxwell's equations, the amplitude of evanescent field (\hat{E}) does not fall abruptly to zero at the metal-dielectric interface. Instead, the

evanescent wave produced has amplitude decayed exponentially away from the interface.

$$\hat{E}(z) = \hat{E}_0 \cos(e^{-z/d_p}) \quad \text{Eq. 1.8}$$

$$d_p = \frac{\lambda}{2\pi \sqrt{\sin^2 \theta - \left(\frac{n_m}{n_p}\right)^2}} \quad \text{Eq. 1.9}$$

where \hat{E}_0 is the amplitude of the evanescent field at the interface, z is the distance perpendicular to the surface, d_p is the skin or penetration depth for the electric flux density to decrease by a factor of $e^{-1} = 1/2.7 \sim 1/3$ from \hat{E}_0 , λ is the wavelength of the incident light, and θ is the angle of the incidence in the prism.

In SPR, the intensity of the reflected light is measured as a function of the incident angle. A typical reflectance curve plots the reflectance against the incident angle shown in Figure 1.7. A sharp minimum in the reflectance (or ATR dip) is observed at a particular incident angle as a result of the maximal coupling of the incident light into SPs. This phenomenon is strongly dependent on the refractive indices of all boundary media, including the gold film, the bulk solution close to the gold surface, and the additional layers such as adsorbed molecules on the gold surface. The resonance angle, θ_{spr} , can be determined by the following equation:

$$\theta_{spr} = \sin^{-1} \sqrt{\frac{\epsilon_m \epsilon_d}{\epsilon_p (\epsilon_m + \epsilon_d)}} \quad \text{Eq. 1.10}$$

where ϵ_m , ϵ_d , and ϵ_p are dielectric constant of metal film, dielectric layer, and prism respectively. Most SPR experiments except the electrochemical SPR have a constant

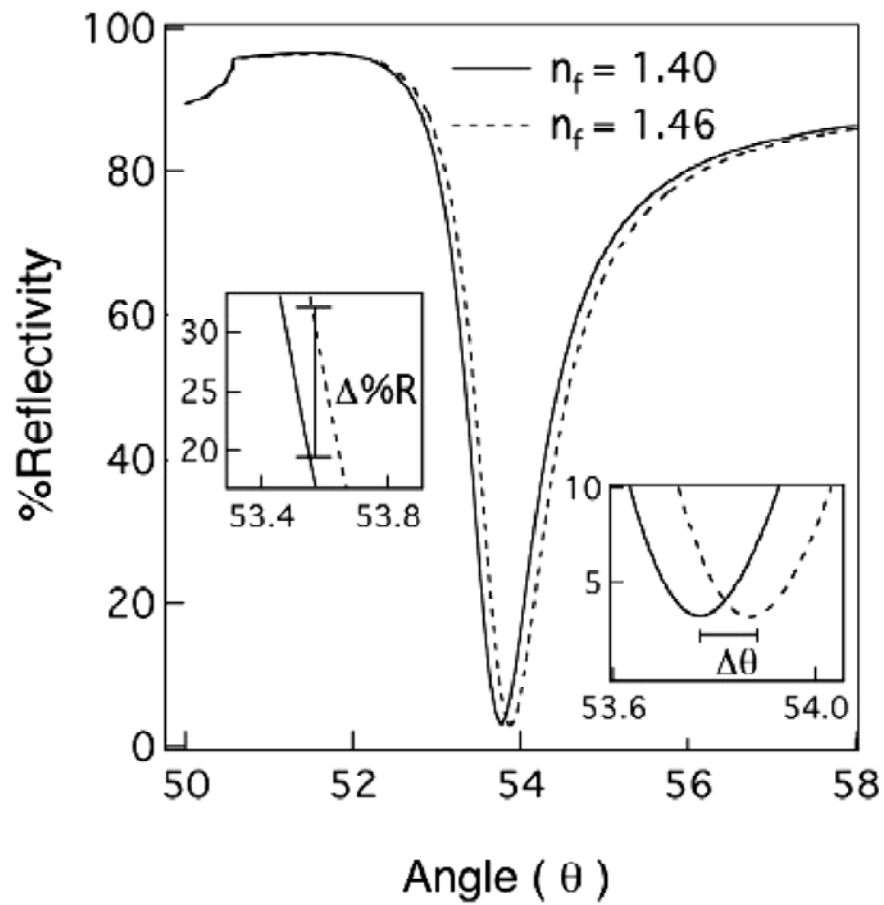


Figure 1.7 The reflectance curve of SPR measurements. Left insert shows the measurement of change in % reflectivity ($\Delta\%R$). Right insert shows the measurement of shift in SPR angle ($\Delta\theta$).⁶⁵

value of θ_m and θ_p . The resonance angle shifts according to the changes in the optical properties of the dielectric layer during the course of the molecular interactions.

The reflectance of the incident light at a given incident angle can be calculated using a three-layer Fresnel equation⁶² where three media, p, m, and s are denoted as prism, metal, and sensing layer respectively. The reflectance R of the incident light varies as a function of the dielectric constant of the three layers, the incident angle, and the wavelength of the incident light. It can be expressed as the following:

$$R = \left| \frac{r_{pm} + r_{md} \exp(2ik_{mz}d)}{1 + r_{pm}r_{md} \exp(2ik_{mz}d)} \right|^2 \quad \text{Eq. 1.11}$$

$$r_{pm} = \frac{k_{pz}\epsilon_m - k_{mz}\epsilon_p}{k_{pz}\epsilon_m + k_{mz}\epsilon_p} \quad \text{Eq. 1.12}$$

$$r_{md} = \frac{k_{mz}\epsilon_d - k_{sz}\epsilon_m}{k_{mz}\epsilon_d + k_{sz}\epsilon_m} \quad \text{Eq. 1.13}$$

$$k_{jz} = \left(\epsilon_j \frac{\omega^2}{c^2} - k_x^2 \right)^{1/2} \quad \text{for } j = p, m, d \quad \text{Eq. 1.14}$$

$$k_x = \sqrt{\epsilon_p} \frac{\omega}{c} \sin\theta \quad \text{Eq. 1.15}$$

where ϵ_j and k_{jz} are the dielectric constant and the wave-vector component perpendicular to the interface in the respective medium j (prism, metal or dielectric), k_x is the component of the incident wave vector parallel to the interface, ω is the angular frequency of the incident light ($\omega(\lambda) = 2\pi c/\lambda$), d is the thickness of the metallic film, and c is the velocity of light. This mathematical model can be used to determine the thickness or the amount of any bound material based on the changes in reflectance from the

dielectric constants of the three layers, the incident angle, and the frequency of the excitation light.

1.6.2 Three modes of SPR measurements

SPR measurements can be conducted in one of the three modes (a) SPR angle shift,⁶³⁻⁶⁶ (b) SPR imaging,⁶⁷⁻⁷⁴ and (c) SPR wavelength shift.⁷⁵⁻⁷⁷ The SPR angle shift is the most widely used technique for an SPR experiment. The reflectivity of monochromatic incident light on a metal is monitored as a function of the incident angle or the reflected angle. In this technique, the entire reflectance curve at each temporal point is measured and the computing algorithm is used to calculate the resonance angle at the inflection point of ATR dip. It has been used as a commercial SPR product such as BIAcore³⁵ and SPReeta.³⁶ Another commonly used technique is the SPR imaging or SPR microscopy. Unlike the SPR angle shift technique, SPR imaging measures the reflectivity at a fixed angle close to the SPR angle, which is obtained from the initial reflectivity curve. As long as the shifts are not too drastic SPR imaging is very effective in monitoring tens, hundreds, or more interactions in a parallel manner. Another alternative method for performing SPR experiment is to measure the reflectivity as a function of wavelength at a fixed incident angle. It has been demonstrated that a Fourier transform spectrometer can be used to perform SPR wavelength shift measurements in the near IR region from 12000 to 6000 cm^{-1} wavenumbers.⁷⁸

1.6.3 SPR based affinity biosensors

Among several experimentally proven concepts of biosensors,⁷⁹⁻⁸¹ the affinity biosensor using SPR is the first commercialized sensor instrument and system.⁸² The SPR affinity biosensors utilize the immobilized biorecognition elements on the gold surface to selectively bind with target molecules in a liquid analyte.^{83,84} When the target molecules captured by the biorecognition elements, the SPR angle shifts due to an increase in the refractive index of the sensing surface. The change in the refractive index varies with the concentration and the dielectric constant of the target molecules. Table 1.2 shows the examples of applications of SPR in biomedical sciences.

The shifts in SPR angle is sometimes reported as resonance unit (RU) which is 0.0001 degree. A response of 1000 RU corresponds to an approximately 1 ng/mm² of the proteins binding to the sensing layer⁸⁵ but this reported sensitivity varies with different instruments used, the dielectric constant of the metal layer, and the type of proteins used in the experiment. With current technology, SPR response can be measured at less than a second per data point. This allows SPR technique to monitor a faster binding kinetic. For example, Zizlsperger & Knoll⁸⁶ used SPR microscopy combined with an image analysis software to measure the binding of streptavidin to the surface-immobilized biotinylated alkanethiols. The time resolution depends on the transfer time of the camera and framegrabber card used in the experiment; resolutions from ~600 to 1000 ms have been reported.⁸⁸ However, the SPR has limited the applications for detecting the analyte containing 1-10 nM of 20 kDa target protein.⁸⁷

1.6.4 Electrochemical SPR

In section 1.6.1, we learned that the resonance angle varies with the complex dielectric constant of the metal film as well as the dielectric properties of the media adjacent to the metal surface. In the electrochemical SPR experiment, the thin gold film serves two functions. One function is for supporting the propagation of the surface plasmons while the other is for conducting electricity as an electrode. Using the SPR to study the effects of the electric potential on the composition of the Helmholtz double layer, the electron density of the metal surface, and faradaic processes on the metal surface has been discussed in the literature.¹⁰⁵⁻¹¹⁰

Electrochemical SPR has been exploited to gain further understanding of the electrochemical processes on the electrode surface.¹¹¹ Chao, et al.¹¹² used SPR and ellipsometry to study the electrochemistry of gold in sulfuric acid. Kötzt, et al.¹¹³ used the Kretschmann configuration to investigate the effects of the electrode potential in the double layer region on the surface plasmon resonance frequency for gold and silver electrodes in perchlorate solution. EC-SPR has been used to study electrode reactions at gold surfaces¹¹⁴⁻¹¹⁶ and to study the conductive polymers^{117,118} and adsorption of alkane thiol monolayers¹¹⁹ at electrode surfaces. Schuessler, et al. suggested that measuring the SPR signals with a potential perturbation shows good spatial and temporal resolution in various bioscience applications^{120,121} such that SPR is capable of detecting changes in the bulk conformational states and the respective dielectric constants.

Table 1.2 Examples of applications of SPR in biomedical sciences

Applications	References
Nuclear receptor-DNA interaction	88
Immunoreactivity of antibody conjugates	89
Peptide-antibody interactions	90
Enzymatic turnover	91
DNA hybridization	39-41
Detection of polymerase chain reaction products	92
Characterization of proteins by epitope mapping with monoclonal antibody	93
Quantitative immunoassays	94-96
Quantitative receptor assays	97
Drug absorption extrapolation	98
Drug-protein interactions	99
Analysis of structure-function relationship of proteins and ligands	101
Analysis of antibody-antigen interactions	102-103
Quantitative structure-activity relationship	104

1.7 Surface enhanced Raman spectroscopy

After the first observation of surface enhanced Raman spectroscopy¹²² (SERS) in 1974, SERS has recently been the subject of renewed interest,^{123,124} motivated in part by the ultra sensitivity in detecting single molecules.^{125,126} Each year the number of SERS publications increase as the nanoscaled material fabrication technique advances and the importance of the trace analysis increases. There are excellent reviews of SERS.^{127,128} A recent Faraday Discussion on SERS¹²⁹ is reflective of the breadth of modern SERS research. One must understand the principles of the Raman spectroscopy before the comprehension of SERS principles.

1.7.1 Raman spectroscopy

Since its discovery in 1928 by Sir. C. V. Raman,¹³⁰ Raman spectroscopy has been a very powerful characterization tool in a variety of fields such as materials science, biology, chemistry, physics and forensic science.¹³¹⁻¹³³ The Raman effect results from the interaction of vibrational motions of molecules with an electromagnetic wave, providing unique spectral fingerprint of vibrations in the molecules. When a sample is irradiated with an intense beam of light, two types of scattering are observed: (a) Rayleigh scattering and (b) Raman scattering. Rayleigh scattering is intense and has the same frequency as the incident beam, whereas Raman scattering is very weak and has the frequency shifted from the incident frequency. Raman scattering can be explained by using the classical theory for the interaction of the molecule with electromagnetic radiation¹³⁴ or by the quantum theory which relates scattering frequencies and intensities to the vibrational and the electronic energy states of the molecule.¹³⁵

In the classical theory, the interaction of the molecule with electromagnetic radiation gives rise to infrared absorption and Raman scattering.¹³⁶ The interpretation of the optical response mentioned can be explained by using the basic models of the rigid rotator and harmonic oscillator in Herzberg's book (Chapter III, p. 66).¹³⁷ Electromagnetic radiation with an oscillating electric field can induce a change in the dipole moment of the molecule. The induced polarization μ is proportional to the strength of the electric field, \mathbf{E} as given in the equation

$$\mu = \alpha E \quad \text{Eq. 1.16}$$

where the proportionality, α , corresponds to the polarizability of the molecule. The polarizability reflects the ease to distort the electron cloud of a molecule susceptible to an electromagnetic radiation. The electromagnetic radiation can be simply described by the following equation

$$E = E_0 \cos(2\pi\nu_l t) \quad \text{Eq. 1.17}$$

where E_0 is the electric field strength and ν_l is the radiation frequency. Molecular vibrations compose of normal modes, Q_j expressed as

$$Q_j = Q_{j0} \cos(2\pi\nu_j t) \quad \text{Eq. 1.18}$$

where Q_{j0} is normal coordinate amplitude and ν_j is the angular frequency of molecular vibrational mode j . During the molecular vibration, the polarizability varies with the conformation of the molecule and the amplitude of the polarizability can be summed with all the possible vibration modes as

$$\alpha = \alpha_0 + \left[\frac{\partial \alpha}{\partial Q_j} \right] \cdot Q_j + \dots \quad \text{Eq. 1.19}$$

When a molecule interacts with the electromagnetic field of the radiation, equation 1.16 becomes

$$\mu = \alpha E = \alpha E_0 \cos(2\pi\nu_l t) \quad \text{Eq. 1.20}$$

Substituting equation 1.18 and 1.19 into 1.20 yields

$$\mu = \alpha_0 E_0 \cos(\omega_l t) + \left[\frac{\partial \alpha}{\partial Q_j} \right] \cdot E_0 \cos(2\pi\nu_l t) Q_{j0} \cos(2\pi\nu_j t) + \dots$$

Eq. 1.21

Using the trigonometric identity,

$$\cos A \cdot \cos B = \frac{1}{2} [\cos(A + B) + \cos(A - B)] \quad \text{Eq. 1.22}$$

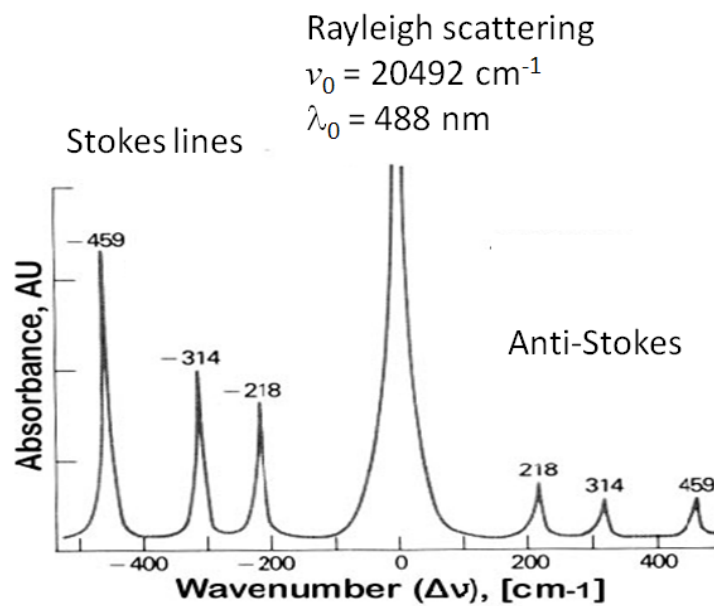
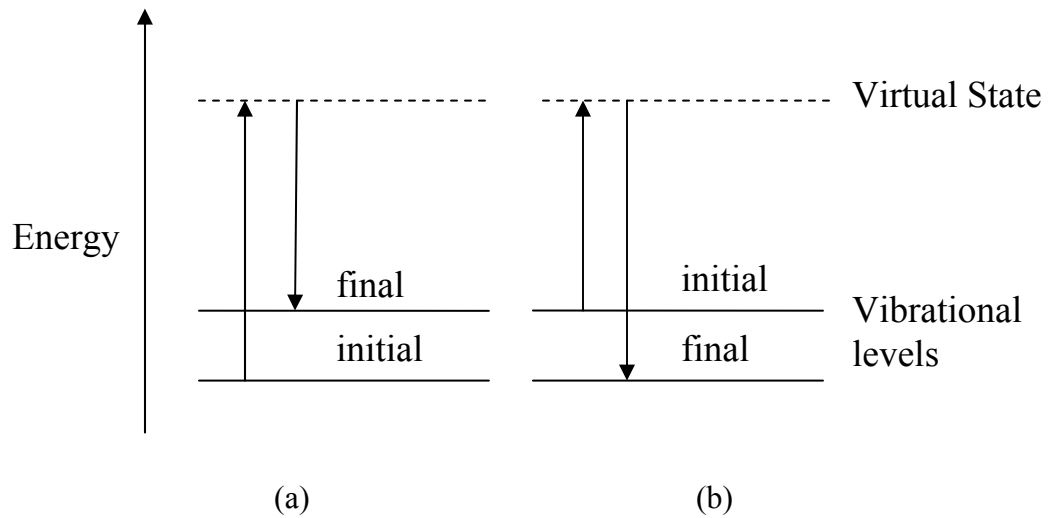
the induced dipole expression is derived as

$$\mu = \alpha_0 E_0 \cos(2\pi\nu_l t) + \frac{1}{2} \left[\frac{\partial \alpha}{\partial Q_j} \right] \cdot E_0 Q_{j0} \cos 2\pi(\nu_l + \nu_j) t +$$

$$\frac{1}{2} \left[\frac{\partial \alpha}{\partial Q_j} \right] \cdot E_0 Q_{j0} \cos 2\pi(\nu_l - \nu_j) t + \dots \quad \text{Eq. 1.23}$$

The first term in the equation 1.23 will account for the Rayleigh scattering. The second and third terms in the equation 1.23 consist of a frequency shift due to the molecular vibration and they are called anti-Stokes scattering and Stokes scattering respectively.

The quantum theory of Raman spectroscopy is depicted by Figure 1.8. When a molecule in a low quantized energy state absorbs the energy from the radiation and is excited to a higher quantized state, the excited molecule decays back to an alternate lower state by re-emitting the light having a frequency different from the incident light. If the re-emitted frequency is lower than the radiation frequency, this refers to Stokes scattering shown in Figure 1.8(a) and vice versa for anti-Stokes scattering in Figure 1.8(b). Since most of the molecules under standard conditions are in the lowest-lying quantized energy



(c)

Figure 1.8 Quantum theory for (a) the Stokes and (b) anti-Stokes scattering. The arrow lines indicate the electron transition. (c) Raman spectra of CCl_4 showing Rayleigh, Stokes and anti-Stokes scattering.¹³⁸

state, the Stokes scattering occurs more frequently than the anti-Stokes scattering. As a result, the intensity of Stokes signals is always higher than the anti-Stokes scattering, illustrated by the Raman spectra of CCl_4 in Figure 1.8(c). The Stokes signals are most often used for measuring Raman shift and it has a unit of cm^{-1} . The Stokes intensity for a particular mode is proportional to the fourth order of radiation frequency¹³⁹ and is a function of polarizability shown as equation 1.24.

$$I_{Stokes} \sim (\nu_l - \nu_j)^4 \left[\frac{\partial \alpha}{\partial Q_j} \right]^2 \cdot I_0 \quad \text{Eq. 1.24}$$

The equation shows that higher Raman signal can be produced from higher radiation frequency and larger change in the polarizability.

The polarizability of the molecule depends on the vibration mode of different molecular bonds and the surface plasmon assisted enhancement. The Raman signals from a highly polar moiety, such as the O-H bonds in water, are usually weak. An external electric field cannot induce a large change in the polarizability of the O-H bond. Therefore, Raman spectroscopy is insensitive to water, herein makes Raman spectroscopy or SERS an excellent fingerprinting technique for the unknown in an aqueous solution. Strong Raman scattering is often observed from the moieties with distributed electron clouds, such as carbon-carbon double bonds due to the fact that the pi-electron cloud of the double bond can be easily distorted through bending or stretching mode by the electric field of radiation.

1.7.2 Surface enhanced Raman spectroscopy

Surface enhanced Raman spectroscopy was first observed by Fleischmann and coworkers¹²⁴ in 1974 when they found Raman spectra for pyridine adsorbed on a roughened silver electrode has an intensity a million fold more intense than the normal Raman counterpart. At first the observed SERS signal was attributed to the increase in surface area when the silver electrode was roughened.¹²⁴ However, two research groups, Jeanmarie and Van Duyne¹³⁹ and Albrecht and Creighton,¹⁴⁰ recognized that the electrode roughening process could increase the signal only up to one magnitude higher. They postulated that the origins of the enhancement related to the strength of the local electromagnetic field.¹³⁹ It is now generally accepted that the enhancement of Raman spectra on a roughened silver surface comes from two major contributions: an electromagnetic (EM) enhancement¹²⁵ and a chemical enhancement (or more precisely charge transfer enhancement).¹⁴¹ The electromagnetic enhancement arises from the localized surface plasmons (discussed in section 1.5) while the chemical enhancement arises from chemisorption of the adsorbate on the metal surface. The electromagnetic enhancement accounts for 10^5 - 10^6 of enhancement and the chemical enhancement only accounts for 10^2 of enhancement.¹⁴²

The basis of EM enhancement is the capacity of metallic nanoparticles or nano-size structured metallic substrates to support the localized surface plasmons with resonant frequencies in the visible region of the electromagnetic spectrum.¹⁴³⁻¹⁴⁵ When a small spherical metallic nanoparticle is irradiated with a light, the oscillating electric field causes the conduction electrons to oscillate coherently. This is schematically pictured in Figure 1.5. When the electron cloud is displaced relative to the nuclei, a restoring force

arises from Coulomb attraction between electrons and nuclei that results in oscillation of the electron cloud relative to the nuclear framework. The oscillation frequency is determined by four factors: the density of electrons, the effective electron mass, and the shape and size of the charge distribution. The collective oscillation of the electrons is called the localized surface plasmon resonance to distinguish from propagating surface plasmon on the planar metal surface. These localized surface plasmons enhance the native Raman signal by producing an increased electric field in the vicinity of the target molecules.^{146,147}

The nature of the metal surface plays an important role in the surface enhancement. The surface morphology and the shape of the roughness features at the metal surface can interact with photons and “store the electromagnetic energy into the surface plasmons”.¹²⁵ Noble metal particles in the 10-200 nm size range tend to generate LSPR which results in amplification of the electric field E near the particle surfaces such that the $|E|^2$ can be 10^2 - 10^4 times greater in intensity than the incident field.¹⁴⁸

Over the years, several different techniques have been developed to fabricate noble metal SERS substrates. The substrates involved with the easiest and most accessible fabrication techniques are nanoparticles with different shapes, metal colloidal films,^{149,150} and electrochemically roughened silver electrodes,^{151,152}. However, limitations in these techniques include the complexity of these irregular surfaces, the variation from one experiment to another, and the heterogeneity of the surface, which escalate the task in elucidating details in the mechanisms of SERS. Recent literature has reported the possibility in preparing the metal particles with tunable shapes and sizes using chemical reactions in solution wet chemistry such as rods,¹⁵³⁻¹⁵⁵ cubes,^{156,157} triangles,¹⁵⁸

nanorings,¹⁵⁹ nanoshells,¹⁶⁰ and disks.¹⁶¹ Another method to prepare more uniform and controllable SERS substrates is the metal film over nanospheres (FONS) and nanosphere lithography.¹⁶² However, the best way to fabricate SERS substrate is using microfabrication techniques such as electron beam lithography (EBL) with reactive ion etching, which allow for the precise control of the periodic structure, shape, and spacing.¹⁶³⁻¹⁶⁵ But one disadvantage of EBL technique is associated with high preparation cost and scale-up issues.

Progressing with the development of the plasmonic nanostructures, systematic investigations on the role of localized plasmon resonances in the magnitude of the EM enhancement have been reported.^{166,167} As mentioned earlier, the evanescent wave near the metal surface contributes to the significantly enhanced near field intensity compared to the incident light. If E_0 denotes an incident plane wave, the local field (E_L) in the vicinity of a metal surface can be modeled as $E_L = g E_0$. If the incident light has wavelength close to an LSP resonance, the amplitude enhancement factor, g , can be considerably greater than unity in certain regions of a SERS substrate. It varies with the frequency-dependent dielectric constant of the nanoparticle, the dielectric constant of the medium, and the excitation frequencies.¹⁶⁸ For a single silver nanoparticle, the value of g has been calculated¹⁶⁸ to be on the order of 10–100 without considering the enhancement effect from particle aggregation.

Since evanescent fields decay exponentially away from the surface, Whitney, et al.¹⁶⁹ and Carron, et al.¹⁷⁰ conducted separate experiments to probe the distance dependence of SERS. Figure 1.9 shows the SERS spectra of pyridine spaced from the metal surface by alumina layers of variable thickness. The spectrum is most enhanced

when the particle is directly adsorbed to the metal surface. As the thickness of the alumina spacer increases, the intensity of the SERS spectra decreases and the intensity can be modeled by the equation shown below.^{169,170}

$$I = \left(1 + \frac{r}{a}\right)^{-10} \quad \text{Eq. 1.25}$$

where I is the Raman intensity, a is the size of the enhancing nanoparticle feature, and r is the distance from the surface to the adsorbate. The best fit line to equation 1.25 is shown in Figure 1.9 and yields a value of $a = 12.0$ nm.

1.8 Conclusions

This chapter has attempted to elaborate the basic principles of the surface plasmon resonance and to discuss the sensing applications of SPR particularly in surface plasmon resonance spectroscopy and in surface enhanced Raman spectroscopy. Surface plasmon resonance occurs when the light is reflected on the metal surface under the total reflectance geometry. The electrons on the metal surface interact with the incident photons, creating an electromagnetic field normal to the surface or an evanescent wave at the interface between the dielectric and the metal. The evanescence wave can be either propagating or localized on the metal surface depending on the size of the metal surface. Both types of the evanescent wave contributing different ways of signal transduction for the sensing applications.

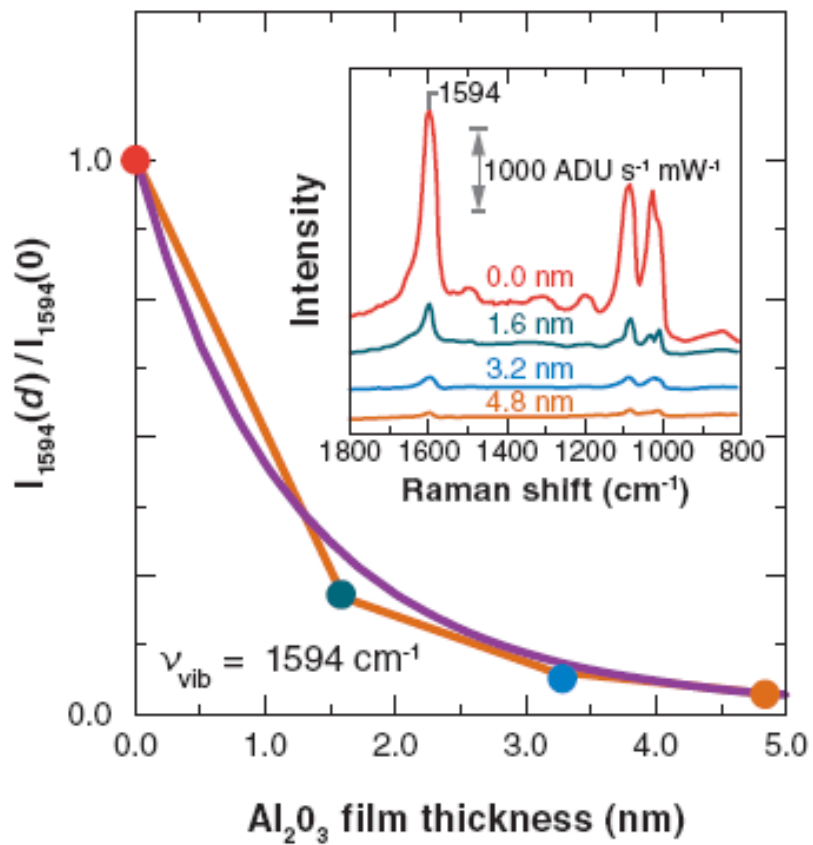


Figure 1.9 Distance dependence of SERS. Plot of normalized surface-enhanced Raman scattering (SERS) intensity as a function of alumina thickness for the 1594 cm^{-1} band of pyridine. Insert is SERS spectra from which the normalized SERS intensity is calculated. Reproduced with permission from citation 170 Copyright 1999 American Chemical Society.

Surface plasmon resonance spectroscopy is based on a sharp decrease in the reflected light intensity at the resonance conditions. From the mathematical model, SPR angle varies with the radiation frequency and the dielectric constants of the prism, the metal, and the dielectric layer. Since the dielectric constant of the prism and the metal remain constant in a typical SPR experiment, the shift in SPR angle corresponds to the change in the dielectric constant of the dielectric at the metal-dielectric interface. Due to this unique property, SPR has been used to characterize the formation of thin films, to evaluate the biocompatibility of the biomaterials, to study the biomolecular interactions, and to carry out chemical sensing. A variety of electrochemical processes have been studied using the electrochemical SPR to gain further understanding on the electrochemical processes at the electrode surface. They provide invaluable information for analyzing the data in this dissertation.

Surface enhanced Raman spectroscopy is based on the localized enhanced electromagnetic field produced from the evanescent wave on the metallic nanostructures or metallic nano-objects. Raman effects are the inelastic scattering of the light by a molecule, observed as Stokes scattering and anti-Stokes scattering. The Stokes signals are most often used for measuring the Raman shift because they have higher intensity than the anti-Stokes scattering. SERS uses the nanoscaled metallic surface to create a localized surface plasmon wave, which is responsible for the enhancement in Raman signal. The enhancement factor can be sixth order of magnitude higher than the normal Raman. Since the Raman spectra can provide the fingerprint of the molecule, SERS is ultra sensitive for chemical sensing.

1.9 References

- [1] Reather, H. Surface Plasmons on Smooth and Rough Surfaces and on Grating, Springer Tracts Modern Physics 111 (Springer, Berlin, Heidelberg 1988).
- [2] Agranovich, V. M.; Mills D. L. (Eds.), Surface Polaritons, Modern Problems in Condensed Matter Sciences (North-Holland, Amsterdam 1982).
- [3] Nylander, C.; Liedberg, B.; Lind, T. *Sens. and Actuators* **1982**, *3*, 79-88.
- [4] Liedberg, B.; Nylander, C.; Lundstrom, I. *Sens. and Actuators* **1983**, *4*, 299-304.
- [5] Homola, J. *Anal. Bioanal. Chem.* **2003**, *377*, 528–539.
- [6] Homola, J. (Eds) *Surface Plasmon Resonance Based Sensors, Springer Series on Chemical Sensors and Biosensors, Volume 4* (Springer-Verlag, Berlin, Heidelberg 2006).
- [7] Nishimura, T.; Hifumi, E.; Fujii, T.; Niimi, Y.; Egashira, N.; Shimizu, K.; Uda, T. *Electrochemistry* **2000**, *68*, 916–919.
- [8] Mullett, W. M.; Lai, E. P. C.; Yeung, J. M. *Methods* **2000**, *22*, 77–91.
- [9] Hsieh, H. V.; Stewart, B.; Hauer, P.; Haaland, P.; Campbell, R. *Vaccine* **1998**, *16*, 997–1003. [10] Oda, Y.; Owa, T.; Sato, T.; Boucher, B.; Daniels, S.; Yamanaka, H.; Shinohara, Y.; Yokoi, A.; Kuromitsu, J.; Nagasu, T. *Anal. Chem.* **2003**, *75*, 2159–2165.
- [11] Wilkinson, F. L.; Holaska, J. M.; Zhang, Z. Y.; Sharma, A.; Manilal, S.; Holt, I.; Stamm, S.; Wilson, K. L.; Morris, G. E. *Eur. J. Biochem.* **2003**, *270*, 2459–2466.
- [12] Rich, R. L.; Day, Y. S. N.; Morton, T. A.; Myszka, D. G. *Anal. Biochem.* **2001**, *296*, 197–207.
- [13] Baird, C. L.; Courtenay, E. S.; Myszka, D. G. *Anal. Biochem.* **2002**, *310*, 93–99.
- [14] Nilsson, P.; Persson, B.; Uhlen, M.; Nygren, P. A. *Anal. Biochem.* **1995**, *224*, 400–408.

- [15] Peterlinz, K. A.; Georgiadis, R. M.; Herne, T. M.; Tarlov, M. J. *J. Am. Chem. Soc.* **1997**, *119*, 3401–3402.
- [16] Gotoh, M.; Hasebe, M.; Ohira, T.; Hasegawa, Y.; Shinohara, Y.; Sota, H.; Nakao, J.; Tosu, M. *Genet. Anal.-Biomol. Eng.* **1997**, *14*, 47–50.
- [17] Silin, V.; Plant, A. *Trends Biotechnol.* **1997**, *15*, 353–359.
- [18] Green, R. J.; Frazier, R. A.; Shakesheff, K. M.; Davies, M. C.; Roberts, C. J.; Tendler, S. J. B. *Biomaterials* **2000**, *21*, 1823–1835.
- [19] Lechuga, L. M.; Calle, A.; Prieto, F. *Quim. Anal.* **2000**, *19*, 54–60.
- [20] Homola, J.; Koudela, I.; Yee, S. S. *Sens. Actuators, B* **1999**, *54*, 16–24.
- [21] Willets, K. A.; Van Duyne, R. P. *Annual Rev. of Phys. Chem.* **2007**, *58*, 267–297.
- [22] Kneipp, K.; Wang, Y.; Kneipp, H.; Perelman, L. T.; Itzkan, I. *Phys. Rev. Lett.* **1997**, *78*, 1667–1670.
- [23] Nie, S. M.; Emory, S. R. *Science* **1997**, *275*, 1102–1106.
- [24] Jeanmaire, D. L.; Van Duyne, R. P. *J. Electroanal. Chem.* **1977**, *84*, 1
- [25] Geddes, C. D.; Aslan, K.; Gryczynski, I.; Malicka, J.; Lakowicz, J. R. *Rev. Fluoresc.* **2004**, *1*, 365–401
- [26] Goulet, P. J.; Aroca, R. F. *Top. Fluoresc. Spectrosc.* **2005**, *8*, 223–247.
- [27] Liu, Z.; Steele, J. M.; Lee, H.; Zhang, X. *Appl. Phys. Lett.* **2006**, *88*, 171108.
- [28] Sherry, L. J.; Jin, R.; Mirkin, C. A.; Schatz, G. C.; Van Duyne, R. P. *Nano Lett.* **2006**, *6*, 2060.
- [29] Chang, S. –H.; Gray, S. K.; Schatz, G. C. *Opt. Express* **2005**, *13*, 3150.
- [30] Callister, W. D. *Fundamentals of Materials Science and Engineering: An Integrated Approach*, 7th ed. (Wiley and Sons, New York 2007)

- [31] Sambles, J. R.; Bradbery, G. W.; Yang, F. *Comtemp. Phys.* **1991**, 32, 3, 173-183.
- [32] Hanken, D. G.; Jordan, C. E.; Frey, B. L.; Corn, R. M. *Electroanal. Chem.* **1998**, 20, 141-225.
- [33] Otto, A. *Z. Phys.* **1968**, 216, 398-410.
- [34] Kretschmann, E. *Opt. Commun.* **1972**, 6, 185-187.
- [35] Biacore website www.biacore.com
- [36] Soelberg, S. D.; Chinowsky, T.; Geiss, G.; Spinelli, C. B.; Stevens, R.; Near, S.; Kauffman, P.; Yee, Y.; Furlong, C. E. *J Ind. Microbiol. Biotechnol.* **2005**, 32, 669-674.
- [37] Rahn, J. R.; Hallock, R. B. *Langmuir* **1995**, 11, 650-654.
- [38] Brynda, E.; Homola, J.; Houska, M.; Pfeifer, P.; Skvor, J. *Sens. Actuators B* **1999**, 54, 132-136.
- [39] Nilsson, P.; Persson, B.; Uhlen, M.; Nygren, P. A. *Anal. Biochem.* **1995**, 224, 400-408
- [40] Bates, P.J.; Dosanjh, H.S.; Kumar, S.; Jenkins, T.C.; Laughton, C.A.; Neidle, S. *Nucleic Acids Res.* **1995**, 23, 3627-3632.
- [41] Peterlinz, K.A.; Georgiadis, R.M.; Herne, T.M.; Tarlov, M.J. *J. Am. Chem. Soc.* **1997**, 119, 3401-3402.
- [42] Babic, I.; Andrew, S. E.; Jirik, F.R. *Mutat. Res.* **1996**, 372, 87-96.
- [43] Bondeson, K.; Frostell-Karlsson, A.; Fagerstam, L.; Magnusson, G. *Anal. Biochem.* **1993**, 214, 245-251.
- [44] Fisher, R.J.; Fivash, M.; Casas-Finet, J.; Bladen, S.; McNitt, K.L. *Methods Companion Methods Enzymol.* **1994**, 6, 121-133.

- [45] Gotoh, M.; Hasebe, M.; Ohira, T.; Hasegawa, Y.; Shinohara, Y. *Genet. Anal. Biomol. Eng.* **1997**, *14*, 47–50.
- [46] Jory, M. J.; Bradberry, G. W.; Chann, P.S.; Sambles, J. R. *Sens. and Actuators B* **1996**, *35-36*, 197-201.
- [47] Kang, X.; Cheng, G.; Dong, S. *Electrochem. Comm.* **2001**, *3*, 489-493.
- [48] Zhang, N.; Schweiss, R.; Zong, Y.; Knoll, W. *Electrochimica Acta* **2007**, *52*, 2869-2875.
- [49] Bund, A.; Baba, A.; Berg, S.; Johannsmann, D.; Lubben, J.; Wang, Z.; Knoll, W. *J. Phys. Chem. B* **2003**, *107*, 28, 6743 – 6747.
- [50] **Su, X.; Wu, Y.-J.; Knoll, W.** *Biosensors and Bioelectronics* **2005**, *21* (5), 719-726
- [51] Nelson, R.W.; Krone, J.R.; Jansson, O. *Anal. Chem.* **1997**, *69*, *21*, 4363-4368
- [52] Williams, C. and Addona, T.A. *Trends Biotechnol.* **2000**, *18*, 45–48
- [53] Nedelkov, D.; Nelson, R. *Trends Biotechnol.* **2003**, *21*, 301-305
- [54] Agranovich V. M.; Mills, D. L. eds., *Surface Polaritons* (North-Holland, Amsterdam 1982).
- [55] Boardman, A.D. ed., *Electromagnetic Surface Modes* (Wiley, New York 1982).
- [56] S. Kawata, ed., *Near-Field Optics and Surface Plasmon Polaritons* (Springer-Verlag, Berlin, Heidelberg 2001).
- [57] W. L. Barnes, A. Dereux, and T. W. Ebbesen, *Nature* **2003**, *424*, 824–830.
- [58] H. Raether, *Excitation of Plasmons and Interband Transitions by Electrons* (Springer-Verlag, Berlin, Heidelberg 1980).
- [59] Otto, A. *Z. Phys.* **1968**, *216*, 398–410.
- [60] Kretschmann, E.; Raether, H. *Z. Naturforsch. A* **1968**, *23*, 2135–2136.

- [61] Otto, A. "Spectroscopy of surface polaritons by attenuated total reflection," in *Optical Properties of Solids, New Developments*, B. O. Seraphin, ed. (North-Holland, 1976), pp. 677–727.
- [62] Kurihara, K.; Suzuki, K. *Anal. Chem.* **2002**, *74*, 696-701.
- [63] Lyon, L. A.; Musick, M. D.; Natan, M. J. *Anal. Chem.* **1998**, *70*, 5177.
- [64] Advincula, R.; Aust, E.; Meyer, W.; Knoll, W. *Langmuir* **1996**, *12*, 3536.
- [65] Hanken, D. G.; Jordan, C. E.; Frey, B. L.; Corn, R. M. *Surface Plasmon Resonance Measurements of Ultrathin Organic Films at Electrode Surfaces* vol. 20. (Marcel Dekker, New York 1996)
- [66] Jordan, C.E.; Frey, B. L.; Kornguth, F. R.; Corn, R. M. *Langmuir* **1994**, *10*, 3642.
- [67] Frutos, A. G.; Weibel, S. C.; Corn, R. M. *Anal. Chem.* **1999**, *71*, 3935.
- [68] Hickel, W.; Kamp, D.; Knoll, W. *Nature* **1989**, *339*, 186.
- [69] Piscevic, D.; Knoll, W.; Tarlov, M. J. *Supramol. Sci.* **1995**, *2*, 99.
- [70] Rothenhausler, B.; Knoll, W. *Nature* **1988**, *332*, 615.
- [71] Lyon, L. A.; Holliway, W. D.; Natan, M. J. *Rev. Sci. Instrum.* **1999**, *70*, 2076.
- [72] Jordan, C. E.; Frutos, A. G.; Thiel, A. J.; Corn, R. M. *Anal. Chem.* **1997**, *69*, 4939.
- [73] Brockman, J. M.; Nelson, B. P.; Corn, R. M. *Annu. Rev. Phys. Chem.* **2000**, *51*, 41.
- [74] Smith, E. A.; Erickson, M. G.; Ulijasz, A. T.; Weisblum, B.; Corn, R. M. *Langmuir* **2003**, *19*, 1486.
- [75] Hickel, W.; Kamp, D.; Knoll, W. *Nature* **1989**, *339*, 186.
- [76] Zhang, L. M.; Dttamchandani, D. *Electron. Lett.* **1988**, *23*, 1469-1470.
- [77] Jorgenson, R. C.; Yee, S. S. *Sens. and Actuators* **1993**, *B12*, 213-220.
- [78] Frutos, A. G.; Weibel, S. C.; Corn, R. M. *Anal. Chem.* **1999**, *71*, 3935–3940

- [79] Englebienne, P. *Immune and Receptor Assays in Theory and Practice* (CRC Press, Florida 2000).
- [80] Hill, H.O.A.; Davis, J.J. *Biochem. Soc. Trans.* **1999**, *27*, 331–335.
- [81] Haupt, K.; Mosbach, K. *Biochem. Soc. Trans.* **1999**, *27*, 344–350.
- [82] Englebienne, P.; Van Hoonacker, A.; Verhas, M. *Spectroscopy* **2003**, *17*, 255–273.
- [83] Lahiri, J.; Isaacs, L.; Tien, J.; Whitesides, G. M. *Anal. Chem.* **1999**, *71*, 777–790.
- [84] Yoshida, T.; Sato, M.; Ozawa, T.; Umezawa, Y. *Anal. Chem.* **2000**, *72*, 6–11.
- [85] Wilson, W. D. *Science* **2002**, *295*, 2103–2105.
- [86] Zizlsperger, M.; Knoll, W. *Progr. Colloid Polym. Sci.* **1998**, *109*, 244–253
- [87] Wink, T.; van Zuilen, S. J.; Bult, A.; van Bennekom, W, P. *Anal. Chem.* **1998**, *70*, 827–832.
- [88] Cheskis B.; Freedman, L. P. *Biochem.* **1996**, *35*, 3309–3318.
- [89] Adamczyk, M.; Mattingly, P. G.; Shreder, K.; Yu, S. *Bioconjugate Chem.* **1999**, *10*, 1032–1037.
- [90] Van Regenmortel, M. H. V.; Choulier, L. *Comb. Chem. High throughput Screen* **2001**, *4*, 385–395.
- [91] Iwasaki, Y.; Horiuchi, T.; Niwa, O. *Anal. Chem.* **2001**, *73*, 1595–1598.
- [92] Kai, E.; Sawata, S.; Ikebukuro, K.; Iida, T.; Honda, T.; Karube, I. *Anal. Chem.* **1999**, *71*, 796–800.
- [93] Johne, B. *Mol. Biotechnol.* **1998**, *9*, 65–71.
- [94] Laricchia-Robbio, L.; Balzan, S.; Ghione, S.; Montali, U.; Revoltella, R. P. *Biosens. Bioelectron.* **1998**, *13*, 1055–1060.
- [95] Mullett, W.; Lai, E. P.; Yeung, J. M. *Anal. Biochem.* **1998**, *258*, 161–167.

- [96] Mullett, W. M.; Lai, E. P.; Yeung, J. M. *Methods* **2000**, *22*, 77–91.
- [97] Gaus, K.; Hall, E. A. H. *Anal. Chem.* **1999**, *71*, 2459–2467.
- [98] Danielan, E.; Karlen, A.; Karlsson, R.; Winiwarter, S.; Hansson, A.; Löfas, S.; Lennernäs, H.; Hämäläinen, M. *J. Med. Chem.* **2000**, *43*, 2083–2086.
- [99] Frostell-Karlsson, A.; Remaeus, A.; Roos, H.; Andersson, K.; Borg, P.; Hämäläinen, M.; Karlsson, R. *J. Med. Chem.* **2000**, *43*, 1986–1992.
- [100] Van Regenmortel, M. H. *Cell. Mol. Life Sci.* **2001**, *58*, 794–800.
- [101] Adamczyk, M.; Gebler, J. C.; Gunasekera, A. H.; Mattingly, P. G.; Pan, Y. *Bioconjugate Chem.* **1997**, *8*, 133–145.
- [102] Kaganer, E.; Pogreb, R.; Davidov, D.; Willner, I. *Langmuir* **1999**, *15*, 3920–3923.
- [103] Lipschultz, C. A.; Li Y.; Smith-Gill, S. *Methods* **2000**, *20*, 310–318.
- [104] De Genst, E.; Areskoug, D.; Decanniere, K.; Muyldermans, S.; Andersson, K. *J. Biol. Chem.* **2002**, *10*, 174
- [105] Abeles, F.; Lopez-Rios, T. *Solid State Commun.* **1975**, *16*, 843–847.
- [106] Kotz, R.; Kolb, D. M.; Saas, J. K. *Surf. Sci.* **1977**, *69*, 359–364.
- [107] Gordon, J. G.; Ernst, S. *Surf. Sci.* **1980**, *101*, 499–509.
- [108] Tadjeddine, A.; Kolb, D. M.; Kotz, R. *Surf. Sci.* **1980**, *101* (43), 277–285
- [109] Tadjeddine, A.; *Electrochim. Acta* **1989**, *34*, 29–33.
- [110] Lioubimov, V.; Kolomenskii, A.; Merzhin, A.; Nanopoulos, D. V.; Schuessler, H. *A. Applied Optics* **2004**, *43* (17), 3426–3432.
- [111] Abanulo, J. C.; Harris, R. D.; Sheridan, A. K.; Wilkinson, J. S.; Bartlett, P. N. *Faraday. Discuss.* **2002**, *121*, 139–152.

- [112] Chao, F.; Costa, M.; Tadjeddine, A.; Abeles, F.; Lopez-Rios, T.; Theye, M. L. *J. Electroanal. Chem.* **1997**, *83*, 65–86.
- [113] Kötzt, R.; Kolb, D. M.; Sass, J. K. *Surf. Sci.* **1977**, *69*, 359–364.
- [114] Iwasaki, Y.; Tobita, T.; Kurihara, K.; Horiuchi, T.; Suzuki, K.; Niwa, O. *Biosens. Bioelectron.* **2002**, *17*, 783–788.
- [115] Iwasaki, Y.; Horiuchi, T.; Morita, M.; Niwa, O. *Sens. Actuator B* **1998**, *50*, 145–148.
- [116] Iwasaki, Y.; Horiuchi, T.; Morita, M.; Niwa, O. *Electroanalysis* **1997**, *9*, 1239–1241.
- [117] Kang, X.; Jin, Y.; Cheng, G.; Dong, S. *Langmuir* **2002**, *18*, 10305–10310.
- [118] Zhang, N.; Schweiss, R.; Zong, Y.; Knoll, W. *Electrochimica Acta* **2007**, *52*, 2869–2875
- [119] Sheridan, A. K.; Ngamukot, P.; Bartlett, P. N.; Wilkinson, J. S. *Sensors and Actuators B* **2006**, *117*, 253–260.
- [120] Tong, C. W.; Kolomenskii, A.; Lioubimov, V.; Schuessler, H. A.; Trache, A.; Granger, H. J.; Muthuchamy, M. *Biochemistry* **2001**, *40*, 13915–13924.
- [121] Schuessler, H. A.; Mershin, A.; Kolomenskii, A. A.; Nanopoulos, D. V. *J. Mod. Opt.* **2003**, *50*, 2381–2391.
- [122] Fleishmann, M.; Hendra, P. J.; McQuillan, A. *J. Chem. Phys. Lett.* **1974**, *16*, 163
- [123] Moskovits, M. *Rev. Mod. Phys.* **1985**, *57*, 783
- [124] Tian, Z.-Q.; Ren, B. *Annu. Rev. Phys. Chem.* **2004**, *55*, 197
- [125] Kneipp, K.; Wang, Y.; Kneipp, H.; Perelman, L. T.; Itzkan, I.; Dasari, R. R.; Feld, M. S. *Phys. Rev. Lett.* **1997**, *78*, 1667.

- [126] Nie, S.; Emory, S. R. *Science* **1997**, *275*, 1102-1106.
- [127] Moskovits M. *J. Raman Spec.* **2005**, *36*, 485–496.
- [128] Kneipp, K.; Kneipp, H.; Itzkan, I.; Dasari, R.R.; Feld, M.S. *J. Phys. Conden. Matter* **2002**, *14*, R597–R624.
- [129] Cohen, L. F. ed., *Faraday Discussion Vol 132* (RSC Publishing, Cambridge, UK, 2006).
- [130] Raman, C. V.; Krishnan, K. S. *Nature* **1928**, *121*, 501.
- [131] Roy, D.; Barber, Z. H.; Clyne, T. W. *J. Appl. Phys.* **2002**, *91* (9), 6085.
- [132] Rao, A. M.; Richter, E.; Bandow, S.; Chase, B.; Eklund, P. C.; Williams, K. A.; Subbaswamy, K. R.; Menon, M.; Thess, A.; Smalley, R. E.; Dresselhaus, G.; Dresselhaus, M. S. *Science* **1997**, *275*, 187.
- [133] Ryder, A. G.; O'Connor, G. M.; Glynn, T. J. *J. Raman Spectrosc.* **2000**, *31*, 221-227.
- [134] Long, D. A. *The Raman Effect* (JohnWiley & Sons, Ltd., Chichester 2001).
- [135] Graybeal, J. D. *Molecular Spectroscopy*, (McGraw-Hill, Inc, New York 1988) p. 368-369.
- [136] Nakamoto, K. *Infrared and Raman Spectra of Inorganic and Coordination Compounds. Part A: Theory and Applications in Inorganic Chemistry* (John Wiley & Sons, Inc., New York 1997).
- [137] Herzberg, G. *Molecular Spectra and Molecular Structure. I. Infrared and Raman Spectra of Polyatomic Molecules*, (van Nostrand, Princeton 1945).
- [138] Skoog, D. A.; Holler, F. J.; Nieman, T. A. *Principles of Instrumental Analysis*, 5th ed. (Saunders College publishing, Philadelphia 1998) p. 431.

- [139] Jeanmarie, D. L.; Van Duyne, R. P. *J. Electroanal. Chem.* **1977**, *84*, 1.
- [140] Albrecht, M. G.; Creighton, J. A. *J. Am. Chem. Soc.* **1977**, *99*, 5215.
- [141] Kambhampati, P.; Child, C. M.; Foster, M. C.; Campion, A. *J. Chem. Phys.* **1998**, *108*, 5013.
- [142] Shatz, G. C.; Van Duyne, R. P. in *Electromagnetic Mechanism of Surface Enhanced Spectroscopy*, Chalmers, J. M.; Griffiths, P. R. ed. (John Wiley and Sons Ltd., Chichester 2002).
- [143] Maher, R. C.; Cohen, L. F.; Etchegoin, P.; Hartigan, H. J. N.; Brown, R. J. C.; Millington, M. J. T, *J. Chem. Phys.* **2004**, *120*, 11746.
- [144] Michaels, A. M.; Jiang, J.; Brus, L. *J. Phys. Chem. B* **2000**, *104*, 11965.
- [145] Kneipp, K.; Wang, Y.; Kneipp, H.; Itzkan, I.; Dassari, R. R.; Feld, M. S. *Phys. Rev. Lett.* **1996**, *76*, 2444.
- [146] Doering, W. E.; Nie, S. *J. Phys. Chem. B* **2002**, *106*, 311.
- [147] Munro, C. H.; Smith, W. E.; Garner, M.; Clarkson, J.; White, P. C. *Langmuir*, **1995**, *11*, 3712.
- [148] Young, M. A.; Dieringer, J. A.; Van Duyne, R. P. “Plasmonic materials for surface-enhanced and tip-enhanced Raman spectroscopy”, in *Tip Enhancement* Kawata, S.; Shalaev, V. M. (Eds.), (Elsevier, Amsterdam 2007) p. 4
- [149] Musick, M. D.; Keating, C. D.; Lyon, L. A.; Botsko, S. L.; Pena, D. J.; Hollay, W. D.; McEvoy, T. M.; Richardson, J. N.; Natan, M. J. *Chem. Mater.* **2000**, *12*, 2869–2881.
- [150] Park, S.-H.; Im, J.-H.; Im, J.-W.; Chun, B.-H.; Kim, J.-H. *Microchem. J.* **1999**, *63*, 71–91.
- [151] Li, J.; Fang, Y. *Spectrochim. Acta Part A* **2007**, *66A*, 994–1000.

- [152] Murgida, D.; Hildebrandt, P. *Top. Appl. Phys.* **2006**, *103*, 313–334.
- [153] Orendorff, C. J.; Gearheart, L.; Jana, N. R.; Murphy, C. J. *Phys. Chem. Chem. Phys.* **2006**, *8*, 165–170.
- [154] Yang, Y.; Xiong, L.; Shi, J.; Nogami, M. *Nanotechnology* **2006**, *17*, 2670–2674.
- [155] White, D. J.; Mazzolini, A. P.; Stoddart, P. R. *J. Raman Spectrosc.* **2007**, *38*, 377–382.
- [156] Tian, Z.-Q.; Yang, Z.-L.; Ren, B.; Li, J.-F.; Zhang, Y.; Lin, X.-F.; Hu, J.-W.; Wu, D.-Y. *Faraday Discuss.* **2006**, *132*, 159–170.
- [157] McLellan, J. M.; Siekkinen, A.; Chen, J.; Xia, Y. *Chem. Phys. Lett.* **2006**, *427*, 122–126.
- [158] Haynes, C. L.; Van Duyne, R. P. *J. Phys. Chem. B*, **2003**, *107*, 7426.
- [159] Aizpurua, J.; Hanarp, P.; Sutherland, D. S.; Kall, M.; Bryant, G. W.; de Abajo, F. J. *G. Phys. Rev. Lett.* **2003**, *90*, 57401.
- [160] Jackson, J. B.; Halas, N. J. *Proc. Natl. Acad. Sci. USA*, 2004, *101*, 17930.
- [161] Lu, L.; Kobayashi, A.; Tawa, K.; Ozaki, Y. *Chem. Mater.* **2006**, *18*, 4894–4901.
- [162] Zhang, X.; Yonzon, C. R.; Van Duyne, R. P. *J. Mater. Res.* **2006**, *21*, 1083–1092.
- [163] Gunnarsson, L.; Bjerneld, E. J.; Xu, H.; Petronis, S.; Kasemo, B.; Kall, M. *Appl. Phys. Lett.* **2001**, *78*, 802–804.
- [164] Haynes, C. L.; McFarland, A. D.; Zhao, L.; Van Duyne, R. P.; Schatz, G. C.; Gunnarsson, L.; Prikulis, J.; Kasemo, B.; Kaell, M. *J. Phys. Chem. B* **2003**, *107*, 7337–7342.
- [165] Hicks, E. M.; Zou, S.; Schatz, G. C.; Spears, K. G.; Van Duyne, R. P.; Gunnarsson, L.; Rindzevicius, T.; Kasemo, B.; Kaell, M. *Nano Lett.* **2005**, *5*, 1065–1070.

- [166] P. M. Tessier, O. D. Velev, A. T. Kalambur, J. F. Rabolt, A. M. Lenhoff and E. W. Kaler, *J. Am. Chem. Soc.* **2000**, 122, 9554.
- [167] Surawara, Y.; Kelf, T. A.; Baumberg, J. J.; Abdelsalam, M. E.; Bartlett, P. N. *Phys. Rev. Lett.* **2006**, 97, 266808.
- [168] Kelly, K. L.; Coronado, E.; Zhao, L. L.; Schatz, G. C. *J. Phys. Chem. B* **2003**, 107, 668–677.
- [169] Dieringer, J. A.; McFarland, A. D.; Shah, N. C.; Stuart, D. A.; Whitney, A. V. *Faraday Discuss.* **2005**, 132, 9–26.
- [170] Kennedy, B. J.; Spaeth, S.; Dickey, M.; Carron, K. T. *J. Phys. Chem. B* **1999**, 103, 3640–3646.

CHAPTER 2

SIMULTANEOUS SENSING OF TRACE SELENITE IONS AND TELLURITE IONS BY ELECTROCHEMICAL-SURFACE PLASMON RESONANCE TECHNIQUE

2.1 Introduction

Surface plasmon resonance spectroscopy (SPR) is a well-known method for monitoring binding events occurring at a solid-liquid interface in the field of biochemistry, material science, and electrochemistry. The basis of SPR is the sensitivity of the evanescent field to the dielectric constant of the sensing layer which is just few hundred nanometers above the metal surface. SPR is initiated from the optical excitation of the surface plasmons at a metal-prism interface and the resulting collective oscillation of electric charges propagates along the metal-prism and metal-dielectric interfaces.

One SPR measuring technique is the incident angle modulation, which uses a monochromatic excitation light to excite the surface plasmons on the planar metal surface and measures the reflectivity of the light (defined as the intensity of reflected light over the intensity of incident light) as a function of incident angle. As the incident angle approaches the resonance angle, the intensity of the reflected light sharply decreases and reaches a minimum at the resonance angle. This optical phenomenon is due to the energy transfer from the coupled photons to the electrons at the resonance condition. The resonance angle, θ_{SPR} , can be modeled by the following equation:

$$\theta_{spr} = \sin^{-1} \sqrt{\frac{\epsilon_m \epsilon_d}{\epsilon_p (\epsilon_m + \epsilon_d)}} \quad \text{Eq. 2.1}$$

where ϵ_m , ϵ_d , and ϵ_p are dielectric constant of metal film, dielectric layer, and prism respectively. In a typical experiment, the resonance angle shifts according to the change in the dielectric constant of the dielectric layer. Therefore, SPR has been widely used for the characterization of thin films, the analysis of biomolecular interactions, the study of the self-assembly of the thiol molecules on metal surface, and the studies of the conformational change of the protein molecules.

Due to its great surface sensitivity, an electrochemist would expect that SPR could provide details related to the interfacial events occurring at the electrode surface beyond the typical the current-potential relationship. In the electrochemical SPR (EC-SPR) the thin gold film on the glass slide provides the support of the surface plasmons and also provides the electric conductive media as a function of a working electrode. Electrochemistry typically involves two types of processes: the adsorptions (non-faraday process) and faraday process. Both processes can change the dielectric constant of the dielectric layer. Therefore, SPR is very suitable for the study of different electrochemical processes. These include the determination of the electric field profile within the multilayer films of zirconium phosphonate,¹ detecting trace metals,^{2,3} studies of the diffusion and adsorption processes on electrode surface,⁴⁻⁶ determination of the surface coverage of hydrated proteins at a fixed potential,⁷ study of the electrochemical doping/dedoping process⁸ and developing an electrochemical SPR sensor.^{9,10}

Selenium is an important element in biological and environmental systems.¹¹⁻¹² Selenium can exist in several oxidation states (-II, 0, +IV, +VI). The bioavailability and

toxicity of selenium depends on its chemical form. Both selenate (Se^{6+}) and selenite (Se^{4+}) are water-soluble inorganic species which are present in natural waters. Selenite ion is approximately 10-fold more toxic than selenate ion.¹³ The most bioavailable form of selenium is organic selenium as selenide (Se^{2-}). Since selenium is an essential trace element for human body, a lack of selenium can lead to several diseases. However, excess selenium in the body has proven to be fatal. EPA set the drinking standard at a level of 0.05 ppm (or 0.633 mM) of selenium.¹⁴ The selenium gap between toxic concentration and concentration as supplement is very small. A sensitive method of determining selenium can aid to uncover the importance of selenium in health. The analytical methods for determining traces of selenium in the environmental samples are atomic absorption spectrometry (AAS),^{15,16} inductively coupled plasma atomic emission spectrometry (ICP-AES),¹⁷ inductively coupled plasma mass spectrometry (ICP-MS),¹⁸ neutron activation analysis,¹⁹ and stripping voltammetry.²⁰⁻²³

For portable sensors, anodic stripping voltammetry²⁴ (ASV) is perhaps the most promising method for determining the concentration of metal ions. Metal ions are electrodeposited on the rotating disk electrode followed by stripping of the metal film at a certain applied potential. The current measured during the stripping process is proportional to the metal ion concentration in the solution, and the potential, at which the stripping of the metal film occurs, corresponds to the standard oxidation potential of the specific metal deposited on the electrode. There are two limitations for ASV. The presence of background current in ASV measurement makes it difficult to detect the small stripping current associated with the oxidation of the analyte. The ASV is

responsive to the oxidation and reduction of the redox-active species such that the formation of the intermetallic compounds can interfere with stripping peak of the analyte.

It has been reported that SPR can be used to detect metal ions by SPR-ASV,²⁵⁻²⁷ use of functionalized self-assembled monolayer,^{28,29} use of immobilized enzyme,³⁰ and use of polymeric thin film.³¹⁻³³ In APR-ASV, it has been shown that SPR is insensitive to the background current introduced by the dissolved oxygen³⁴ and SPR is sensitive to detect intermetallic compounds.

Herein, we attempt to further extend the scope of the SPR technique to the analysis of the underpotential growth of selenium and the detection of the selenite solution. Fundamental study for the characteristics of SPR under a potential modulation has been designed by choosing a well documented electrochemical system such as gold oxide formation and stripping in the 1 M HClO₄ solution. The effects of faradaic and non-faradaic process on SPR signals will be discussed. The underpotential deposition of the selenium film on the gold surface is monitored in situ with SPR measurement. Regarding to the ion sensing, we use EC-SPR to study the constant potential deposition of the selenium at various selenite concentrations. The anodic stripping of selenium, the interference effect from tellurite ions in the solution, and implementation of the standard addition technique for simultaneous sensing of the mixed selenite ions and telluride ions are explored in our study.

2.2 Experimental

2.2.1 Materials

The chemicals were of all analytical reagent grades. SeO_2 (99.99% purity) and TeO_2 (99.99% purity) were obtained from Merck Chemical Company. HClO_4 was obtained from Fisher Scientific. Stock solution of 1 mM selenite was prepared from SeO_2 in 0.1M HClO_4 while 1 mM of tellurite solution was prepared in 0.1M HClO_4 . Due to the low solubility of the TeO_2 in water, solid TeO_2 was stirred and heated in a concentrated solution for 30 minutes before dilution to 1 mM with the deionized water. All of the aqueous solutions were prepared with deionized water purified by Millipore-Q (18 m Ω).

2.2.2 Electrochemistry

All cyclic voltammetry experiments were performed in homemade single-compartment glass cells (ca. 25 mL total volume) using a BAS-100 workstation. A standard three-electrode configuration was used in which the SPReeta sensor surface was the working electrode, a Pt mesh was the counter electrode, and a silver wire in a 3 M AgCl solution (Ag/AgCl) was the reference electrode. All potentials are referenced to Ag/AgCl. The solution was thoroughly degassed with ultrapure Ar and was isolated from air with a blanket of Ar during experiments. All cyclic voltammetry was conducted with a scan rate of 10 mV/s.

2.2.3 Instrumentation

SPReeta sensors developed by Texas Instrument (TI) were used. This SPR system employs a light emitting diode (840 nm) with a polarizer, reflecting mirror, and 128 pixel Si-photodiode array. Each detection pixel corresponds to a narrow range of incident angle. The sensing region is coated with a semitransparent gold film (ca. 50 nm) with a Cr-adhesion layer (1 – 2 nm). A 12-bit three-channel electronic control box completes the interface between the sensor and a PC. Multichannel SPREETA software provided by TI monitors the changes in RI or resonance angle near the sensing surface calculates the statistical noise in the signal and displays the results.

The SPReeta evaluation module (SPR-EVM-BT) was purchased from Nomadics (Stillwater, OK, USA). The major components of the module were a SPReeta sensor, integrated flow cell, interface controller, and application software. A 12-bit analog-to-digital converter was utilized to provide a high resolution of 1×10^{-7} refractive index units (RIU), which corresponding to 0.001 degree in angle.

2.3 Results and discussion

2.3.1 Study of stripping and formation of the gold oxide

The effects of the non-faradaic and faradaic processes on the bare gold surface of the SPReeta in 0.1 M HClO₄ solution was investigated simultaneously by SPR and cyclic voltammetry. Prior to the cyclic voltammetry measurement, the gold electrode has been oxidized by applying a potential of 1650 mV for 10 seconds. The voltammetric behavior of and the SPR responses of the gold electrode immersed in 0.1 M HClO₄ solution are shown in Figure 2.1. There are only two characteristic peaks observed in the cyclic

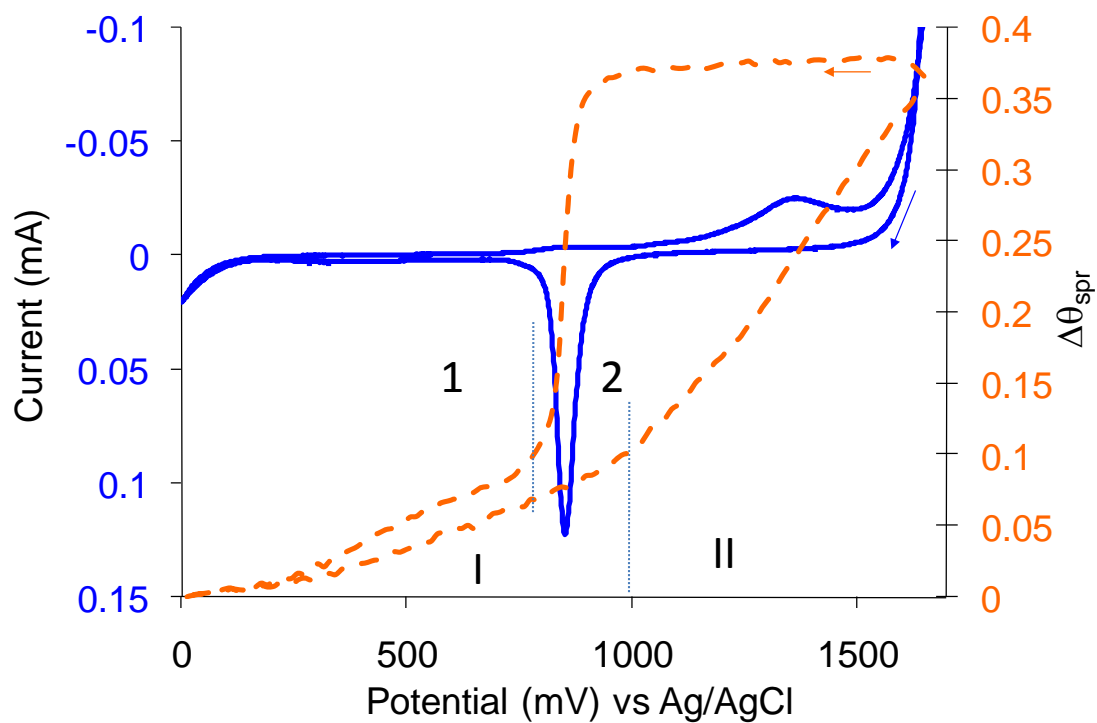


Figure 2.1 The simultaneous measurement of cyclic voltammetry (solid line) and SPR (dash line) for a gold electrode in 0.1 M HClO₄. The scan rate is 10 mV/second.

voltammogram. They are attributed to the reduction and oxidation of the gold respectively. As the potential decreases from 1650 mV to 950 mV, the shift in SPR angle, $\Delta\theta_{\text{SPR}}$, remains unchanged due to the well-covered stable gold oxide layer which has a higher dielectric constant than the supporting electrolyte.⁴⁰ At 950 mV, there is a sharp decrease in $\Delta\theta_{\text{SPR}}$ due to the reduction of the gold oxide. This decrease in $\Delta\theta_{\text{SPR}}$ continues until the potential reaches 700 mV. At this point, the decrease in $\Delta\theta_{\text{SPR}}$ has a linear trend, which can be attributed to the depleting of the charging from double layer. The rate of the decrease in $\Delta\theta_{\text{SPR}}$ slows down at the applied potential of 365 mV as it approaches to the potential of zero charge (pzc).

It is apparent from Figure 2.1 that the SPR response in the forward and the reverse scan has two distinct regimes. The pzc for gold in the 0.1M HClO₄ has been reported as 365 mV (vs Ag/AgCl).^{35,36} During the reverse potential scan from 0 mV to 1000 mV, the first regime for the SPR signals was observed when the applied potentials are deviates away from the pzc of the gold. The increase in $\Delta\theta_{\text{SPR}}$ was attributed to the double layer charging. This observation is similar to the results of reflectance measurement by and Kolb, et al.^{37,38} and Ernst, et al.³⁹ The second regime was observed at potential more positive than 1000 mV when the $\Delta\theta_{\text{SPR}}$ increases dramatically due to the formation of the gold oxide.

An explanation for the first regime has been made by Kolb, et al.⁴⁰ to address the electroreflectance effect^{41,42} in which the dielectric constants of the electrode are altered by the changes in the free-electron concentration at the surface of the gold electrode. The SPR signal is affected by the dielectric constant of the metal and the adjacent dielectric

layer. The dielectric constant of the metal surface layer, ϵ_{ms} , under the applied potential can be represented as the following:

$$\epsilon_{ms} = \epsilon_{ms,0} + \Delta\epsilon_{ms} \quad \text{Eq. 2.2}$$

where $\epsilon_{ms,0}$ and $\Delta\epsilon_{ms}$ are the dielectric constant of the metal surface layer without and with applied potential respectively. The magnitude of the change in $\epsilon_{ms,0}$ can be estimated using the Drude equation for a free electron gas^{42,43} as the following:

$$\Delta\epsilon_{ms} = (\epsilon_m - 1) \left(\frac{\Delta N}{N} \right) \quad \text{Eq. 2.3}$$

where ϵ_m is dielectric constant of bulk metal, N is the bulk free electron density and ΔN the change in free electron density in the surface layer. Finally the ratio $\Delta N/N$ can be related to the charge on the electrode surface⁴⁰ by

$$\left(\frac{\Delta N}{N} \right) = \left(\frac{C_{DL}}{Ned} \right) (E - E_{pzc}) \quad \text{Eq. 2.4}$$

where C_{DL} is the double layer capacitance, e the charge on the electron, d the layer thickness (also called the Thomas-Fermi screening length; assumed to be 0.6 Å) and E_{pzc} the potential of zero charge. From the model and experimental results, as the potential changes from E_{pzc} , the change in the electron density increases and the shift in SPR angle increases. This explains the observed increase in $\Delta\theta_{SPR}$ in the potential range from 365 mV to 1060 mV. In addition, the accumulation of ion species on the metal surface or double layer charging effect accounts for such change in $\Delta\theta_{SPR}$.

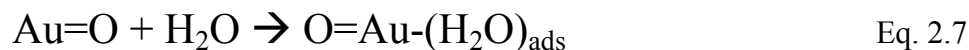
As the potential increases to 1060 mV, a larger increase in the shift of SPR angle is observed. This is attributed to the gold oxide formation. Evidences of the gold oxide formation has been studied using electrochemical EQCM^{44,45} and infrared

spectroscopy.⁴⁶⁻⁴⁹ Gold oxide formation under potential sweep consists of two steps.⁵⁰

The first step is the conversion of adsorbed water on the Au surface to an adsorbed hydroxyl radical according to the following equation,



and the second step, the formation of Au oxide and the adsorption of water on gold oxide, occurs concurrently.



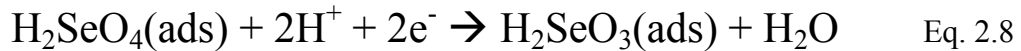
The shift in SPR angle increases steadily as the gold oxide forms.

The hysteresis of SPR signals was observed in the first regime. It is also apparent in Figure 2.1 that the hysteresis is more distinctive at the anodic potential than at the cathodic potential to the E_{pzc} . The observed hysteresis behavior cannot be explained by the changes in the electronic density of the metal alone but this phenomenon may be due to the slower kinetics in the reduction of the gold oxide.

2.3.2 Study of selenium underpotential deposition

Shannon et al⁵¹ has investigated the voltammetric behavior of a Au (111) electrode immersed in 1 mM SeO_2 and a 0.1M of HClO_4 supporting electrolyte. It has been reported that there are three cathodic surface-limited peaks C1, C2, and C3. The peak C1 and C2 attribute to the reduction of an adsorbed selenate species to selenite while the peak C3 attributes to the selenium underpotential deposition associated with the four-electron reduction of adsorbed selenite to selenium.

Figure 2.2 shows the polycrystalline gold surface such as the SPR electrode has a similar behavior to the Au (111) for the selenium underpotential deposition. Three reduction peaks C1, C2, and C3 were observed in the EC-SPR. The system shows good stability and reproducibility in the optical responses. The changes in SPR angle associated with the deposition and the removal of the Se UPD layer are reversible. For the cathodic scan from 900 mV to 0 mV, the shift of the SPR angle, $\Delta\theta_{\text{SPR}}$, initially decreases due to the decreasing double layer charging effects, mentioned in the earlier discussion. At potential around 400 mV, we observed a current peak yet there was no shift in SPR angle. The SPR signal for the electrochemical process occurring at C1 reduction peak was overwhelmed by the dominating effect from the charging in double layer. At the potential of 300 mV, C2 current peak was observed aligned with the increase in $\Delta\theta_{\text{SPR}}$. This observation can be attributed to the adsorption and the conversion of the selenic acid to the seleneous acid shown as:



As the potential reaches 250 mV, we observed the Se UPD current peak and $\Delta\theta_{\text{SPR}}$ increases monotonically as the surface confined seleneous acid was converted to elemental selenium, which has higher refractive index than the solution. Finally, at the bulk deposition potential of 100 mV, we could not observe any further increase in current or in $\Delta\theta_{\text{SPR}}$ because the deposition in this regime is limited by the transport and the sluggish four-electron kinetics of converting from selenic acid to element selenium.

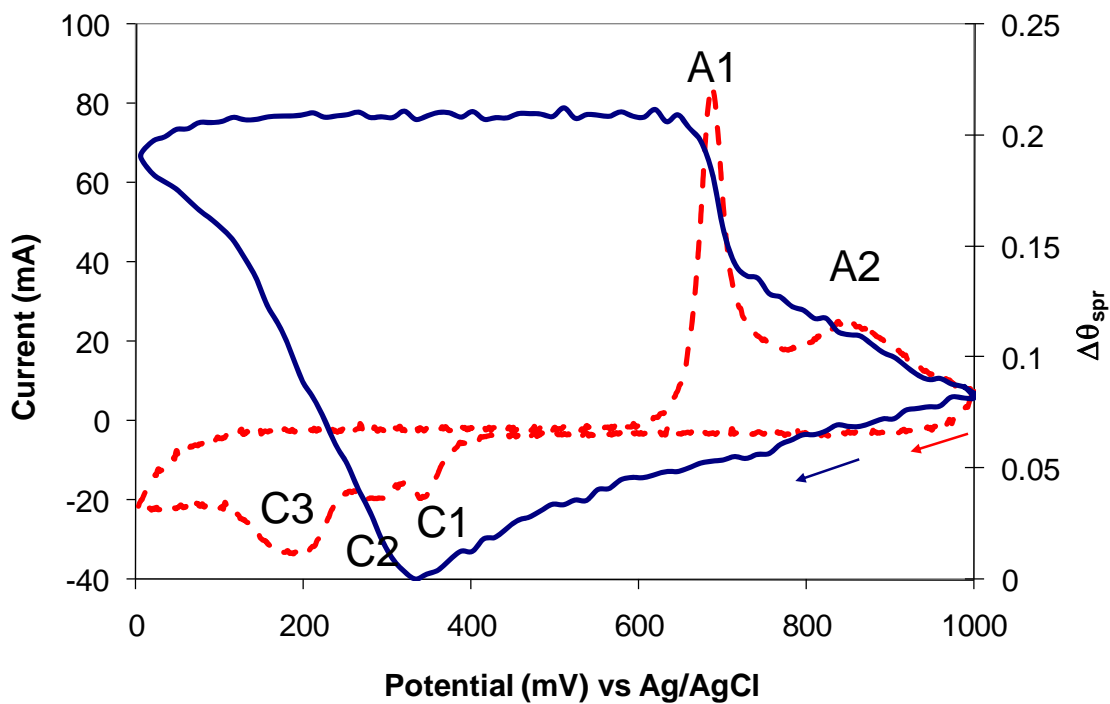


Figure 2.2 The simultaneous measurement of cyclic voltammetry (dash line) and SPR (solid line) for a gold electrode in 1 mM SeO_3^{2-} . The scan rate is 10 mV/second.

2.3.3 EC-SPR for selenite detection using constant potential deposition method

Fick's law of diffusion states that the diffusion flux at steady state is proportional to the diffusion coefficient and the concentration gradient. After perturbing the electrode with step potentials of 500 mV and 900 mV, the electrode was allowed to replenish the adsorbed selenous acid at a more negative potential such as 200 mV. The rate of the replenishment is governed by the concentration gradient of the selenite in the vicinity of the electrode surface. We relied on the working principle of the diffusion flux using EC-SPR to detect the concentration of selenite ions in the solution.

Figure 2.3 shows the SPR responses in the 200 μ M selenite solution during a three-step potential program. Initially two potentials, 500 mV and 900 mV, were applied and the corresponding SPR signal showed a reversible behavior under the step potential perturbations. When the deposition of the selenium was carried out at 200 mV, the $\Delta\theta_{\text{SPR}}$ increased and reached plateau after 1200 seconds. The earlier work showed when the selenium was deposited at the bulk deposition potential $\Delta\theta_{\text{SPR}}$ continuously increased and did not reach a plateau. After the deposition stopped, the potential was held at 500 mV for 100 seconds. The $\Delta\theta_{\text{SPR}}$ remained constant due to the stable film formation. When the stripping potential of 900 mV was applied, the θ_{SPR} decreased sharply and returned to the same starting resonance angle.

The UPD deposition of selenium at 200 mV was monitored using EC-SPR at various selenite concentrations ranging from 100 nM to 500 μ M. Figure 2.4 shows the rate of the shift in SPR angle depends on the concentrations of the selenite solution. As the concentration increases, the flux of selenite ions increases, covering the surface a faster rate. The curves are characterized by a rapid increase in $\Delta\theta_{\text{SPR}}$ followed by a slow

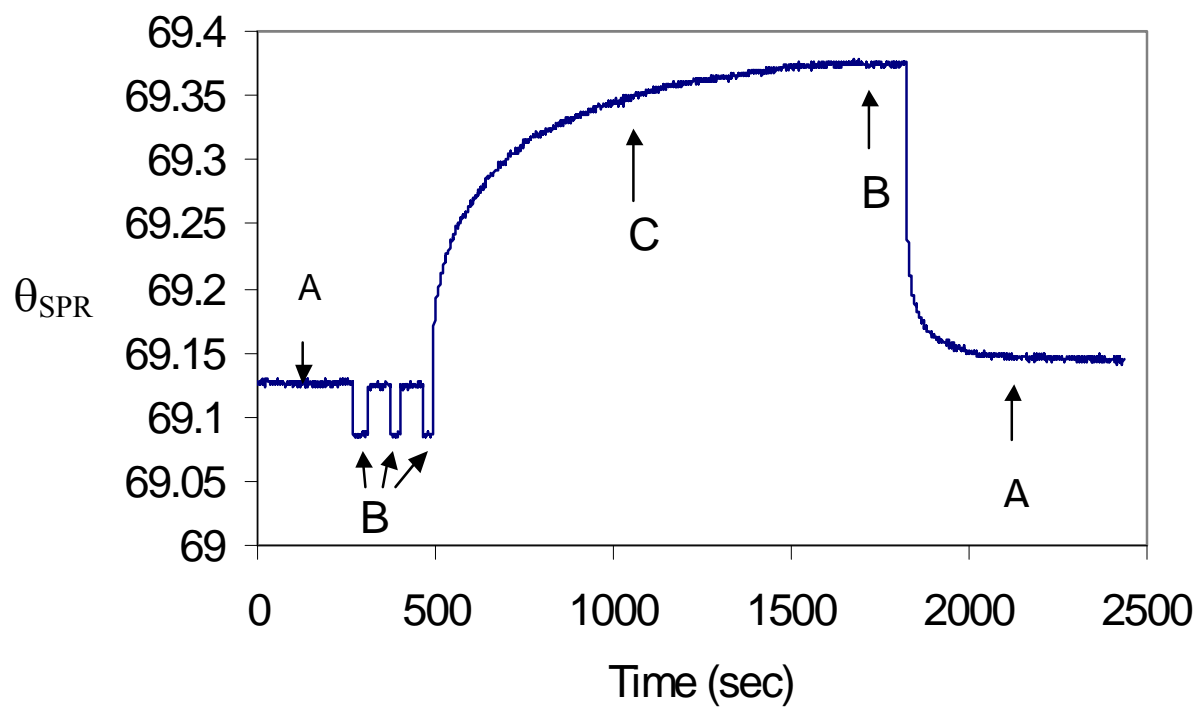


Figure 2.3 The changes in SPR response for three different potentials in the 200 μM selenite solution. (A: 900 mV, B: 500 mV, C: 200 mV).

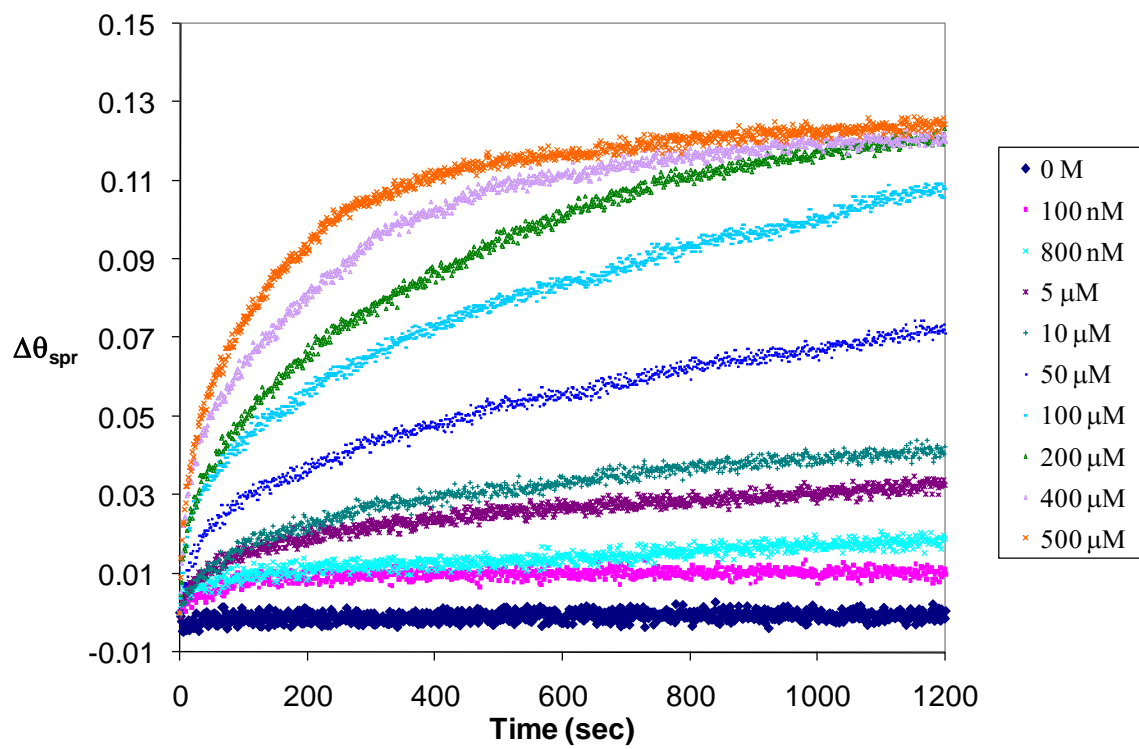


Figure 2.4 The changes in SPR angle for different SeO_3^{2-} concentrations at 200 mV.

approach to steady state. A true saturated response is only observed at the highest concentration consistent with our assertion that selenite mass transport is the rate determining step in selenium uptake. At zero concentration, we did not observe any significant shift in SPR angle.

The detection limit for selenite ions using EC-SPR is found to be 800 nM since the noise level was measured as 0.006 degree. The dynamic range is three orders of magnitude. A calibration curve shown in Figure 2.5 was generated from the values of $\Delta\theta_{\text{SPR}}$ for the various selenite concentrations at 500 seconds of deposition time.

The EC-SPR characterization on the pure selenite solution shows good reproducibility and good dynamic range; however, this constant potential method suffers severely from the interference effects of other metal ions. Figure 2.6 shows the interference effect arises from the presence of the tellurite ions. The telluride ions compete with selenite ions in mass transport to the electrode surface. With the same concentration of the selenite concentration, the solution containing tellurite ions had higher $\Delta\theta_{\text{SPR}}$ than the solution without the tellurite ions.

2.3.4 EC-SPR for selenite detection using electrochemical stripping method

SPR can be used to monitor the electrochemical stripping of the selenium from the gold surface as seen in Figure 2.3. The shift in SPR angle was later found to be proportional to the amount of the selenium deposited on the surface. When the deposited selenium is electrochemically stripped off the gold surface, the SPR signals are proportional to the amount of selenium deposited. Figure 2.7 shows the SPR response to a potential sequence for the stripping analysis. Selenium was electrodeposited from a

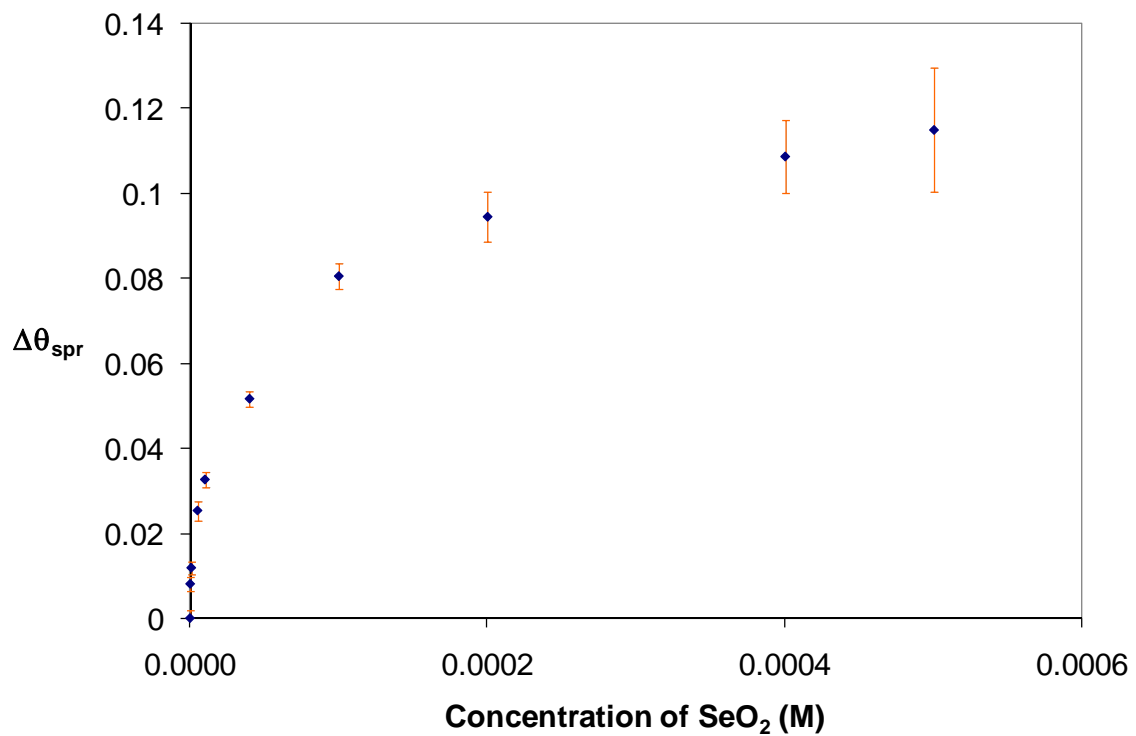


Figure 2.5 The changes in SPR angle for different SeO₃²⁻ concentrations at 200 mV from Figure 2.4 at time 500 seconds.

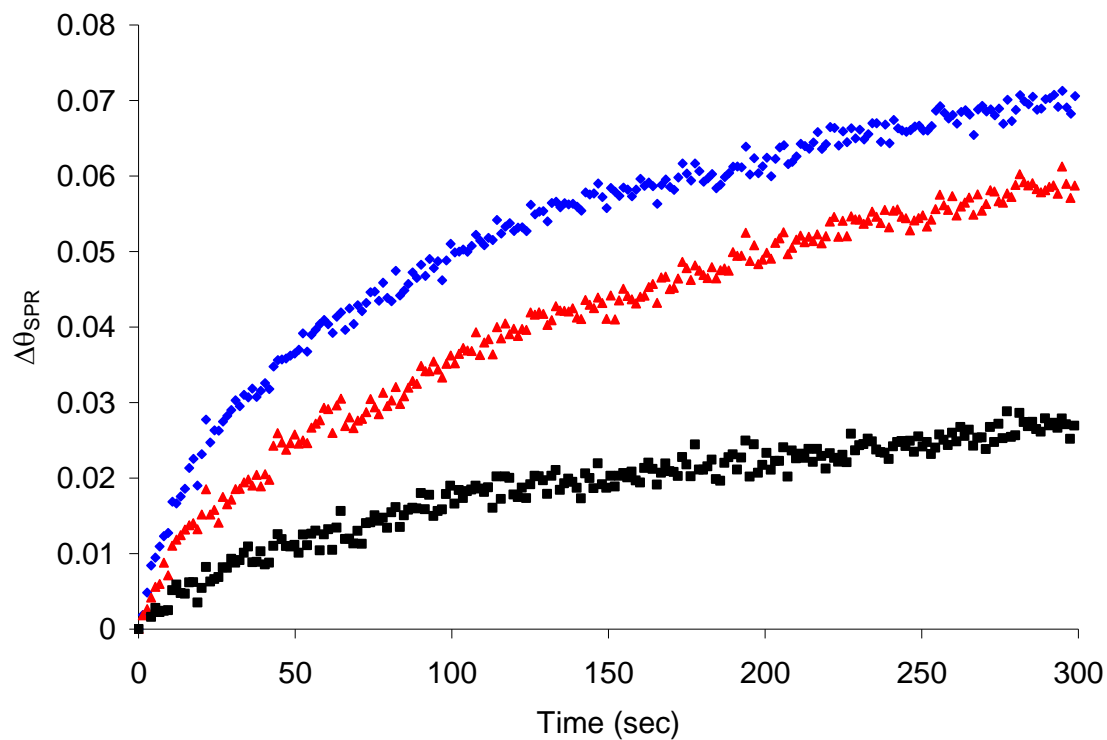


Figure 2.6 Interference study of EC-SPR constant potential deposition. The square represents the EC-SPR response for 10 μM SeO_3^{2-} , the triangle represents EC-SPR response for 1 mM TeO_3^{2-} and 10 μM SeO_3^{2-} , and the diamond represents EC-SPR response for 1 mM TeO_3^{2-} .

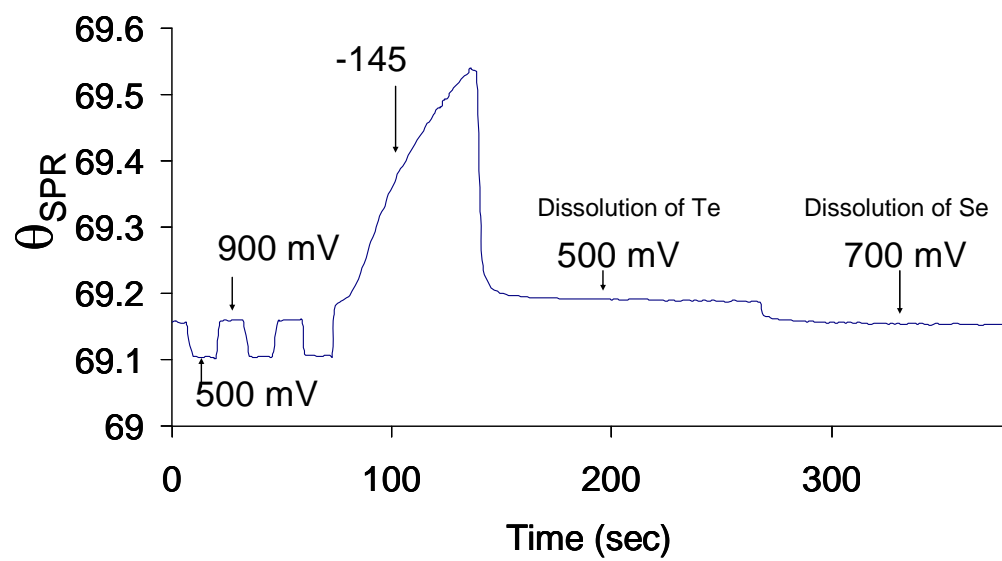


Figure 2.7 The potential step program for the EC-SPR stripping analysis.

solution containing 500 μM of tellurite ions and 500 μM of selenite ions using a potential of -145 mV for 60 second. A stripping potential of 500 mV was chosen for the stripping of tellurium while the potential of 700 mV was chosen for the stripping of selenium. Since the standard reduction potential of tellurium is more negative than that of selenium, tellurium deposits preferentially and thus more abundantly than the selenium at the same applied potential. Although the deposition was carried out with equal molar of both ions, the stripping of tellurium shows greater $\Delta\theta_{\text{SPR}}$ than the stripping of selenium due to a larger amount of tellurium deposited on the electrode.

Figure 2.8 shows the $\Delta\theta_{\text{SPR}}$ from the stripping of (a) the pure tellurium and (b) pure selenium on the gold surface. The potential sequence for the stripping analysis starts at 500 mV for 120 seconds followed by a potential at 700 mV for 120 seconds. Figure 2.8 shows that the stripping of selenium and tellurium can be monitored using SPR. The shift in SPR angle for the tellurium stripping appears to be more dramatic than that for the selenium stripping. This may be due to the larger amount of the tellurium deposited than selenium at the same deposition potential.

Simultaneous sensing on a solution containing selenite ions and telluride ions is investigated. By varying the telluride concentration from 200 μM to 500 μM and keeping the selenite concentration constant, we observed an increase in $\Delta\theta_{\text{SPR}}$ at 500 mV and a constant $\Delta\theta_{\text{SPR}}$ at 700 mV shown in Figure 2.9. Varying only the concentration of selenite 25 μM to 50 μM results a similar $\Delta\theta_{\text{SPR}}$ at 500 mV and an increase in $\Delta\theta_{\text{SPR}}$ at 700 mV shown in Figure 2.10.

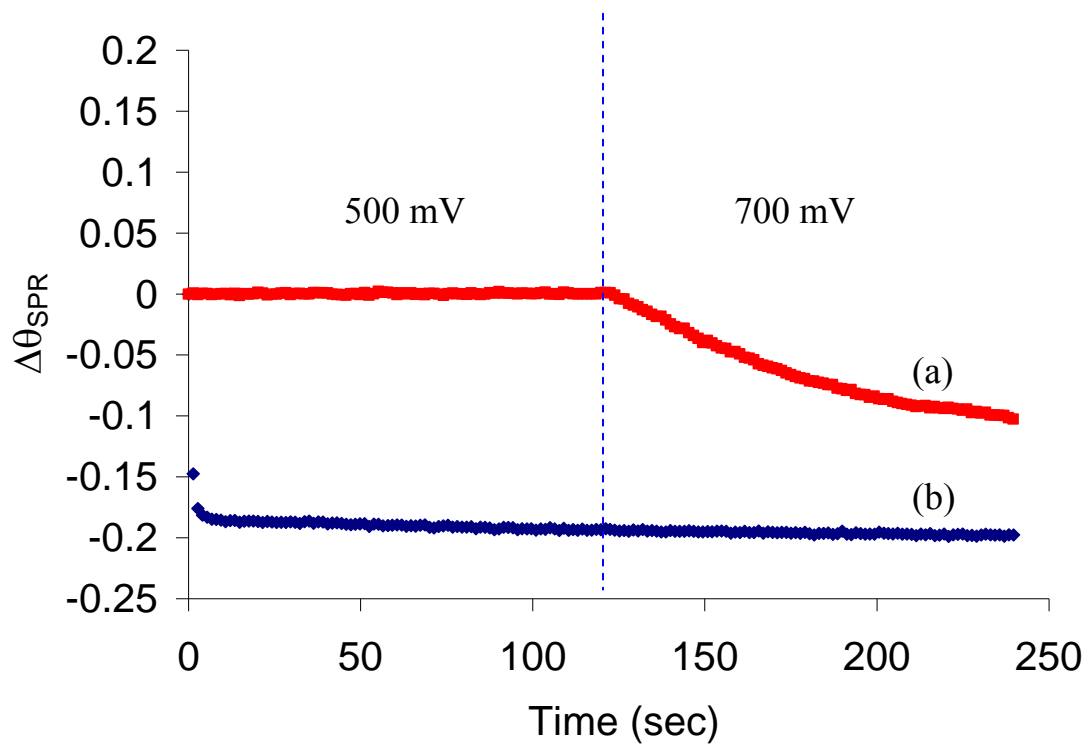


Figure 2.8 Effect of stripping potential on (a) selenium electroplated and (b) tellurium electroplated gold electrode. A potential of 500 mV was applied for 120 seconds before another potential of 700 mV was applied.

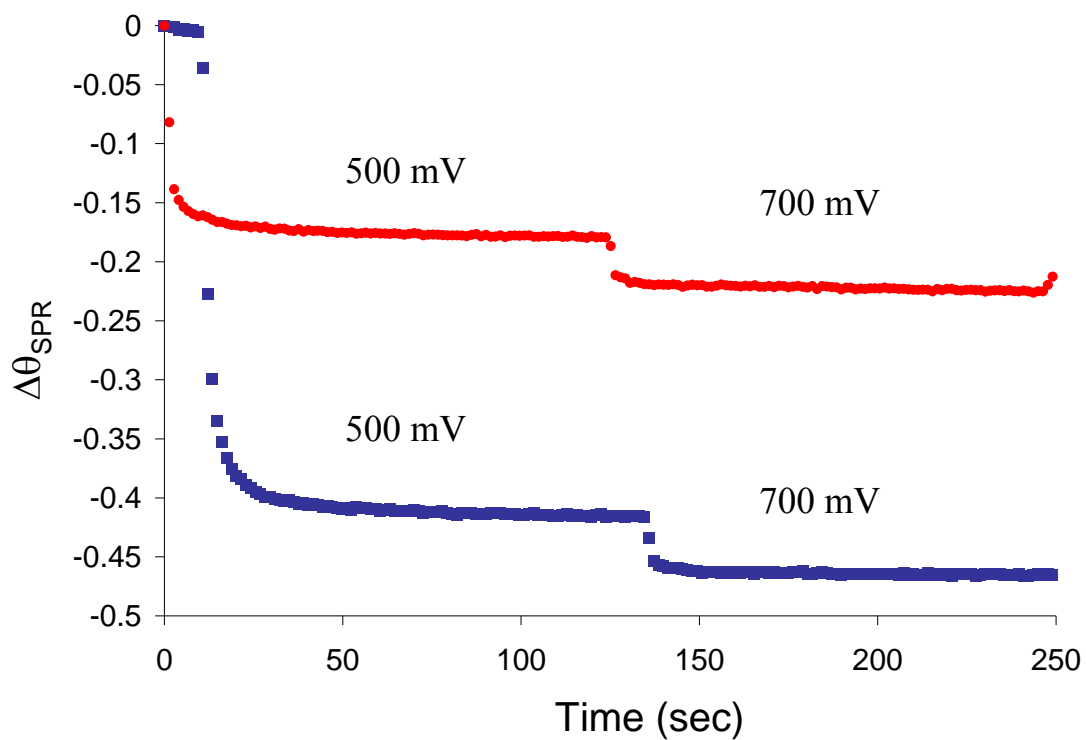


Figure 2.9 The TeO_3^{2-} concentration effect on the EC-SPR stripping response. The circles correspond to the solution containing $200 \mu\text{M}$ of tellurite and $50 \mu\text{M}$ of selenite. The squares correspond to the solution containing $500 \mu\text{M}$ of tellurite and $50 \mu\text{M}$ of selenite.

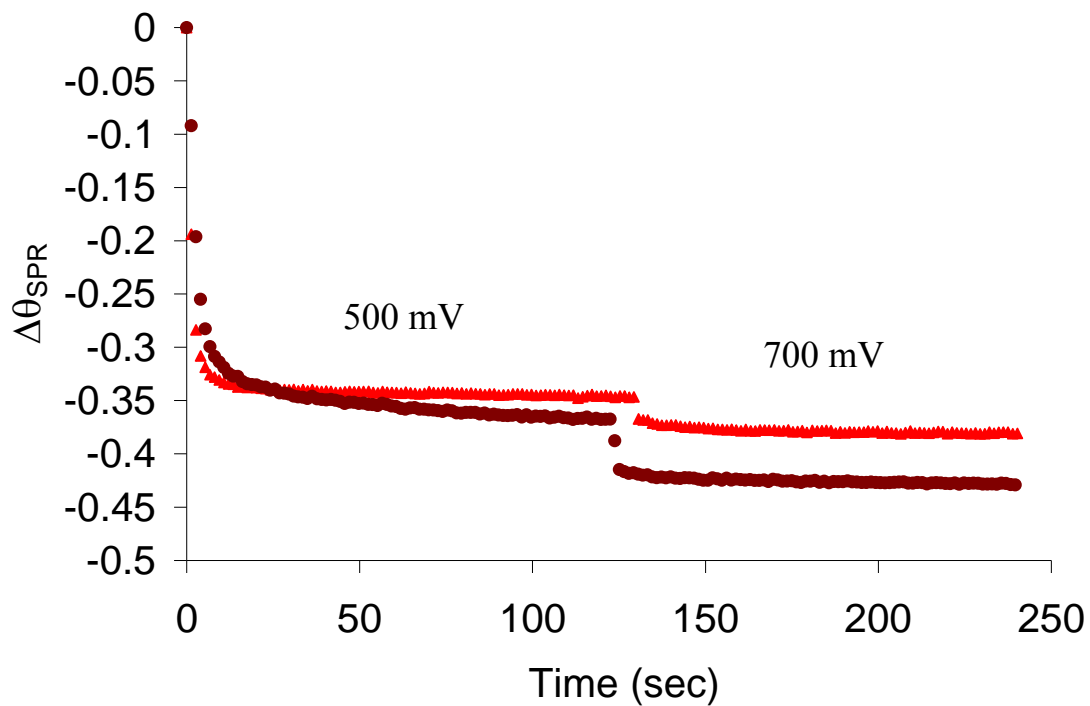


Figure 2.10 The SeO_3^{2-} concentration effect on the EC-SPR stripping response.

The triangles correspond to the solution containing 400 μM tellurite and 25 μM selenite.

The circles correspond to the solution containing 400 μM tellurite and 50 μM selenite.

Due to the fact that the magnitude of $\Delta\theta_{\text{SPR}}$ is proportional to the amount of ion species at different stripping potential, we implement the standard addition technique for the stripping analysis with EC-SPR to determine the unknown concentrations of tellurite ions and selenite ions in a solution. A 25 ml of unknown solution containing an equal molar of tellurite ions and selenite ions was used in the experiment. An increment of one milliliter of the standard solution containing equal molar (500 μM) of tellurite ions and selenite ions was added to the unknown solution and was monitored for the change in $\Delta\theta_{\text{SPR}}$ at stripping potentials of 500 mV and 700 mV shown in Figure 2.11. The change in $\Delta\theta_{\text{SPR}}$ for both potentials shows a linear trend which can be extrapolated for the determination of the x-intercepts. The concentration of the unknown was determined by multiplying the value of the x-intercept with the concentration of the standard solution over the initial volume of the unknown solution. The results were tabulated in Table 2.1 for the unknown solution contains equal molar of 50 μM of selenite and tellurite. Quantitative analysis shows the unknown solution containing 48 μM tellurium ions and 52 μM of selenium ions. The EC-SPR with the standard addition was able to determine the values close to the true values.

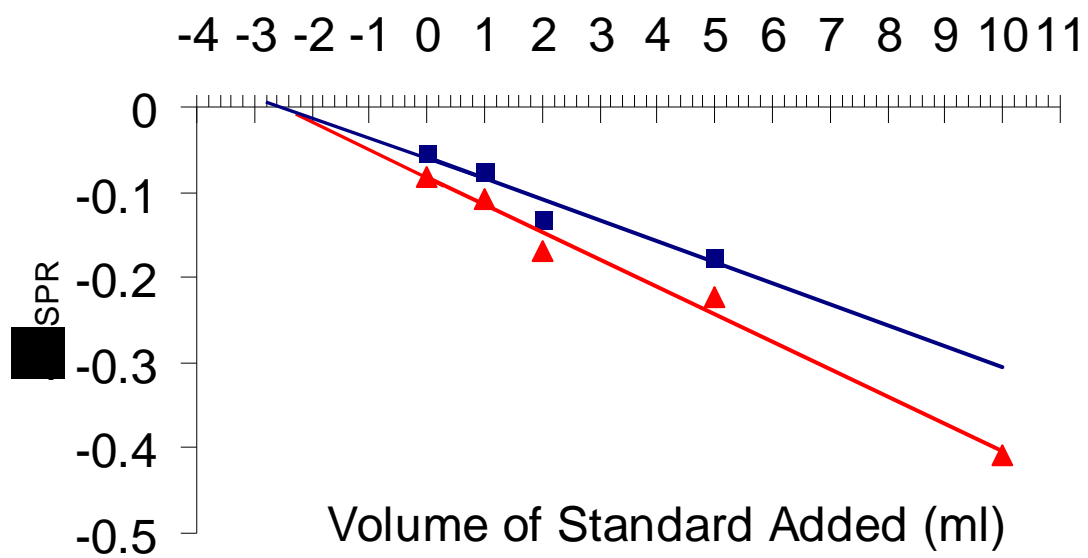


Figure 2.11 The standard addition method to determine the concentration of an unknown analyte containing TeO_3^{2-} and SeO_3^{2-} ions. (squares: tellurite; triangles: selenite)

Table 2.1 The calculated value for the concentration of TeO_3^{2-} and SeO_3^{2-} ions in the unknown analyte. X-intercept was determined from Figure 2.11.

	Te	Se
x-intercept (ml)	2.4	2.6
[Unknown] (μM)	48	52

2.4 Conclusions

Herein, we utilized the sensitivity of the surface plasmon resonance spectroscopy to probe the electrode-analyte interface in-situ with electrochemical experiments. The EC-SPR study on the gold oxide formation in 0.1 M HClO₄ shows that the SPR is sensitive to both faradaic and non-faradaic processes. The change in SPR angle during the faradaic process attributes to the change in the dielectric constant of the dielectric layer due to the deposition or stripping of the gold oxide at the gold-dielectric interface. The change in SPR angle during the nonfaradaic process attributes to the charging of the double layer which alters the electron density on the gold surface. This effect is more pronounced at the more positive potential relative to the potential of zero charge than at the more negative potential. The hysteresis of SPR signal was also observed and was more distinctive at the more positive potential. Up to now we only can speculate the sluggish kinetics in stripping of the gold oxide layer for the occurrence of hysteresis in SPR signal.

To further understand the underpotential deposition of the selenium on the gold surface, EC-SPR was used to probe the cyclic voltammetry experiment of the 1 mM of selenite solution in 0.1 M HClO₄. The SPR was able to monitor the conversion of the selenate, the Se UPD, and the stripping of selenium film on the gold surface. However, SPR could not resolve the C1 current peak due to the overwhelming double layer charging effect. Further study for that process is required.

The EC-SPR was used to probe the mass transport of the selenite ions to the electrode surface under a constant potential of 200 mV. The SPR is sensitive to detect the selenium film formation. EC-SPR sensor for pure selenium has a detection limit of 800

nM. However, the selenium detection using this method was impeded by the severe interference effect of other ions such as tellurite ions.

The stripping voltammetry in situ with EC-SPR was used to exploit the possibility of separating the contributions of selenium and tellurium deposition to the SPR signals. Initial study shows the SPR signal can be monitored at two different potentials 500 mV and 700 mV which correspond to the stripping potential of tellurium and selenium respectively. An increase in the change in SPR angle was observed when the concentration of one component increases. Due to this fact, the standard addition method was used in conjunction with EC-SPR experiment. This combined method show a promising result for the simultaneous sensing of tellurite and selenite in the solution.

2.5 References

- [1] Hanken, D. G.; Corn, R. M. *Anal. Chem.* **1997**, *69*, 3665-3673.
- [2] Chinowsky, T. M.; Saban, S. B.; Yee, S. S. *Sens. Actuators, B* **1996**, *35-36*, 37-43.
- [3] Jung, C. C.; Saban, S. B.; Yee, S.S.; Darling, R. B. *Sens. Actuators, B* **1996**, *32*, 143-147.
- [4] Iwasaki, Y.; Horiuchi, T.; Morita, M.; Niwa, O. *Surf. Sci.* **1999**, *427-428*, 195-198.
- [5] Iwasaki, Y.; Horiuchi, T.; Morita, M.; Niwa, O. *Sens. Actuators, B* **1998**, *50*, 145-148.
- [6] Iwasaki, Y.; Horiuchi, T.; Morita, M.; Niwa, O. *Electroanalysis* **1997**, *9*, 1239-1241.
- [7] Terrettaz, S.; Stora, T., Duschl, C.; Vogel, H. *Langmuir* **1993**, *9*, 1361-1369.
- [8] Georgiadis, R.; Peterlinz, K. A.; Rahn, J. R.; Peterson, A. W.; Grassi, J. H. *Langmuir* **2000**, *16*, 6759-6762.
- [9] Kang, X.; Cheng, G.; Dong, S. *Electrochem. Commun.* **2001**, *3*, 489-493.

- [10] Koide, S.; Iwasaki, Y.; Horiuchi, T.; Niwa, O.; Tamiya, E.; Yokoyama, K. *Chem. Commun.* **2000**, *9*, 741-742.
- [11] Rederstorff, M.; Krol, A.; Lescure, A. *Cell. Mol. Life Sci.* **2006**, *63*, 52–59.
- [12] Levander, O.A. “Selenium.” in: *Trace elements in human and animal nutrition 5th ed.* Mertz, W. ed. (Academic Press Inc.Orlando, Florida 1986) p 209-279.
- [13] Lemy, A.D.; Finger, S. E.; Nelson, M. K. *Environ. Toxicol. Chem.* **1993**, *12*, 2265.
- [14] www.epa.gov/safewater/dwh/hfacts.html
- [15] Carnrick, G. R.; Manning, D. C.; Slavin, W. *Analyst* **1983**, *108*, 1297 – 1312.
- [16] Örnemark, U.; Pettersen, J.; Olin, A. *Talanta* **1994**, *39*, 1089.
- [17] Buckley, W. T.; Budac, J. J.; Godfrey, D. V.; Koenig, K. M. *Anal. Chem.* **1992**, *64*, 724.
- [18] McCurdy, E. J.; Lange, J. D.; Haygarth, P. M. *Sci. Total Environ.* **1993**, *135*, 131.
- [19] Blotcky, A. J.; Ebrahim, A.; Rack, E.P. *Anal. Chem.* **1988**, *60*, 2734.
- [20] Prasad Pamidi, V. A.; Arunachalam, F. J.; Gangadbaran, S. *Electroanalysis* **1994**, *6*, 589.
- [21] Adeljou, S. B.; Bond, A. M.; Briggs, M. H.; Hughes, C. H. *Anal. Chem.* **1983**, *55*, 2076.
- [22] Tan, S. H.; Kounaves, S. P. *Electroanalysis* **1998**, *10*, 364.
- [23] McLaughlin, K.; Boyd, D.; Hua, Ch.; Smyth, M. R. *Electroanalysis* **1992**, *4*, 689.
- [24] Wang, J. *Stripping Analysis: Principles, Instrumentation, and Applications*, (VCH Publishers, Florida 1985).
- [25] Chinowsky, T. M.; Saban, S. B.; Yee, S. S. *Sens. Actuators, B* **1996**, *35-36*, 37-43.

- [26] Jung, C. C.; Saban, S. B.; Yee, S. S.; Darling, R. B. *Sens. Actuators, B* **1996**, *32*, 143-147.
- [27] Wang, S.; Forzani, E.; Tao, N. *Anal. Chem.* **2007**, *79*, 4427-4432
- [28] Chah, S.; Yi, J.; Zare, R. *Sens. and Actuators B* **2004**, *99*, 216-222
- [29] Hong, S.; Kang, T.; Moon, J.; Oh, S.; Yi, J. *Colloids and surf. A: Physicochem. Eng. Aspects* **2007**, *292*, 264-270.
- [30] May, L.; Russell, D. *Analytica Chimica Acta* **2003**, *500*, 119-125.
- [31] Mirkhalaf, F.; Schiffrin, D. J. *J. Electroanal. Chem.* **2000**, *484*, 182-188.
- [32] Ock, K.; Jang, G.; Roh, Y.; Kim, S.; Kim, J.; Koh, K. *Microchemical J.* **2001**, *70*, 301-305.
- [33] Nishimura, S.; Yoshidome, T.; Kyuutoku, W.; Mitsushio, M.; Higo, M. *Anal. Sci.* **2002**, *18*, 267-271.
- [34] Iwasaki, Y.; Horiuchi, T.; Morita, M.; Niwa, O. *Sens. Actuators, B* **1998**, *50*, 145-148.
- [35] Chen, J. H.; Nie, L. H.; Yao, S. Z. *J. Electroanal. Chem.* **1996**, *414*, 53-59.
- [36] Borkowska, Z.; Stimming, U. *J. Electroanal. Chem.* **1991**, *312*, 237-244.
- [37] Schultz, W. J.; Dickertmann, D. *Surface Sci.* **1976**, *54*, 489.
- [38] Beckmann, H. O.; Gerischer, H.; Kolb, D. M.; Lehmpfuhl, G. *Symp. Faraday Soc.* **1977**, *12*, 51
- [39] Gorden, J. G.; Ernst, S. *Surface Sci.* **1980**, *101*, 499
- [40] Kotz, R.; Kolb, D. M.; Sass, J. K. *Surface Sci.* **1977**, *69*, 359
- [41] Hansen, W. N.; Prostak, A. *Phy. Rev.* **1968**, *174*, 500

- [42] McIntyre, J. D.E. in *Advances in Electrochemistry and Electrochemical Engineering*, Vol. 9, Eds. P. Delahay and C. W. Tobias (Wiley, New York, 1973) p. 61.
- [43] Kolb, D. M.; Kotz, R. *Surf. Sci.* **1977**, *64*, 96
- [44] Uchida, H.; Ikeda, N.; Watanabe, M. *J. Electroanal. Chem.* **1997**, *424*, 5.
- [45] Uchida, H.; Hiei, M.; Watanabe, M. *J. Electroanal. Chem.* **1998**, *452*, 97.
- [46] Ataka, K.; Yotsuyanagi, T.; Osawa, M. *J. Phys. Chem.* **1996**, *100*, 10664.
- [47] Calvente, J. J.; Marinkovic, N. S.; Kovacova, Z.; Fawcet, W. R. *J. Electroanal. Chem.* **1997**, *421*, 49.
- [48] Kitamura, F.; Ohsaka, T.; Tokuda, K. *Electrochim. Acta* **1997**, *42*, 1235.
- [49] Kitamura, F.; Nanbu, N.; Ohsaka, T.; Tokuda, K. *J. Electroanal. Chem.* **1998**, *452*, 241.
- [50] Bruckenstein, S.; Shay, M. *J. Electroanal. Chem.* **1985**, *188*, 131.
- [51] Hayes, W. A.; Shannon, C. *Langmuir* **1996**, *12*(15), 3688-3694.

CHAPTER 3

STUDY OF PROTEIN-PROTEIN INTERACTION USING SURFACE PLASMON RESONANCE SPECTROSCOPY

3.1 Introduction

Protein-protein interactions are important for many biological functions and are one of the main fields in proteomics. Protein-protein interactions play major roles in mediating signals from the exterior of a cell to the interior (i.e. signal transduction),^{1,2} in programming cell death,³ and in acting as receptors in our immune system.⁴ Scientific methods of studying protein-protein interactions were reviewed⁵ since they have great significance in revealing the work of nature and in conducting medical research.

Proteins can exist as multi-subunit proteins⁵ and examples of such proteins are hemoglobin, tryptophan synthetase, aspartate transcarbamylase, core RNA polymerase, Q β -replicase, and glycyl-tRNA synthetase. Protein scientists have proposed a few reasons^{5,6} to explain why the living organism prefers to make multi-subunit proteins than to make a single large protein with multiple active sites. First, it is more efficient to build proteins from simpler subunits than to require multiple copies of the coding information to synthesize oligomers. Second, simple subunit proteins require less amino acid in their protein sequence and thus the translational errors can be minimized. Third, simple subunits can be synthesized at one locale, diffusing at a faster rate than a large multi-site protein and assembling to a multi-subunit at another locale. Finally, simple subunits can

be assembled in different ways to alter the magnitude of catalytic activity or type of biological responses.

One characteristic of the multi-subunit complexes is the ability to form substrate channels for the delivery of a reaction intermediate from one enzymatic active site to another within the enzymatic environment.⁷⁻⁹ The substrate channeling within the enzymatic system allows faster transfer of the reaction products from one active site to another,^{10,11} prevents decomposition of the intermediates from the extra-enzymatic environment,¹² and segregates the intermediates from other substrates which may compete for the same enzymatic reactions.^{13,14} For example, the alkanesulfonate monooxygenase system in our study consists of two protein components, the NAD(P)H-dependent flavin mononucleotide FMN reductase (SsuE) and monooxygenase (SsuD), which utilize reduced flavin (FMNH₂) as a substrate to convert alkanesulfonates to aldehyde and sulfite ion.^{15,16} The overall processes are summarized in scheme 1. Since the reduced flavin can be rapidly oxidized to generate oxygen radicals as intermediate products, the transfer of the reduced flavin may be more favorable through substrate channeling within the enzymatic environment than the free diffusion in the bulk solvent.¹⁷⁻²⁰ Previous studies from affinity chromatography, crosslinking experiments, and the spectroscopic studies showed strong evidence of the formation of a stable complex between the FMN reductase (SsuE) and monooxygenase (SsuD).²⁰



Scheme 1.

There are many methods for detection and analysis of protein-protein interactions, which have been summarized in a review article.⁵ Physical methods such as protein affinity chromatography, crosslinking, affinity blotting, and immunoprecipitating can be used for the detection of the protein-protein interaction. However, these methods can not determine the actual value of binding constant between two proteins. For the determination of the binding constant, there are two different categories of physical methods such as surface-based and solution-based methods. The surface based method tethers one type of protein onto a surface and monitors the binding in real time as another protein is introduced to the protein modified surface using the microfluidic flow. Unlike the surface based method, the solution based method determines the binding constant by titrating a protein against another protein and simultaneously monitoring the change in fluorescence of the reaction substrate bound between two proteins²⁰ (known as fluorometric titration) or the change in the heat release under isothermal condition²¹ (known as isothermal titration calorimetry). The binding constants determined by the surface based methods may not match with those obtained from the solution based methods due to a variety of potential artifacts.^{22,23} For example, the tethered protein on the surface could restrict the rotational freedom or hinder the folding/unfolding mechanism, altering the binding thermodynamics and kinetics. The surface based method also requires that the protein in mobile phase be transported to and from the bound protein in a rapid and uniform manner, avoiding effects of concentration gradients on the apparent rate constant.²⁴ Despite these shortcomings, the application of the surface based methods such as the protein arrays²⁵ are highly sought after since they allow parallel and high throughput screening of protein based pharmaceuticals.

The surface based method monitors the binding of two proteins under different concentrations of the protein analyte by different readout strategies, such as fluorescence,^{26,27} piezoelectricity,²⁸ chemiluminescence,²⁹ electrochemistry,³⁰ surface enhanced Raman spectroscopy,³¹ atomic force microscopy,³² and surface plasmon resonance spectroscopy.³³ There are three main advantages of surface plasmon resonance over other techniques. First, because the SPR measurements are based on refractive index changes, detection of protein-protein interaction does not require any fluorescent labels. Second, the measurements can be performed in real time. Finally, SPR is capable of detecting analytes over a wide range of molecular weights and binding affinities,³⁴ Because of its unique features, SPR has become a powerful tool for studying biomolecular interactions. For example, SPR has been used to investigate the protein-peptide interactions,³⁵ the cellular ligation,³⁶ the protein-DNA interactions,^{37,38} and the DNA hybridization.^{39,40}

The prior study²⁰ provides the evidence of the strong interactions between SsuE and SsuD using the solution based methods such as protein affinity chromatography, crosslinking, and fluorometric titration. Herein, the goal of the current study is to evaluate how closely the results from SPR experiments match with those performed by using the solution based method. The real-time measurements on the two-component alkanesulfonate monooxygenase system using SPR are demonstrated. The reported kinetic model²⁵ is used to determine the adsorption rate constants (k_a) and desorption rate constants (k_d), which yield the dissociation constant (K_d). The reported results will be compared with those in the prior study.²⁰

3.2 Experimental

3.2.1 Chemicals and proteins

Thioctic acid, butanethiol, 1-ethyl-3-(3-dimethylaminopropyl) carbodiimide hydrochloride (EDC), ethaneamine were obtained from Aldrich and were used as received. SsuD and SsuE are prepared as described in the reference 16.

3.2.2 Instrumentation

SPReeta sensors developed by Texas Instrument (TI) were used. This SPR system employs a light emitting diode (840 nm) with a polarizer, reflecting mirror, and Si-photodiode array. Each detection pixel corresponds to a narrow range of incident angle. The sensing region is coated with a semitransparent gold film (ca. 50 nm) with a Cr-adhesion layer (1 – 2 nm). A 12-bit three-channel electronic control box completes the interface between the sensor and a PC. Multichannel SPREETA software provided by TI monitors the changes in RI or resonance angle near the sensing surface calculates the statistical noise in the signal and displays the results.

The SPReeta evaluation module (SPR-EVM-BT) was purchased from Nomadics (Stillwater, OK, USA). The major components of the module were a SPReeta sensor, integrated flow cell, interface controller, and application software. A 12-bit analog-to-digital converter was utilized to provide a high resolution of 1×10^{-7} reflective index units (RIU), which corresponding to 0.001 degree in angle.

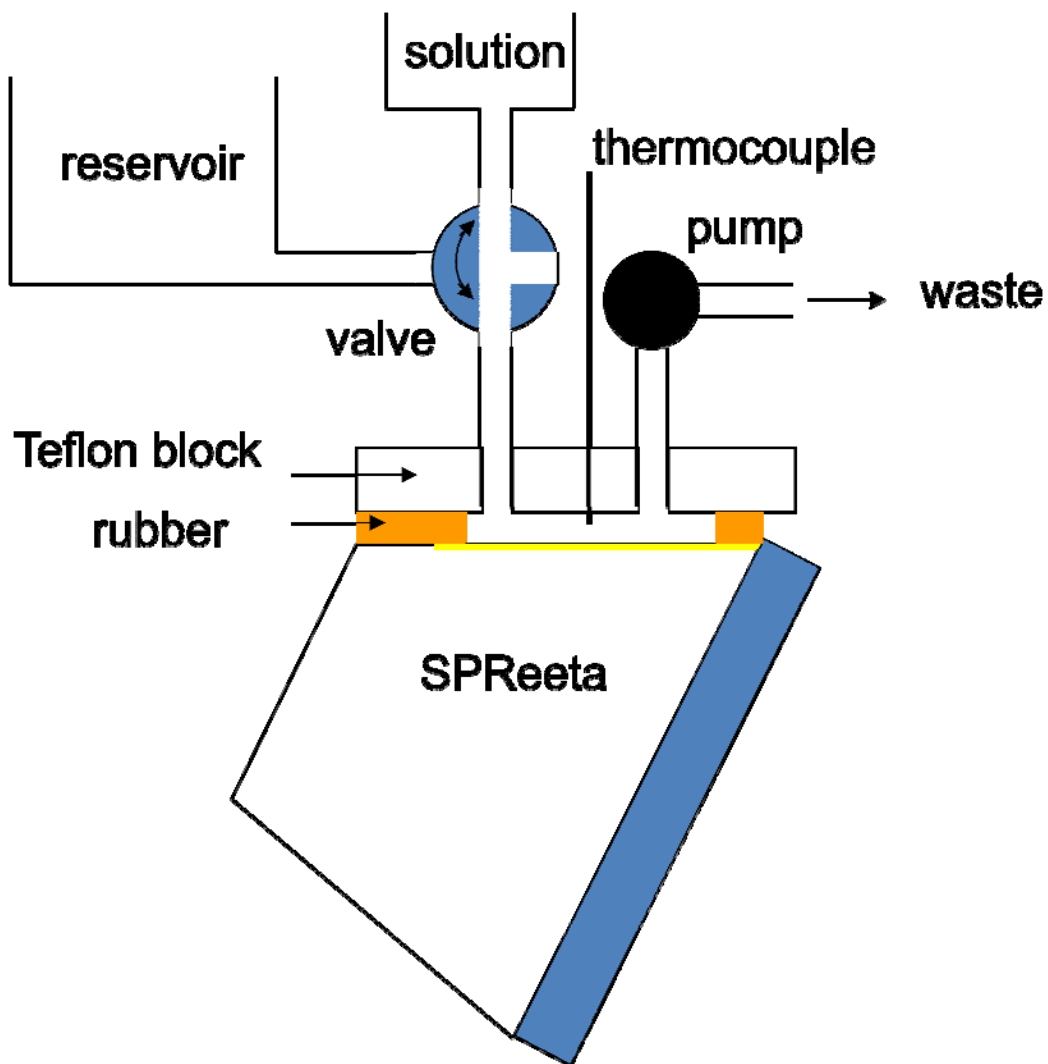


Figure 3.1 The flow-cell setup for SPR measurement.

3.2.3 Covalent immobilization of SsuD on SPReeta sensing surface

Simplified scheme for the covalent immobilization of SsuD was shown in Figure 3.2. The SPReeta sensing surface was first cleaned with 1% (v/v) Triton X 100 aqueous solution before it was soaked in the ethanol solution consisting of 0.5 M butanethiol and 0.5 M thioctic acid for 24 hours. The modified surface was rinsed with copious of pure ethanol to remove excess thiols before the series of experiments for protein interactions.

The thioctic acid modified surface was activated by flowing 4 ml of 1 mM EDC solution using the flow cell, followed by introducing 5 $\mu\text{g/ml}$ of SsuD solution at 4 $^{\circ}\text{C}$ and at a flow rate of 1 ml/min for 20 seconds. The SsuD modified surface was rinsed with distilled water for 90 seconds. In order to deactivate the unbound active EDC modified surface, 1 ml of 1 mM ethaneamine solution was flowed through the surface for 1 minute, followed by rinsing with distilled water. At this point, the flow rate was slowed down from 1 ml/min to 100 $\mu\text{L/min}$.

The SPR measurements for the protein binding were conducted using the same SsuD modified surface and three different concentrations of SsuE solution, 5.6 μM , 10 μM , and 14 μM . The SsuE solutions are free from buffer solution and FMN substrates. They were kept at 4 $^{\circ}\text{C}$ during the experiments. Between each binding experiment, a surface regeneration step was used. The surface regeneration was done by introducing 10 mM glycine and 10 mM hydrochloride solution, followed by rinsing with distilled water.

3.3 Results and discussion

Since SPR can monitor the change in the refractive index close to sensing surface, SPR can be used to probe binding events occurring at proximity of 100 nm from the

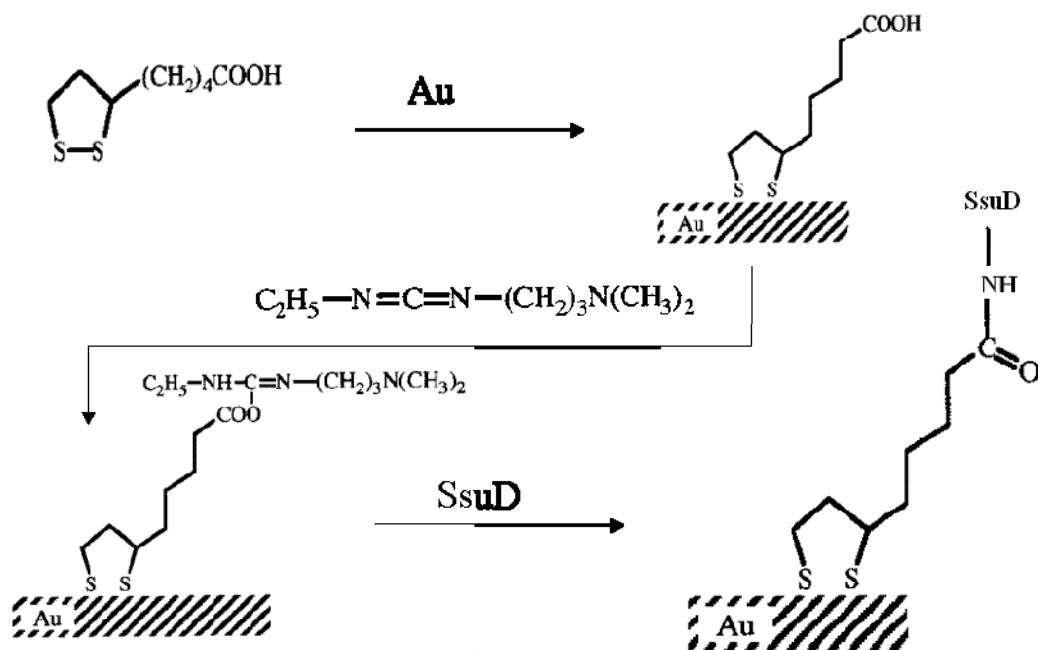


Figure 3.2 Schematic representation of the immobilization of the SsuD on gold surface.

sensing surface. The sensing surface is thin gold film, which allows generation of surface plasmons upon the excitation with photons and allows surface modification using thiol molecules. Figure 3.3 shows the SPR sensorgram of immobilization of SsuD. Initially when the SPR sensing surface was covered with thiol molecules, the SPR angle maintains at 69.64° under the distilled water. During the surface activation using EDC solution, the SPR angle increases to 69.81° , due to the surface modification. After the SsuD solution was introduced to the activated surface, the SsuD was bound to the surface via amine coupling, indicated by an increase in the resonance angle from 69.64° to 69.84° shown in Figure 3.3. The performance of the SPR was reported that every 0.1° shift in SPR angle corresponds to approximately 1ng/mm^2 of the protein immobilized on the surface.⁴¹ Therefore, the SPR shift in our experiment shows approximately 2 ng/mm^2 immobilized on the sensing surface. Finally, the surface was treated with ethaneamine to deactivate any unbound surface active site.

Figure 3.4 shows the real-time SPR measurement of the immobilized SsuD binding with SsuE and the surface regeneration. At point A in Figure 3.4, 5.6 mM of SsuE was introduced to the SsuD modified surface, resulting an increase in the SPR angle. At point B, the distilled water was used to rinse the surface to minimize any nonspecific adsorption. The SPR angle shifted from 69.834° to 69.854° and this indicates the binding of the SsuE on the immobilized SsuD. At point C, an equal molar of glycine and hydrochloride solution was used to cleave off the SsuE, regenerating the sensing surface.

The binding constant reveals the strength of protein-protein interaction and it is often expressed as dissociation constant or association constant (affinity constant).

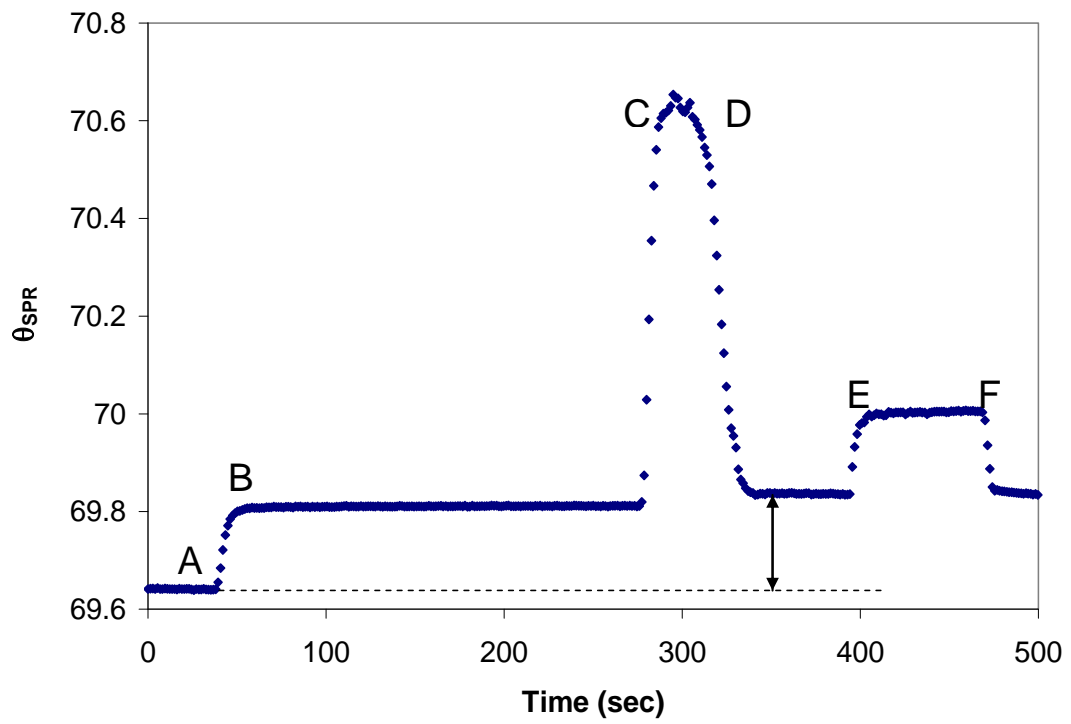


Figure 3.3 The SPR sensogram for the SsuD immobilization. (A) thioctic acid modified surface. (B) surface activation by EDC. (C) introduction of SsuD. (D) rinsing with distilled water. (E) surface deactivation by ethaneamine (F) rinsing with distilled water.

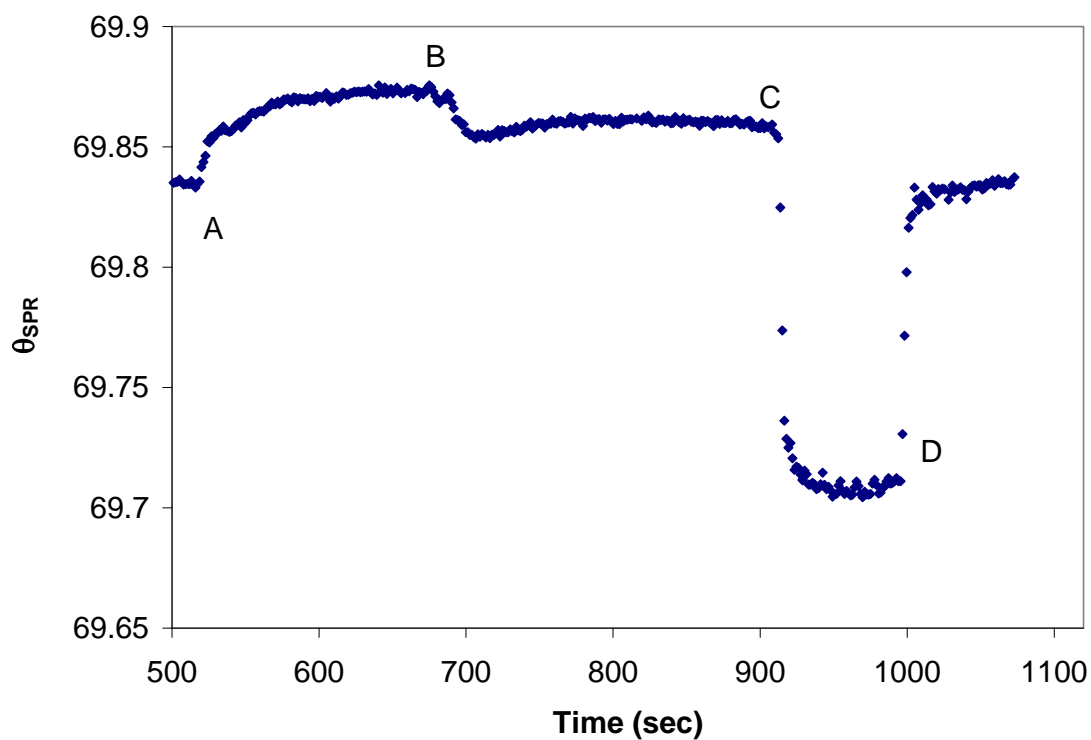


Figure 3.4 The SPR measurement of protein interactions between SsuE and immobilized SsuD. (A) introduction of SsuE. (B) rinsing with water (C) surface regeneration by glycine/hydrochloride solution (D) rinsing with water.

Equation 3.1 shows the formation of the protein complex at equilibrium.



where P_1^f and P_2^f are different free proteins and P_1P_2 is the protein-protein complex. The most common used terminology for the binding constant by biochemists is the dissociation constant (K_d). The dissociation constant is expressed as the following equation:

$$K_d = \frac{[P_1^f][P_2^f]}{[P_1P_2]} \quad \text{Eq. 3.2}$$

where $[P_1^f]$, $[P_2^f]$, and $[P_1P_2]$ are the concentrations of the free protein 1, the free protein 2 and the protein complex respectively. A smaller value of K_d indicates the equilibrium favors the formation of the protein complex and also indicates the strength of protein-protein interaction is high. Another terminology for the binding constant is association or affinity constant (K_a), which is reciprocal of the dissociation constant.

Both dissociation and association constant can be determined by the concentrations of the free protein and the protein complex. However, these concentrations may be difficult to be determined experimentally. Since SPR monitors the binding of two proteins in real time, the SPR signals correspond to the kinetic model of the protein binding, which has been developed by Brooks, et al.⁴² and Corn, et al.²⁵. For the reversible interaction shown in equation 3.1, the rate of formation of the protein complex at time, t , can be written as

$$\frac{d[P_1P_2]}{dt} = k_a[P_1^f][P_2^f] - k_d[P_1P_2] \quad \text{Eq. 3.3}$$

where k_a is the association rate constant and k_d is the dissociation rate constant. After protein interactions for some time, t , the remaining of protein 2 can be expressed as equation 3.4 if a stoichiometric ratio for the binding between two proteins is 1:1.

$$[P_2^f] = [P_2^f]_0 - [P_1P_2] \quad \text{Eq. 3.4}$$

where $[P_2^f]_0$ is the concentration of protein 2 at $t=0$. In the SPR experiment, one protein is immobilized on the surface while another protein is present in the mobile phase. If P_2 is the surface bound protein (s denotes as surface bound protein) and P_1 is the mobile protein, Equation 3.4 can be rewritten as

$$[P_2^s] = [P_2^s]_0 - [P_1P_2] \quad \text{Eq. 3.5}$$

Substituting Eq. 3.5 into Eq. 3.3 yields

$$\frac{d[P_1P_2]}{dt} = k_a[P_1^f]([P_2^s]_0 - [P_1P_2]) - k_d[P_1P_2] \quad \text{Eq. 3.6}$$

The observed SPR signal, R , is proportional to the formation of protein complex at the surface and the maximum SPR signal, R_{\max} , will be proportional to the concentration of the bound protein 2.⁴³ Therefore the Eq. 3.6 can be expressed as

$$\frac{dR}{dt} = k_a[P_1^f](R_{\max} - R) - k_d R \quad \text{Eq. 3.7}$$

where dR/dt is the rate of formation of protein complex on the surface.

Rearranging Eq. 3.7 gives

$$\frac{dR}{dt} = k_a[P_1^f]R_{\max} - (k_a[P_1^f] + k_d)R \quad \text{Eq. 3.8}$$

Solving the differential equations yields,

$$R = \frac{k_a [P_1^f] R_{\max} (1 - e^{-(k_a [P_1^f] + k_d)t})}{k_a [P_1^f] + k_d} \quad \text{Eq. 3.9}$$

Figure 3.6 shows the data points from the real time SPR measurements of SsuD binding with SsuE at different concentrations of SsuE and the mathematical fitting (solid line) using the Eq. 3.9. Apparently as the concentration of SsuE increases the surface saturates at a faster rate and the shift in resonance angles increases at a faster rate. The SPR measures the kinetics of the protein binding. Another observation is that the plateau of each curve occurring at different levels suggested that the stoichiometric ratio of SsuE and SsuD may change as a function of protein concentration in the solution. Equation 3.9 was used to fit the SPR curves shown as solid lines to obtain the value of k_a and k_d at different SsuE concentrations and the results were summarized in Table 3.1. The average association and dissociation rate constant are $4400 \pm 230 \text{ M}^{-1} \text{ s}^{-1}$ and $0.0010 \pm 0.00069 \text{ s}^{-1}$ respectively. The dissociation constant (K_d) was calculated to be $0.24 \pm 0.17 \text{ }\mu\text{M}$ which is two order of magnitudes higher than the reported value²⁰ of $0.0022 \text{ }\mu\text{M}$. This implies that SPR measured a weaker interaction between SsuD-SsuE than the solution based method. The free SsuD in the solution exists as a tetramer at equilibrium condition.¹⁶ When SsuD was immobilized on the surface, the subunits of SsuD facing towards the surface might be blocked and were unable to bind to SsuE. Since the amount of SsuE binds to the immobilized SsuD reduces, this reflects on the higher value of the dissociate constant.

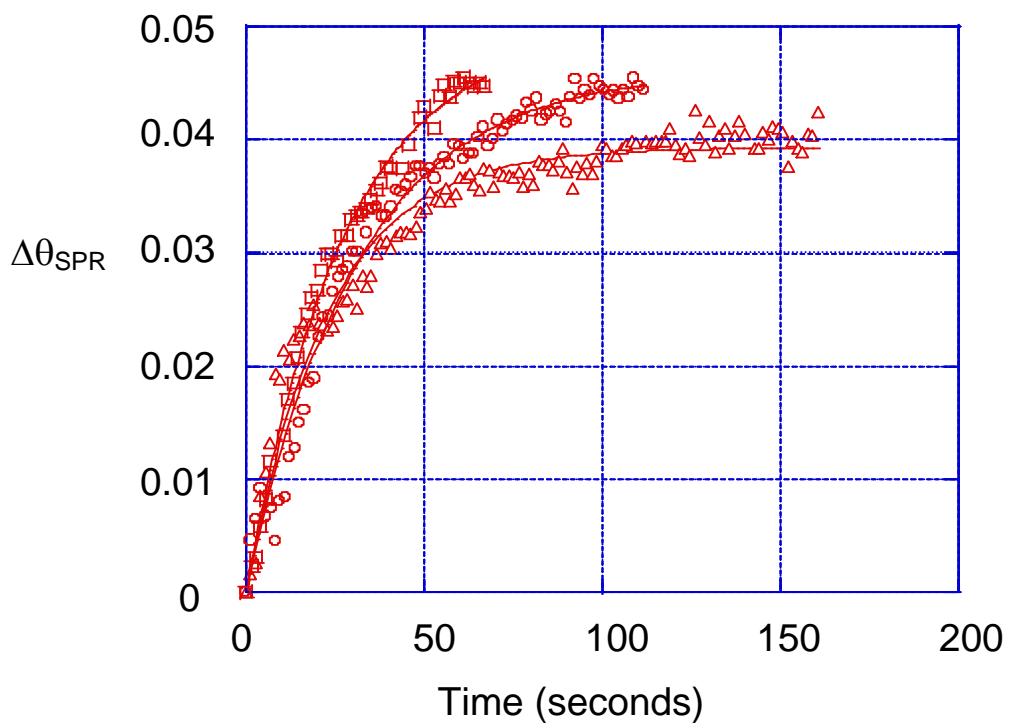


Figure 3.5 The shifts in SPR angle upon the loading of SsuE at different concentrations. (triangle: 5.6 μM ; circle: 10 μM ; square: 14 μM)

Table 3.1 The data fitting results

[SsuE] (M)	R_{max}	k_a (M⁻¹ s⁻¹)	k_d(s⁻¹)	K_d (M)	k_a Error	k_d Error	Corr. Coef
5.6E-06	0.041	7400	1.8E-03	2.4E-07	220	3.3E-04	0.975
1.0E-05	0.047	3100	6.2E-04	2.0E-07	71	3.0E-04	0.991
1.4E-05	0.051	2600	6.8E-04	2.7E-07	49	5.2E-04	0.997

3.4 Conclusions

The protein interactions between SsuD and SsuE in the alkanesulfonate monooxygenase system were used as the model system to compare the dissociation constants determined from the surface based and the solution based methods. Since the surface based method allows the high throughput analysis and is very suitable for the proteomic explorations, the direct comparison between two different methods makes the biochemistry community aware of the difference in the determination of the dissociation constant. The surface based method employed in our current study is the surface plasmon resonance spectroscopy. The real time SPR measures the kinetic parameters of the protein binding between the immobilized SsuD and the mobile SsuE. The developed mathematical model was used to determine the values of the association and dissociation rate constant ($4400 \pm 230 \text{ M}^{-1} \text{ s}^{-1}$ and $0.0010 \pm 0.00069 \text{ s}^{-1}$ respectively). The calculated dissociation constant (K_d) was $0.24 \pm 0.17 \text{ }\mu\text{M}$ which is two orders of magnitudes higher than the reported value of $0.0022 \text{ }\mu\text{M}$ from the solution based method. The different plateau level for each protein uptake curve suggested that the stoichiometric ratio between SsuE and SsuD may change as a function of protein concentration in solution. The mathematical model, assumed a constant 1:1 stoichiometric ratio, could not account for such stoichiometric change during the binding. However, the fitting results suggested the surface based method measures weaker SsuD-SsuE interactions compared with the solution based method. This discrepancy may also arise from the steric effects for some interaction sites after the immobilization of SsuD tetramers.

3.5 References

- [1] Eyster, K. M. *Biochem. Pharmac.* **1998**, *55*, 1927–1938.
- [2] Souroujon, M. C.; Mochly-Rosen, D. *Nat. Biotechnol.* **1998**, *16*, 919–924.
- [3] Arkin, M. R.; Wells, A. J. *Drug Discovery* **2004**, *3*, 301.
- [4] von Mehren, M.; Adams, G. P.; Weiner, L. M. *Annual Review of Medicine* **2003**, *54*, 343-369.
- [5] Phizicky, E.; Fields, S. *Microbiological Reviews* **1995**, *59*(1), 94-123.
- [6] Klotz, I. M., Darnall, D. W.; Langerman, N. R. “Quarternary structure of proteins”, p. 293–411. In H. Neurath and R. L. Hill (ed.), *The proteins*. (Academic Press, Inc., New York 1975).
- [7] Spivey, H. O.; Ovadi, J. *Methods* **1999**, *19*, 306-321.
- [8] Anderson, K. S. *Methods Enzymol.* **1999**, *308*, 111-145.
- [9] Srere, P. A. *Annu. Rev. Biochem.* **1987**, *56*, 89-124.
- [10] Easterby, J. S. *Biochem J.* **1981**, *199*, 155-161.
- [11] Westerhoff, H. V.; Welch, G. R. *Curr. Top. Cell. Regul.* **1992**, *33*, 361-390.
- [12] Rudolph, J.; Stubbe, J. *Biochemistry* **1995**, *34*, 2241-2250.
- [13] Ushiroyama, T.; Fukushima, T.; Styre, J. D.; Spivey, H. O. *Curr. Top. Cell. Regul.* **1992**, *33*, 291-307.
- [14] Ovadi, J.; Huang, Y.; Spivey, H. O. *J. Mol. Recognit.* **1994**, *7*, 265-272.
- [15] Eichhorn, E.; Van der Ploeg, J. R.; Leisinger, T. *J. of Biol. Chem.* **1999**, *274*(38), 26639-26646.
- [16] Gao, B.; Ellis, H. R. *Biochem. and Biophys. Research Comm.* **2005**, *331*(4), 1137-1145.

- [17] Bruice, T. C. "A progress report on studies of the activation of molecular oxygen by dihydroflavins", p. 265–277. In V. Massey and C. H. Williams (ed.), *Flavins and flavoproteins*. (Elsevier North-Holland, Inc., New York 1982).
- [18] Imlay, J. A. *Annu. Rev. Microbiol.* **2003**, *57*, 395–418.
- [19] Walsh, C. *Annu. Rev. Biochem.* **1978**, *47*, 881–931.
- [20] Abdurachim, K.; Ellis, H. R. *J. of Bacteriology* **2006**, *188* (23), 8153-8159.
- [21] Pierce, M. M.; Raman, C. S.; Nall, B. T. *Methods* **1999**, *19* (2), 213-221.
- [22] Myszka, D. G. *Curr. Opin. Biotechnol.* **1997**, *8*, 50–57.
- [23] Day, Y. S. N.; Baird, C. L.; Rich, R. L.; Myszka, D. G. *Protein Science* **2002**, *11*(5), 1017-1025.
- [24] Myszka, D. G.; He, X.; Dembo, M.; Morton, T. A.; Goldstein, B. *Biophys. J.* **1998**, *75*, 583–594.
- [25] Wegner, G. J.; Wark, A. W.; Lee, H. J.; Codner, E.; Saeki, T.; Fang, S.; Corn, R. M. *Anal. Chem.* **2004**, *76*(19), 5677-5684.
- [26] Vuori, J.; Rasi, S.; Takala, T.; Vaananen, K. *Clin. Chem.* **1991**, *37*, 2087.
- [27] Xu, Y.-Y.; Pettersson, K.; Blomberg, K.; Hemmila, I.; Mikola, K.; Lovgren, T. *Clin. Chem.* **1992**, *38*, 2038.
- [28] Chu, X.; Lin, Z. H.; Shen, G. L.; Yu, R. Q. *Analyst.* **1995**, *120*, 2829–2832.
- [29] Brown, C. R.; Higgins, K. W.; Frazer, K.; Schoelz, L. K.; Dyminski, J. W.; Marinkovich, V. A.; Miller, S. P.; Burd, J. F. *Clin. Chem.* **1985**, *31*, 1500.
- [30] Hayes, F. J.; Halsall, H. B.; Heineman, W. R. *Anal. Chem.* **1994**, *66*, 1860.
- [31] Ni, J.; Lipert, R. J.; Dawson, G. B.; Porter, M. D. *Anal. Chem.* **1999**, *71*(21), 4903-4908.

- [32] Dong, Y.; Shannon, C. *Anal. Chem.* **2000**, 72(11), 2371-2376.
- [33] Lyon, L. A.; Musick, M. D.; Natan, M. J. *Anal. Chem.* **1998**, 70, 5177.
- [34] McDonnell, J. M. *Curr Opin Chem Biol.* **2001**, 5, 572-577.
- [35] Shliom, O.; Huang, M.; Sachais, B.; Kuo, A.; Weisel, J. W.; Nagaswami, C.; Nassar, T.; Bdeir, K., Hiss, E.; Gawlak S.. *J. Biol. Chem.* **2000**, 275, 24304-24312.
- [36] Quinn, J. G.; O'Neill, S.; Doyle, A.; McAtamney, C.; Diamond, D.; MacCraith, B. D.; O'Kennedy, R. *Anal. Biochem.* **2000**, 281, 135-143.
- [37] Shumaker-Parry, J. S.; Aebersold, R; Campbell, C. T. *Anal. Chem.* **2004**, 76, 2071-2082.
- [38] Mischiati, C.; Borgatti, M.; Bianchi, N.; Rutigliano, C.; Tomassetti, M.; Feriotto, G.; Gambari, R. *J. Biol. Chem.* **1999**, 274, 33114-33122.
- [39] Peterlinz, K. A.; Georgiadis, R. M. *J Am Chem Soc.* **1997**, 119,3401-3402.
- [40] Peterson; A. W.; Wolf, L. K.; Georgiadis, R. M. *J Am Chem Soc.* **2002**, 124, 14601-14607.
- [41] Wilson, W. D. *Analyzing Science* **2002**, 295, 2103–2105.
- [42] O'Shannessy, D. J.; Brigham-Burke, M.; Soneson, K. K.; Hensley, P.; Brooks, I. *Anal. Biochem.* **1993**, 212, 457-468.
- [43] Karlsson, R.; Michaelsson, A.; Mattsson, L. *J. Immuno. Methods* **1991**, 145, 229-240

CHAPTER 4

**SENSITIVITY STUDIES OF SURFACE ENHANCED RAMAN SCATTERING
ON Au/Ag FILM OVER NANOSPHERES AND Au/Ag COATED HIGH
EFFICIENCY PARTICULATE AIR FILTER**

4.1 Introduction

Surface enhanced Raman spectroscopy (SERS) has been exploited as a tool to quantify analytes at trace level.¹⁻⁵ The basis for the ultra sensitivity of SERS is the huge enhancements in the effective Raman cross section of molecules within the electromagnetic field of the localized surface plasmon (LSPR) wave. This LSPR field has strongly associated with the surface roughness⁶ from the nanoscaled features of the noble metal surface. The pioneer works in SERS were carried out using the roughened noble metal surface⁷ or the aggregation of colloidal metal particles⁸ to produce an enhancement factor of 10^5 - 10^6 . Such substrate that can produce the surface enhanced effect is called SERS substrate. As the fabrication techniques advance, new SERS substrates such as metal film over nanospheres (FONS) and silver nanoisland array have been introduced and their sensing applications have been investigated.⁹

Vibrational spectroscopic methods are valuable analytical tools because they provide the unique vibrational fingerprints for small molecule analytes and the capability for quantitative analysis. Surface enhanced Raman spectroscopy has been proven as a versatile vibrational spectroscopic method for the sensing of polycyclic aromatic

compounds,¹⁰ organophosphorus compounds,¹¹ chlorinated pesticides,¹² fungicides,¹³ and other growth inhibitors.¹⁴ As far as the detection for the bio-agents is concerned, SERS is capable of detecting bacillus spores¹⁵ and bacteria.¹⁶ The sensitivity of the SERS can reach as low as single molecule;^{1,17} however, such sensitivity depends on the nature of the target molecule and the degree of the interaction between the target molecule and the SERS substrate.

There are few ways to evaluate the performance of any SERS based sensors. One way is to introduce an internal standard to the analyte solution which shows a similar interaction behavior towards the sensing surface. The detection of dipicolinic acid and glucose in the presence of NO_3^- ions as an internal standard^{18,19} and the quantification of creatinine in the presence of isotopic labeled creatinine²⁰ are two of the examples. Another way to evaluate the performance of any SERS sensors in terms of the detection limit and the dynamic range is to monitor the SERS signal as a function of known surface coverage.²¹ Finally, a standard addition technique can be implemented to determine the unknown concentration of sample molecules on the surface at a fixed location after the incremental amount of standard solution is added to the SERS substrate.

In modern aircraft, a high efficiency particulate air or HEPA filter is used to efficiently dissipate any particulate matter, smoke, odor, and bacteria that are present in the air cabin.²² It is the only line of defense to ensure the safety of the passenger from exposure to toxic substances which might be released during the flight. A HEPA filter based SERS substrate can serve as both the sample collection medium and Raman signal amplifier in the detection of airborne chemicals.

The work presented herein uses both metal FONS and metal coated HEPA filter as tools for the quantitative 4-aminothiophenol (4-ATP) detection. In our study, the SERS substrates were prepared by coating the monolayer of nanospheres and the HEPA filter with sequent depositions of 5.3 μm base layer of silver and 5.3 μm top layer of gold (Au/Ag). For the characterization of the Au/Ag coated FONS, we used the mixed self-assembled monolayer of 4-ATP and decanethiol (DT). The coverage of the 4-ATP, adjusted by changing the 4-ATP concentrations, is monitored by the SERS and the electrochemical method. From the reduction current of the 4-ATP, we can determine the number of 4-ATP molecules on the gold surface, which can be related to the SERS intensity to generate a calibration curve. For the Au/Ag coated HEPA filter, we used the standard addition technique to overcome the irreproducibility of the surface roughness in quantitative analysis of 4-ATP solution concentrations.

4.2 Experimental

4.2.1 Materials

All the chemicals used were reagent grade or better. Perchloric acid and potassium chloride were purchased from Fisher Scientific Inc. Decanethiol and 4-aminothiophenol were purchased from Aldrich. Decanethiol was used without further purification while 4-aminothiophenol was purified by the following steps.²² 4-ATP was dissolved in water by adding sulfuric acid (1 N). The solution was decolorized by adding activated charcoal followed by filtration to remove the charcoal. The remained solution was titrated with sodium hydroxide to a neutral pH. The organic phase was extracted with a small amount of dichloromethane. The light yellow solid 4-ATP was obtained by

evaporating the dichloromethane and stored in the dark at 4 °C. Monodispersed polystyrene latex spheres with a diameter of 600 nm as 8.1 wt% solutions in water were purchased from Interfacial Dynamics Corporation. All solutions were prepared using reagent grade water (18.2 MΩ cm) from a Barnstead “NANO infinity” ultrapure water system.

4.2.2 SERS substrate fabrication

Au/Ag FONS. The polystyrene nanospheres suspension was diluted to 4 wt% solution in water. The 20 μL of diluted suspension was used to spin-coate a polystyrene nanosphere film at 500-1000 rpm on the freshly cleaved mica with an area of 4 cm². The specimen-to-specimen reproducibility of the nanosphere film was excellent. After allowed air dry for 24 hours, the nanosphere film was sputter-coated with base layer of silver and the top layer of gold, resulting Au/Ag FONS. The sputter coating was carried out by PELCO SC-7 sputter coater from Ted Pella Inc. Following the operation conditions such as 70 mm working distance between the metal target and the substrate, 0.08 mbar of the sputtering chamber under Argon gas environment, 30 mA of sputtering current, and 60 seconds of the sputtering time, the thickness of the gold and silver produced is estimated to be 5.3 nm. After sputter coating, each Au/Ag FONS on mica was divided radially into 10 triangular pieces for self-assembly of the mixed monolayer.

Au/Ag coated HEPA. The HEPA filter was used as received and was sputter coated with base layer of silver and the top layer of gold with the same conditions used to prepare FONS.

4.2.3 Self-assembled monolayer preparation

Previously prepared SERS substrates were rinsed with ethanol, air dried and then immersed for 6 hours in an ethanol solution containing a total thiol (one or two types of thiol molecules) concentration of 1mM. Upon emersion, the specimen was rinsed with copious amount of ethanol.

4.2.4 Electrochemical measurement

All electrochemistry experiments were carried out using a BAS Epsilon Potentiostat workstation. A conventional three electrode configuration was employed and all cell components were constructed from Teflon. In all cases, the gold wire electrode or Au/Ag FONS were the working electrode, a platinum net was the counter electrode, and Ag|AgCl(sat) was the reference electrode. All electrochemical behaviors obtained are corresponding to SAMs adsorbed on polycrystalline Au surfaces. All electrochemistry is carried out under a blanket of Ar after degassing the cell for 15 minutes.

Cyclic voltammograms of a clean Au electrode in a solution containing 1mM $K_3Fe(CN)_6$, and 0.1 M KCl were recorded at a range of scan rates. The gold surface area was determined by the slope of the line where peak current was plotted against the square root of the scan rate as the following equation:

$$i_p = (2.69 \times 10^5)n^{3/2}AD_0^{1/2}C_0\nu^{1/2} \quad \text{Eq. 4.1}$$

where i_p is the peak current in amperes, n is the number of electrons in the half redox reaction ($n = 1$ for $Fe(CN)_6^{3-} / Fe(CN)_6^{4-}$ redox couple), A is the total electrode area (cm^2), D_0 is the diffusion coefficient of the analyte ($7.63 \times 10^{-6} cm^2/sec$ for ferricyanide anion in 0.1 M KCl), C_0 is the bulk concentration of $K_3Fe(CN)_6$, and ν is the scanning rate.

4.2.5 Atomic force microscopy imaging

All AFM images were acquired using an atomic force microscope Autoprobe CP from Park Scientific, and an Acquisition Module from Thermomicroscope. The imaging probes were ULNC-AUMT-AB mounted silicon cantilevers with spring constant 2.1 N/m (Digital Instruments). All images were acquired with a 100 μm Scanner Master with contact mode in air at room temperature. The images obtained were analyzed with PSI ProScan 1.5 data analysis software.

4.2.6 SERS apparatus

Raman measurements were carried out by a Renishaw inVIA microscope system with a 514.5 nm argon ion laser and a 50 \times long working distance objective lens to focus the laser beam and to generate the laser beam size of 1 μm diameter. A low laser power (<0.30 mW) was used to avoid laser heating on the sample. Using 180 $^\circ$ backscattering geometry, the scattered light was collected by the objective lens and passed through a holographic notch filter to remove the Rayleigh line. The detector was a thermoelectrically cooled charge-coupled device (CCD) detector of 576 \times 384 pixels. The accumulated exposure time of the CCD detector was between 10 and 40 seconds and the instrumental spectral resolution ranged from 1.0 to 1.5 cm^{-1} .

4.3 Results and discussions

As mentioned earlier, one requirement to calibrate the performance of SERS based sensor is to relate the SERS signals to the known concentrations of surface-bound

analyte molecules. Self-assembled monolayer of the thiol compounds offers a way to produce a well-defined dimensional, thermodynamically controlled, and highly stable modifying layer on gold electrode for the needs of characterizing SERS substrate. Certain thiol compounds with functional groups such as amino, nitro, and ferrocene have unique electrochemical and spectroscopic properties which can be used to determine the number of functional thiol molecules immobilized on the gold surface.

4.3.1 Characterization of the mixed monolayers of 4-ATP and DT using electrochemistry and SERS

The cyclic voltammogram of a clean gold electrode in 1 M HClO₄ shows one anodic peak at 1.050 V and one cathodic peak at 0.830 V, which correspond to the formation and the stripping of gold oxide respectively. Figure 4.1 shows the cyclic voltammogram of a gold electrode modified with 4-ATP molecules and it is recorded at a scan rate of 100 mV/s in 1 M HClO₄ supporting electrolyte. It is apparent that the 4-ATP molecules on the gold electrode cause an oxidative current peak at 0.800 V and two reductive current peaks at 0.48 V and 0.26 V. These electrochemical features for 4-ATP have been observed from our pioneer work.²² The oxidative current peak at 0.800 V was attributed to the oxidation of 4-ATP molecule to the cation radical.²³ However, if the gold electrode was modified with DT molecules, we would not see these peaks. Therefore, integrating the area under the 4-ATP oxidative peak at 0.8 V can determine the number of 4-ATP molecules on the gold surface.

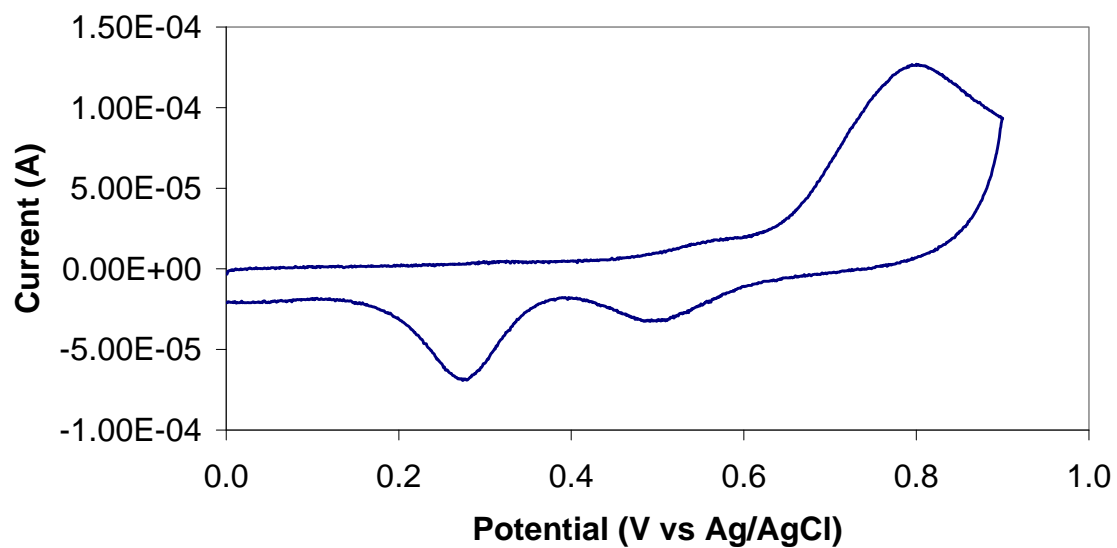


Figure 4.1 The cyclic voltammogram of 4-ATP self-assembled monolayer on a gold electrode in 1 M HClO₄ supporting electrolyte.

Figure 4.2 shows that 4-ATP peak current density at 0.80 V varies with the mole fraction of 4-ATP in the mixed thiol solution used for the preparation of mixed SAMs. Higher concentration of 4-ATP solution generates a higher coverage of 4-ATP molecules on the gold surface, which results a higher oxidative current. In Figure 4.3, the surface coverage density of 4-ATP in the various mixed SAMs is nonlinear with respect to the mole fraction of 4-ATP in the assembling solution. This suggests that 4-ATP interacts with DT in a different degree than 4-ATP molecules interacting among themselves. This behavior is similar to the observation made by Whitesides, et al.²⁵ A quadratic data fitting is applied to the Figure 4.2, yields an equation for calculating the coverage at any given 4-ATP mole fraction in the solution.

$$\Gamma = 3 \times 10^{-10} X_{ATP}^2 + 4 \times 10^{-11} X_{ATP} \quad \text{Eq. 4.2}$$

where Γ is the surface coverage density of 4-ATP molecules and X_{ATP} is the mole fraction of 4-ATP in the assembling solution.

We turn now to the discussion of characterizing mixed monolayer on Au/Ag FONS with SERS measurements. Figure 4.3 shows the normal Raman spectra of 4-ATP crystal and SERS spectra of 4-ATP monolayer on the Au/Ag FONS, which are similar with the literature reported.²⁴ The selected peak assignments are shown in the Table 4.1. Unlike 4-ATP, DT does not have any SERS peak in the wavenumbers ranging from 100 to 2000 cm^{-1} . This optical difference allows us to design an experiment where the SERS intensity of 4-ATP is monitored with different SAMs prepared from various mole fractions of 4-ATP solutions.

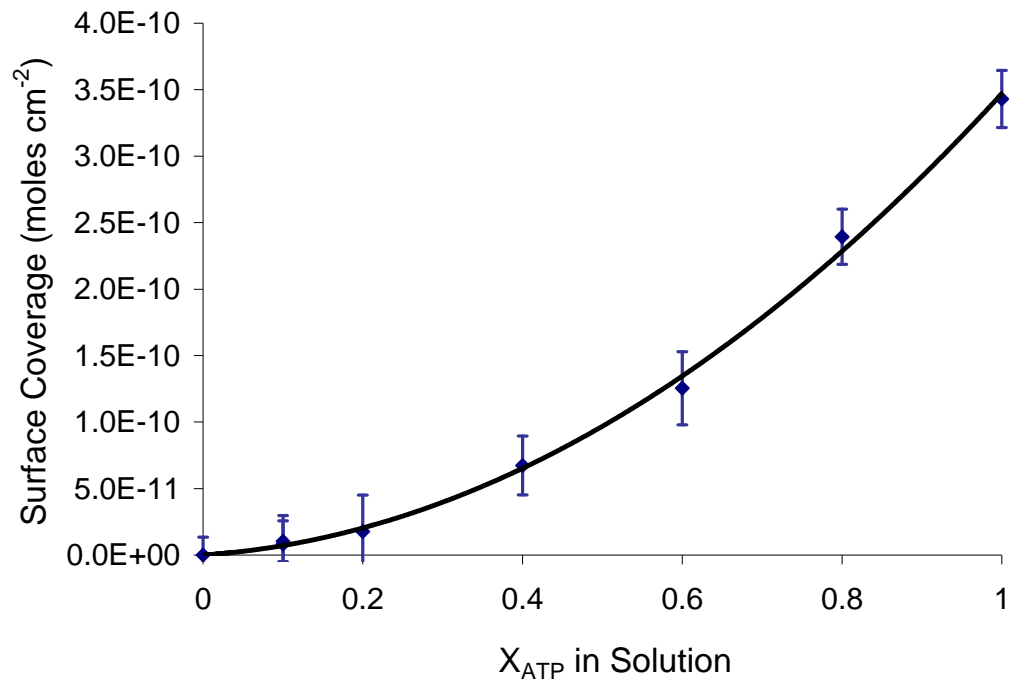


Figure 4.2 The relationship between surface coverage and the mole fraction of ATP in the solution.

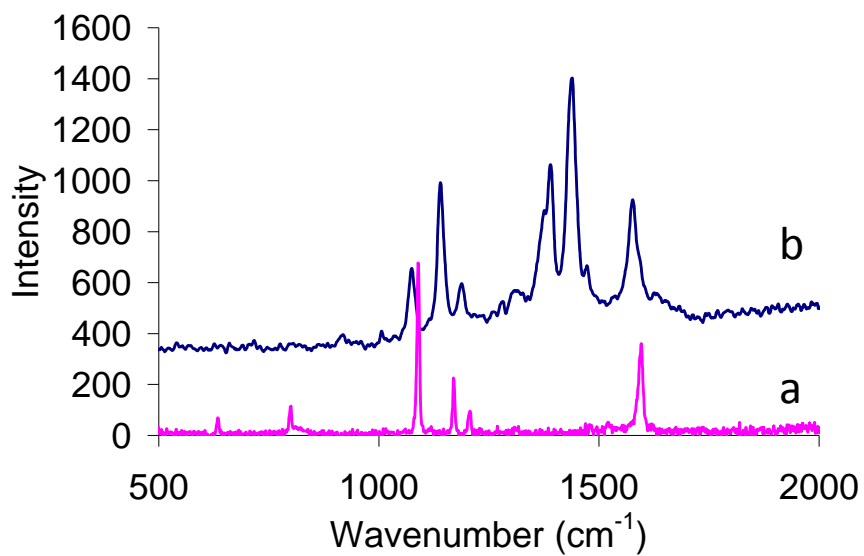


Figure 4.3 The Raman spectrum of 4-ATP. (a) the normal Raman spectra of 4-ATP crystal and (b) the SERS spectra of 4-ATP adsorbed on the Au/Ag FONS.

Table 4.1. The assignment of selected SERS bands for 4-ATP.²⁴

No	ν (cm ⁻¹)	Assignment
1	1077	ν C-S
2	1142	δ C-H
3	1391	δ C-H + ν C-C
4	1440	δ C-H + ν C-C
5	1573	ν C-C

Figure 4.4 shows the AFM image of Au/Ag FONS on mica. The black circle at the center of Figure 4.4 indicates the relative size of laser beam compared to the diameter of the polystyrene nanospheres. SERS experiments were conducted in such a way that the laser beam was focus on the defect-free regions of the FONS and each data point was chosen at least 2 μm apart from one another for statistical analysis.

SERS intensity on the band 1077 cm^{-1} was measured at various 4-ATP solution concentrations shown in Figure 4.5. As the concentration of the 4-ATP solution increase more 4-ATP molecules adsorbed on the FONS surface resulting higher Raman signal. From equation 4.2, we could relate the SERS intensity to the number of moles of 4-ATP molecules adsorbed on the Au/Ag FONS shown in Figure 4.6. One striking observation is that there is a phase transition (a change in slope) occurs at 4-ATP mole fraction of 0.4. This may due to the orientation changes imposed by the increasing concentrations of the 4-ATP on the gold surface. At the low surface concentration of 4-ATP, the orientation of 4-ATP is dictated by the orientation of the DT, which has an estimated $25\text{-}35^\circ$ of tilt angle²⁵ away from surface normal. At the higher surface concentration, the interactions between DT molecules are weakened and ATP molecules tend to form pi stacking and a bending configuration. It is well-known that vibration of surface confined molecules such as 4-ATP with a component along the surface normal will be enhanced more than the vibrations with the components parallel to the surface.²⁶

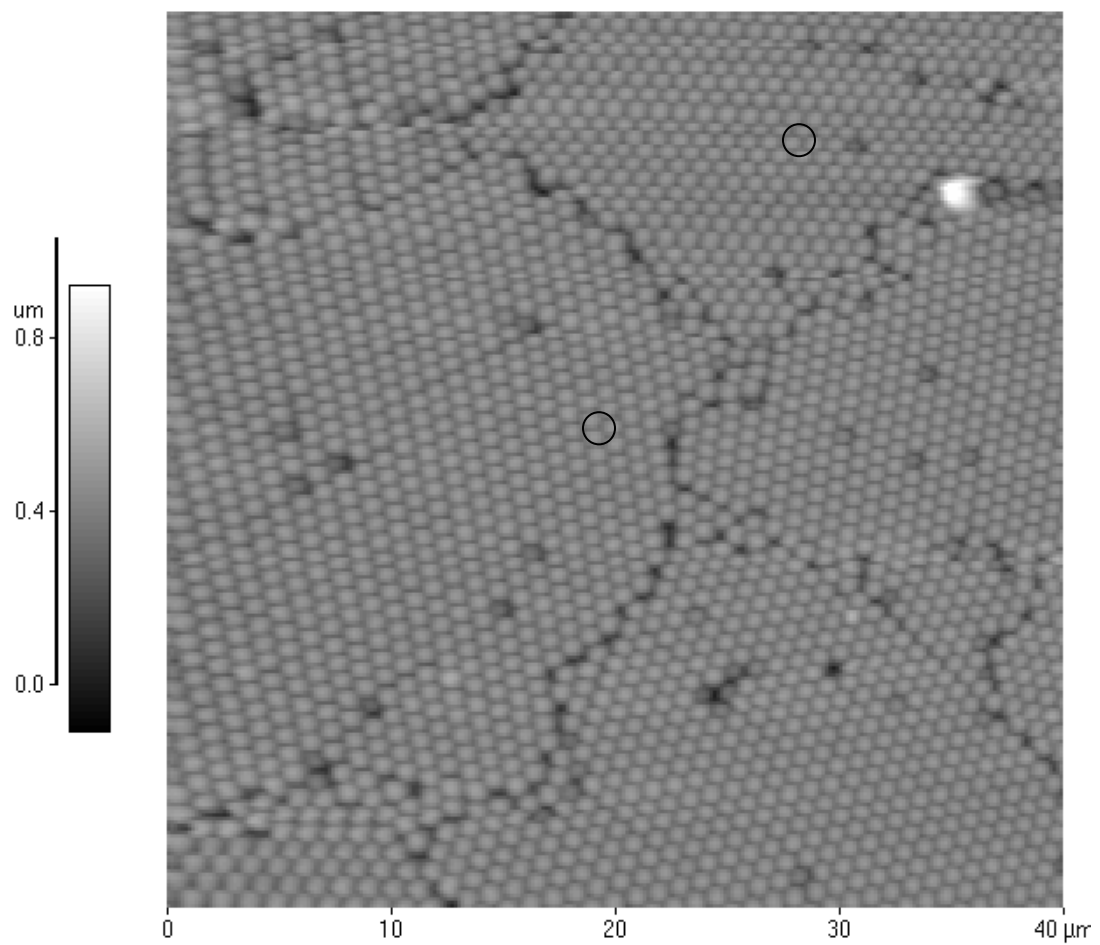


Figure 4.4 The AFM image of Au/Ag FONS on mica. The black circles indicate the size (1 μm diameter) and the location of the laser beam relative to the FONS substrate.

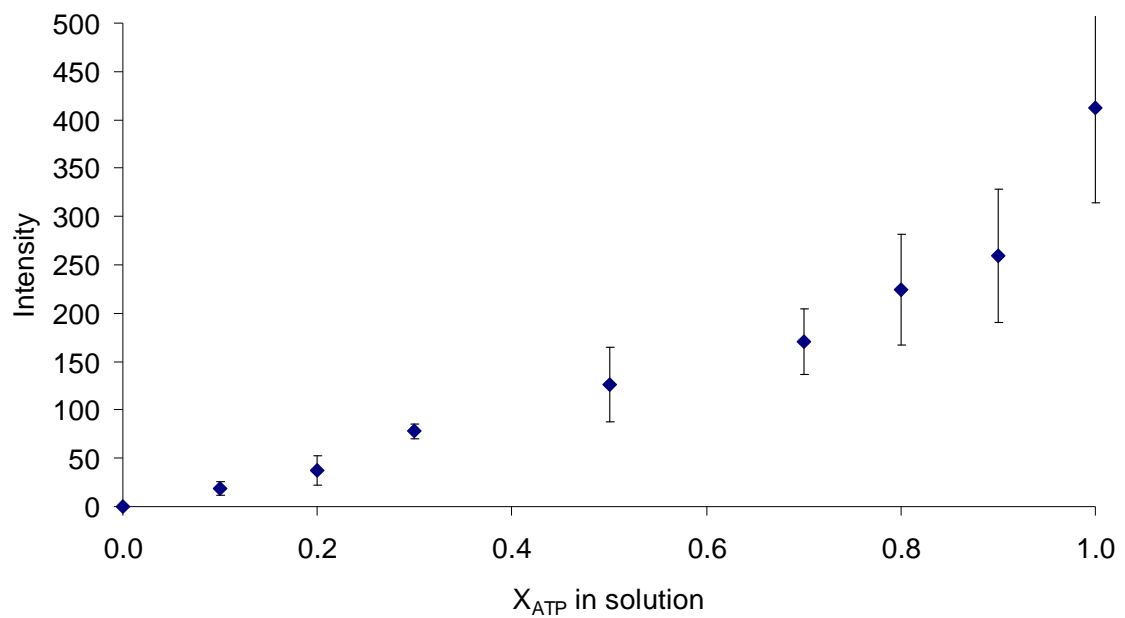


Figure 4.5 Raman intensity of the band 1077 cm⁻¹ for 4-ATP as a function of mole fraction of the 4-ATP in the solution.

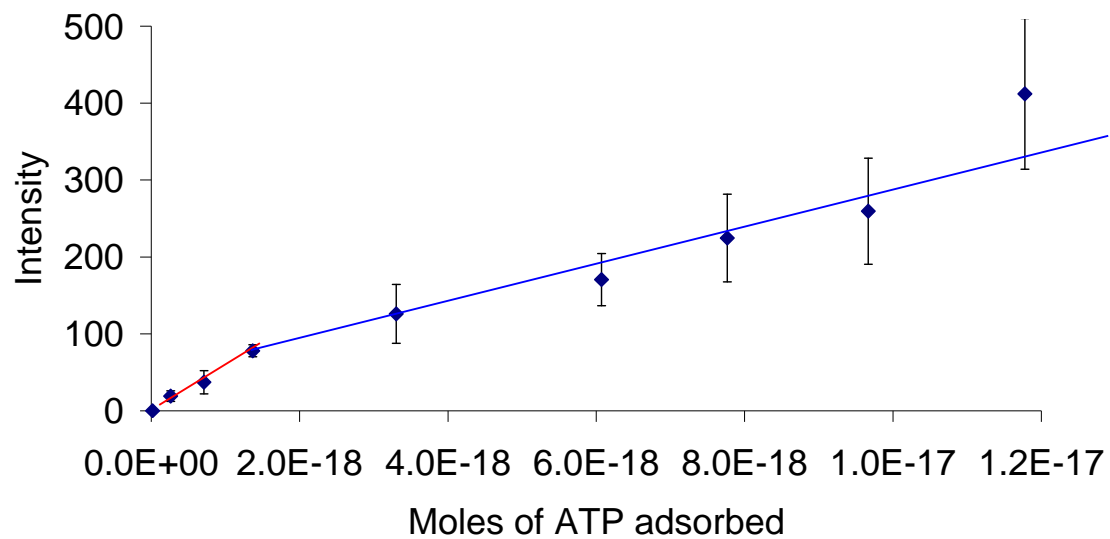


Figure 4.6 The relationship between the SERS intensity to the number of moles of 4-ATP adsorbed on the Au/Ag FONS.

4.3.2 Characterization of the Au/Ag coated HEPA filter

Figure 4.7 shows the SEM image of the Au/Ag coated glass fibers on the HEPA filter. The red circles indicate the nano-scale features with diameters ranging from 200 μm to 600 μm on the fiber which accounts for the surface enhancement. The solid green circle shows the size of laser beam relative to the diameter of the glass fiber.

The feasibility and the sensitivity study of the Au/Ag coated HEPA filter was conducted using the drop coating method to add the analyte to the metal surface. Figure 4.8 shows the uptake curve when 1.0 μM of 4-ATP was applied to the surface. As the volume of 4-ATP solution added increases the Raman intensity increases and reaches a plateau. In order to see if the plateau is real, the modified HEPA filter was soaked in a 1 mM 4-ATP solution for 6 hours and was subsequently rinsed five times with plenty of pure ethanol. The Raman intensity measured representing the saturation point of the 4-ATP molecules on the surface and it was shown as red dot on the graph. If we assume the modified HEPA filter has the same enhancement factor as the FONS, we could use the calibration curve in Figure 4.6 to reveal that the detection limit for this particular batch of modified filter is about 1 attomole of 4-ATP.

The problem with the approach using Au/Ag coated HEPA filter is the irreproducibility of the surface, causing the irreproducible surface enhancement factor. A standard addition technique is designed to overcome this problem shown in Figure 4.9. Herein, a 10 μL of 4-ATP solution with an unknown concentration was added to the modified HEPA filter. The initial SERS intensity was recorded. A standard 4-ATP solution with a concentration of 10 μM was prepared and was added sequentially with a fixed 10 μL increment while monitoring the SERS intensity. The linear trend of the

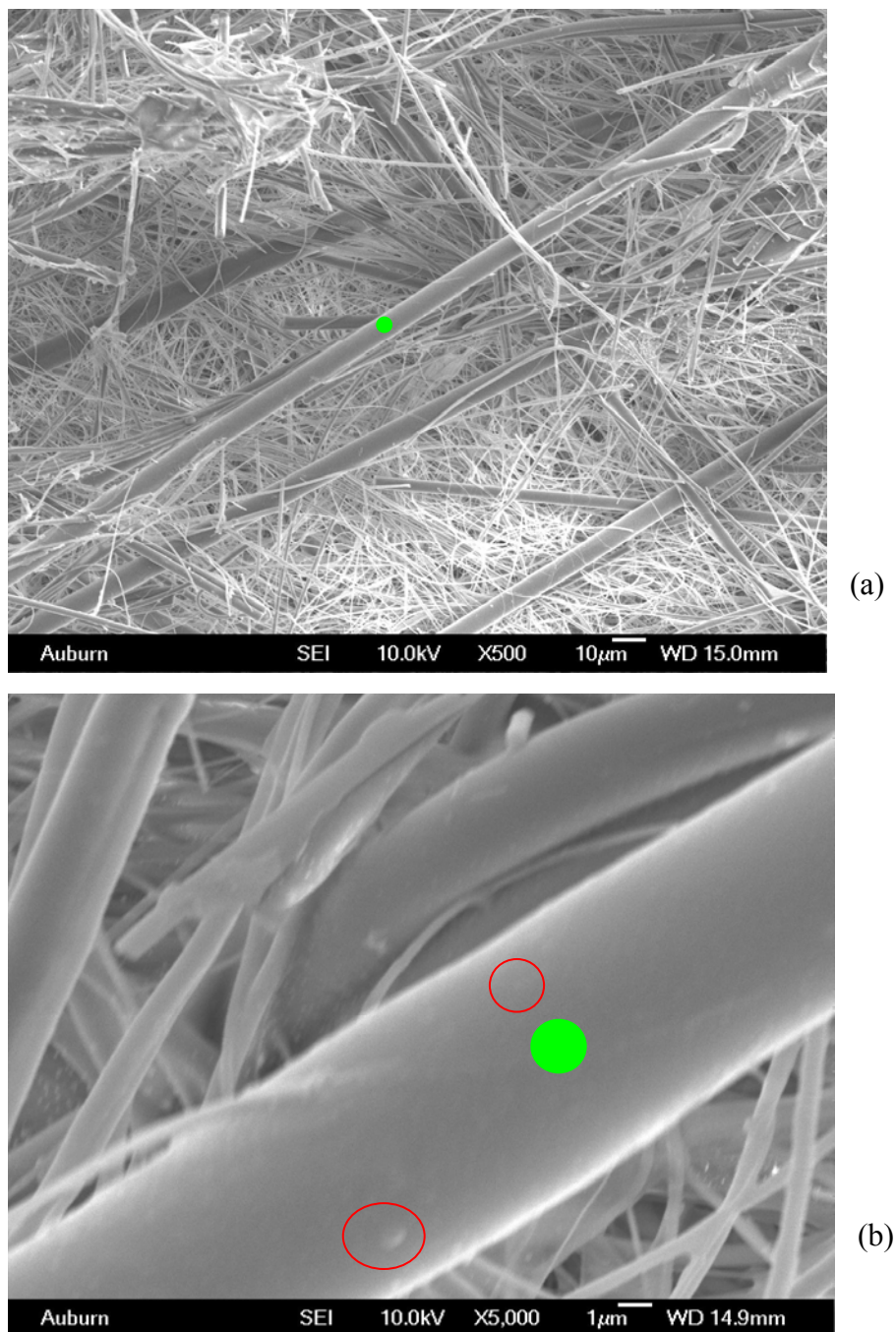


Figure 4.7 The scanning electron microscope image of the Au/Ag coated glass fiber. (a) An overview of the Au/Ag modified HEPA filter. (b) The enlargement of the fiber which was chosen for the Raman experiment. The red circles locate the roughness features on the fiber and the green solid spot representing the size of the laser beam.

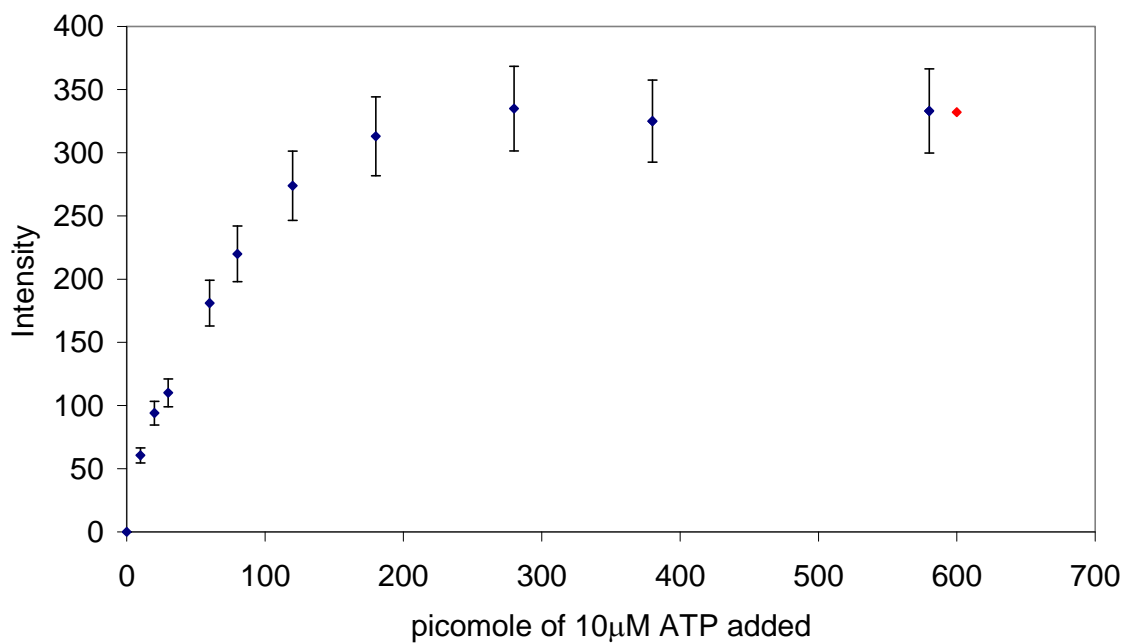


Figure 4.8 The uptake curve of the SERS intensity relative to the picomoles of 4-ATP added to the Au/Ag modified HEPA filter from the addition of 10 μ M ATP solution. The last point was collected after the Au/ Ag modified HEPA filter was soaked in the 1 mM 4-ATP and rinsed with copious pure ethanol.

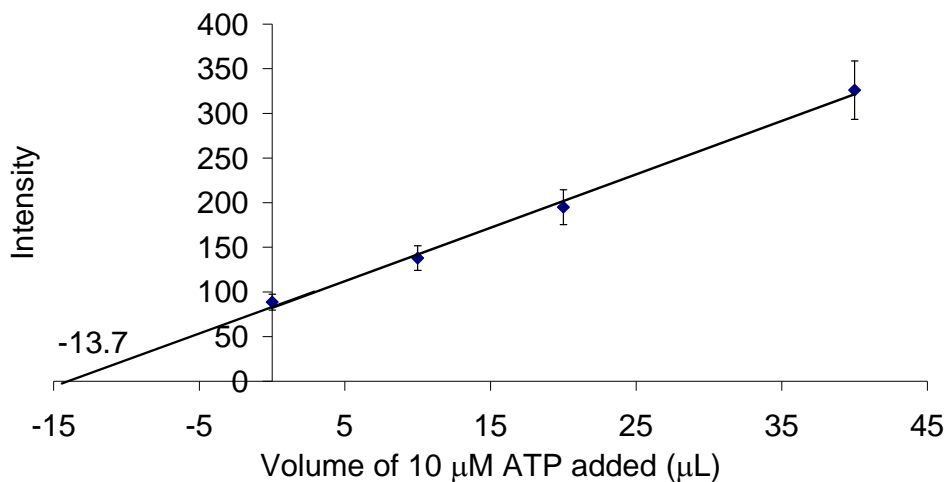


Figure 4.9 The standard addition method is used to determine the unknown concentration of 4-ATP added to the Au/Ag modified HEPA filter. The data point on y-intercept was collected from the addition of the unknown solution onto the modified HEPA filter while the rest of the data points shown were collected as the results of the standard addition. The x-intercept yields the concentration of unknown.

standard addition is able to determine the x-intercept which reveals the concentration of the unknown solution. The concentration of unknown in this particular experiment is supposed to be 15 μM ; however, the additional technique determines it as 13.7 μM . There is a discrepancy of 1.3 μM corresponds to 8.6% error.

4.4 Conclusions

Herein, we studied two strategies to characterize the performance of SERS sensors made from Au/Ag coated FONS and HEPA filter. We utilized the simplicity of using self-assembling technique to producing various surface concentrations of 4-ATP on the SERS substrate and the unique electrochemical and spectroscopic properties of 4-ATP molecules. These surface concentration or surface coverage was determined by electrochemistry and was revealed the range of coverage from 34 nmoles/cm² of a fully 4-ATP covered surface to 8.3 pmole/cm² of a partially covered surface. The equation 4.2 derived from the current-mole fraction relationship was used to reveal the relationship between the SERS intensity and the 4-ATP coverage and the phase transition characteristics at the 4-ATP mole fraction of 0.3 in the mixed thiol solution. This phase transition was speculated by the orientation changes due to the change in the concentrations of 4-ATP. As the concentration of the 4-ATP increases, the interaction force between DT molecules diminishes.

The advantage of using the Au/Ag coated HEPA filter as the chemical sensor is that the modified HEPA can act as a sample collecting medium and a sensing element simultaneously. SEM reveals the presence of the nano-scaled features which are responsible for the surface enhancing effects. The feasibility study shows the SERS

intensity could be monitored by adding the analyte onto the modified HEPA filter and the sensitivity study shows that modified HEPA filter has limit of detection at 1 attomole of 4-ATP.

The second method of characterizing SERS substrate with irreproducible surface such as Au/Ag coated HEPA filter has been investigated. Performing the standard addition technique allows one to extrapolate the concentration of known. The major setback is that this method tends not to be accurate.

4.5 References

- [1] Nie, S.; Emory, S. R. *Science* **1997**, *275*, 1102.
- [2] Yonzon, C. R.; Haynes, C. L.; Zhang, X.; Walsh, J. T.; Van Duyne, R. P. *Anal. Chem.* **2004**, *76*, 78.
- [3] Zhang, X.; Young, M. A.; Lyandres, O.; Van Duyne, R. P. *J. Am. Chem. Soc.* **2005**, *127* 4484.
- [4] Lyandres, O.; Shah, N. C.; Yonzon, C. R.; Walsh, J. T.; Glucksberg, M. R.; Van Duyne, R. P. *Anal. Chem.* **2005**, *77*, 6134.
- [5] Baker, G. A.; Moore, D. S. *Anal. Bioanal. Chem.* **2005**, *382*(8), 1751-1770.
- [6] Fleischmann, M.; Hendra, P. J.; Mcquilla, A. *Chem Phys Lett* **1974**, *26*,163–166.
- [7] Jeanmaire, D. L. ; Van Duyne, R. P. *J. Electroanal. Chem.* **1977**, *84*, 1–20.
- [9] Zhang, X.; Shah, N. C.; Van Duyne, R. P. *Vibrational Spectro.* **2006**, *42*, 2-8.
- [10] Vo-Dinh, T. in: P. Halevi (Ed.), *Photonic Probes of Surfaces*, (Elsevier, New York 1995) pp. 65–95.
- [11] Alak, A. M.; Vo-Dinh, T. *Anal. Chem.* **1987**, *59*, 2149–2153.

- [12] Alak, A. M.; Vo-Dinh, T. *Anal. Chim. Acta* **1988**, *206*, 333–337.
- [13] Narayanan, V. A.; Begun, G. M.; Stokes, D. L.; Sutherland, W. S.; Vo-Dinh, T. *J. Raman Spectrosc.* **1992**, *23*, 281–286.
- [14] Narayanan, V. A.; Begun, G. M.; Bello, J. M.; Stokes, D. L.; Vo-Dinh, T. *Analysis* **1993**, *21*, 107–112.
- [15] Zhang, X.; Matthew, A.; Young, O. L.; Van Duyne, R. P. *J. Am. Chem. Soc.* **2005**, *127*, 4484.
- [16] Sengupta, A.; Mujacic, M.; Davis, E. J. *Anal Bioanal Chem* **2006**, *386*, 1379–1386.
- [17] Kneipp, K.; Wang, Y.; Kneipp, H.; Perelman, L. T.; Itzkan, I.; Dasari, R. R.; Feld, M. *S. Phys. Rev. Lett.* **1997**, *78*, 1667.
- [18] Bell, S. E. J.; Mackle, J. N.; Sirimuthu, N. M. S. *Analyst* **2005**, *130*, 545–549.
- [19] Zhang, X.; Shah, N. C.; Van Duyne, R. P. *Vibration Spectroscopy* **2006**, *42*, 2-8.
- [20] Stosch, R.; Henrion, A.; Schiel, D.; Guettler, B. *Anal Chem* **2005**, *77*, 7386–7392.
- [21] Reilly, T.; Corbman, J. D.; Rowlen, K. L. *Anal. Chem.* **2007**, *79*, 5078-5081.
- [22] Bull, K. *Travel Medicine and Infectious Disease* 2008, *6*, 3, 142-144.
- [23] Hayes, W. A.; Shannon, C. *Langmuir* **1996**, *12*(15), 3688-3694.
- [24] Osawa, M.; Matsuda, N.; Yoshii, K.; Uchida, I. *J. Phys. Chem.* **1994**, *98*, 12702-12707.
- [25] Strong, L.; Whitesides, G. M. *Langmuir* **1988**, *4*, 564.
- [26] Moskovits, M. *Rev. Mod. Phys.* **1985**, *57*, 783.

CHAPTER 5

SUMMARY OF DISSERTATION

This dissertation has exploited the optical phenomenon of surface plasmon resonance on the gold surface for the chemical and biochemical sensing. The surface plasmon resonance occurs when the momentum of light is conserved at the metal-dielectric interface. The photon interacts with the electron in the thin gold film, causing the oscillation of the electrons and generating an evanescent field at the interface. The strength of the evanescent field decays exponentially away from the gold surface, making SPR sensitive to the environment approximately 100 nm above the surface.

Two different mechanisms of producing SPR were discussed in the dissertation. The propagating surface plasmons can be produced on the planar metallic surface by imposing the prism-coupled excitation light on the metal surface. The generation of the surface plasmons with this type of mechanism provides the basis for the surface plasmon resonance spectroscopy, where the resonance angle is measured from the minimum of the reflectance curve. Since the resonance angle is strongly affected by the dielectric constant of the dielectric layer, SPR can be used to monitor the binding events occurring at the gold surface. Another way of producing SPR is to use the nanoscaled surface feature to generate the localized surface plasmons. The oscillation of the localized surface plasmons intensifies the excitation field on the gold surface and provides the key factor for the enhancement of the Raman spectroscopy.

We exploited the sensitivity of the SPR to elucidate the electrochemical processes occurring at the gold electrode surface. The electrochemistry of the gold oxide, the underdeposition of the selenium, and the stripping of the mixed selenium and tellurium layer were studied. The SPR was demonstrated sensitive enough to distinguish the faradaic process and nonfaradaic process during the cyclic voltammetric studies of gold oxide and selenium deposition. The hysteresis of the SPR signals during the potential sweep is puzzling. This may be due to the sluggish kinetics of the stripping process. We were puzzled by another observation in the selenium UPD experiment, where a current peak was observed without any observed change in SPR angle. Overall, we have demonstrated the EC-SPR can be used to quantify the concentration of the selenite ions and telluride ions simultaneously by employing the standard addition technique. The future work includes the sensitivity study of simultaneous sensing using EC-SPR to determine the detection limit for the co-existence of the mixed ions species.

Surface plasmon resonance spectroscopy provides an alternative way in study protein-protein interactions. The protein system chosen is the alkanesulfonate monooxygenase, which consists of SsuD and SsuE. SsuD was first immobilized on the gold surface through the amine coupling and the SPR was used to monitor the kinetics of the protein binding between SsuD and SsuE. Ellis, et al. has investigated the same system in the solution phase and has determined the dissociation constant (K_d) to be $0.0022 \mu\text{M}^{-1} \text{s}^{-1}$. In our surface phase study, the dissociation constant was determined be $0.24 \pm 0.17 \mu\text{M}^{-1} \text{s}^{-1}$. The discrepancy between two methods may be attributed to the unaccounted change in the stoichiometric ratio of two binding proteins and the reduced freedom for

confirmation change during the protein interaction and the size of binding pocket for the surface method compared with the free protein on the solution.

Surface enhanced Raman spectroscopy relies on the localized evanescent field produced on the metallic nanostructure for the enhancement of the Raman spectra. Raman spectroscopy is a molecular fingerprinting method utilizing the inelastic scattering of the light by the various types of the chemical bonds. The presence of the localized evanescent field intensifies the excitation field and imposes an induced electromagnetic field on the adsorbed molecule. This enhancement mechanism is referred as electromagnetic enhancement factor, contributing an enhancement of 10^4 - 10^6 . Another mechanism for the enhancement is the chemical enhancement which contributes an enhancement up to 10^2 . The enormous enhancement on the Raman spectra is promising for sensor development.

The air-filter based chemical sensor using surface enhanced Raman spectroscopy as a readout strategy was conceived with the advent of the metallic nanostructure preparation technique. The mixed monolayers of 4-ATP and decanethiol were studied using SERS. Metal film over nanospheres in our study has produced enhanced Raman spectrum of the 4-aminothiophenol. The detection limit for the Au/Ag FONS is determined to be 1 attomole of 4-ATP. The Au/Ag modified HEPA filter is able to produce enhanced Raman spectra; however, the reproducibility on the Raman intensity of 4-ATP molecules at different locations of the modified filter is poor. Addition technique was employed to overcome the surface irregularity and has been proven useful for estimating the concentration of the unknown solution.